AD_____

Award Number: W81XWH-12-1-0217

TITLE: Metabolic Signaling and Therapy of Lung Cancer

PRINCIPAL INVESTIGATOR: Jing Chen

CONTRACTING ORGANIZATION: Emory University
Atlanta, Georgia 30322

REPORT DATE: September 2013

TYPE OF REPORT: Annual report

PREPARED FOR: U.S. Army Medical Research and Materiel Command
Fort Detrick, Maryland 21702-5012

REPORT DOCUMENTATION PAGE

Form Approved
OMB No. 0704-0188

1. REPORT DATE	2. REPORT TYPE	3. DATES COVERED
September-2013	Annual report	1 September 2012 –31 August 2013

4. TITLE AND SUBTITLE

Metabolic Signaling and Therapy of Lung Cancer

5a. CONTRACT NUMBER

5b. GRANT NUMBER
W81XWH-12-1-0217

5c. PROGRAM ELEMENT NUMBER

6. AUTHOR(S)

Jing Chen

E-Mail: jchen@emory.edu

5d. PROJECT NUMBER

5e. TASK NUMBER

5f. WORK UNIT NUMBER

7. PERFORMING ORGANIZATION NAME(S) AND ADDRESS(ES)

Emory University
Atlanta, Georgia 30322

8. PERFORMING ORGANIZATION REPORT NUMBER

9. SPONSORING / MONITORING AGENCY NAME(S) AND ADDRESS(ES)
U.S. Army Medical Research and Materiel Command
Fort Detrick, Maryland 21702-5012

10. SPONSOR/MONITOR'S ACRONYM(S)

11. SPONSOR/MONITOR'S REPORT NUMBER(S)

12. DISTRIBUTION / AVAILABILITY STATEMENT
Approved for Public Release; Distribution Unlimited

13. SUPPLEMENTARY NOTES

14. ABSTRACT

The purpose of this grant is to decipher molecular mechanisms by which glycolytic enzyme phosphoglycerate mutase 1 (PGAM1) promotes lung cancer cell metabolism and evaluate novel PGAM1 inhibitors as anti-cancer therapy in treatment of lung cancer. We accomplished studies for Month 1-12 as proposed in the approved Statement of Work. We published a featured article in ***Cancer Cell*** and demonstrated that PGAM1 is commonly upregulated in human cancers including lung cancer due to loss of TP53 and is important to coordinate glycolysis and biosynthesis in cancer cells. We developed a novel small molecule PGAM inhibitor PGMI-004A. Inhibition of PGAM1 by shRNA or PGMI-004A results in significantly decreased glycolysis, pentose phosphate pathway flux and biosynthesis in lung cancer cells, as well as attenuated cell proliferation and tumor growth, suggesting PGAM1 as a promising target in treatment of lung cancer. Moreover, in a recent ***Nature Communications*** paper, we reported a novel mechanism in which Y26 phosphorylation activates PGAM1 to promote lung cancer cell proliferation and tumor growth. In addition, we now show that EGFR phosphorylates and activates PGAM1 by promoting cofactor 2,3-BPG binding in lung cancer cells and generated rescue PGAM1 WT and Y26F stable cell lines using different lung cancer cell lines.

15. SUBJECT TERMS
PGAM1 in regulation of lung cancer metabolism; molecular mechanisms underlying PGAM1 activation in lung cancer; PGAM1 inhibitor as novel therapy to treat lung cancer

16. SECURITY CLASSIFICATION OF:			17. LIMITATION OF ABSTRACT	18. NUMBER OF PAGES	19a. NAME OF RESPONSIBLE PERSON
a. REPORT	b. ABSTRACT	c. THIS PAGE			USAMRMC
U	U	U	UU		19b. TELEPHONE NUMBER *(include area code)*

Table of Contents

Introduction

Lung cancer is the leading cause of cancer-related death in the US and worldwide. A substantial percentage of lung cancers express cell surface epidermal growth factor receptor (EGFR) as well as other oncogenic tyrosine kinases including fibroblast growth factor receptor 1 (FGFR1). These receptor tyrosine kinases play a key role in the pathogenesis and disease progression of lung cancer, which makes them attractive therapeutic targets. However, the development of targeted agents in lung cancer is still in its infancy, despite the FDA approval of agents that inhibit EGFR pathways in lung tumors. Thus, it is critical to identify and validate novel promising therapeutic targets to enable significant clinical gains. We found that, phosphoglycerate mutase 1 (PGAM1), which catalyzes the conversion of 3-phosphoglycerate (3-PG) to 2-phosphoglycerate (2-PG) during glycolysis, is commonly upregulated in lung cancer cells. We also found that Y26 phosphorylation of PGAM1 is common in lung cancer cells, which promotes the cofactor, 2,3-bisphosphoglycerate (2,3-BPG), binding to PGAM1, leading to enhanced PGAM1 activity by promoting H11 phosphorylation. Moreover, targeting PGAM1 by shRNA or expression of a catalytically less active mutant Y26F results in aberrant glycolysis and biosynthesis with attenuated pentose phosphate pathway (PPP) and decreased NADPH/NADP+ ratio in cancer cells, and reduced cell proliferation and tumor growth in xenograft nude mice. Furthermore, we screened and developed small molecule *PG*A*M*1 *i*nhibitors (PGMI-004 and 004A), which effectively inhibit PGAM1 and cancer cell proliferation; PGMI-004A treatment attenuates tumor growth in xenograft nude mice and cell proliferation of primary leukemia cells from human patients with minimal toxicity. Therefore, the current funded proposal focuses to decipher molecular mechanisms by which PGAM1 promotes lung cancer cell metabolism and evaluate novel PGAM1 inhibitors as anti-cancer therapy in treatment of lung cancer. In particular, we proposed to elucidate the molecular mechanisms by which protein expression and phospho-Y26-dependent activation of PGAM1 coordinate glycolysis and anabolic biosynthesis to promote lung cancer cell metabolism and tumor growth, and validate PGAM1 as a therapeutic target in treatment of lung cancer *in vitro* and *in vivo* using PGAM1 small molecule inhibitors developed in our laboratory.

Body

We published two papers in top tier journals during the funded period (01-09-2012 to 31-08-2013) from the funded project, demonstrating high impact of our project topic in the cancer research field:

- Hitosugi, T., et al., and Chen, J. (2012) Phosphoglycerate mutase 1 coordinates glycolysis and biosynthesis to promote tumor growth. ***Cancer Cell*** November 13, 2012; 22(5): 585-600. Featured by Cancer Cell, Nature Chemical Biology, SciBX

- Hitosugi, T., et al., and Chen, J. (2013) Y26 phosphorylation of PGAM1 provides a metabolic advantage to tumours by stabilizing the active conformation. ***Nature Communications*** 4, Article number:1790; doi:10.1038/ncomms2759

In addition, we have accomplished all of the proposed studies in the approved Statement of Work for Months 1-12:

Task 1: To elucidate the molecular mechanisms by which expression and phospho-Y26-dependent activation of PGAM1 coordinate glycolysis and anabolic biosynthesis to promote lung cancer cell metabolism and tumor growth. (Month 1-24)

- *We will continue to determine whether EGFR phosphorylates PGAM1 at Y26 in vivo. Lung cancer cells including A549, H157 and H322 expressing EGFR will be treated with increasing doses of EGFR inhibitor Tarceva and decreased Y26 phosphorylation of PGAM1 will be detected by Western blot (Month 1-2).*

Progress: As shown in Fig.1, we treated different human lung cancer cells as proposed with EGFR inhibitor Tarceva. Treatment with Tarceva results in decreased Y26 phosphorylation of PGAM1 in both dose- and time-dependent manners in lung cancer cells including A549 (*upper*), H157 (*middle*) and H322 (*lower*) cells.

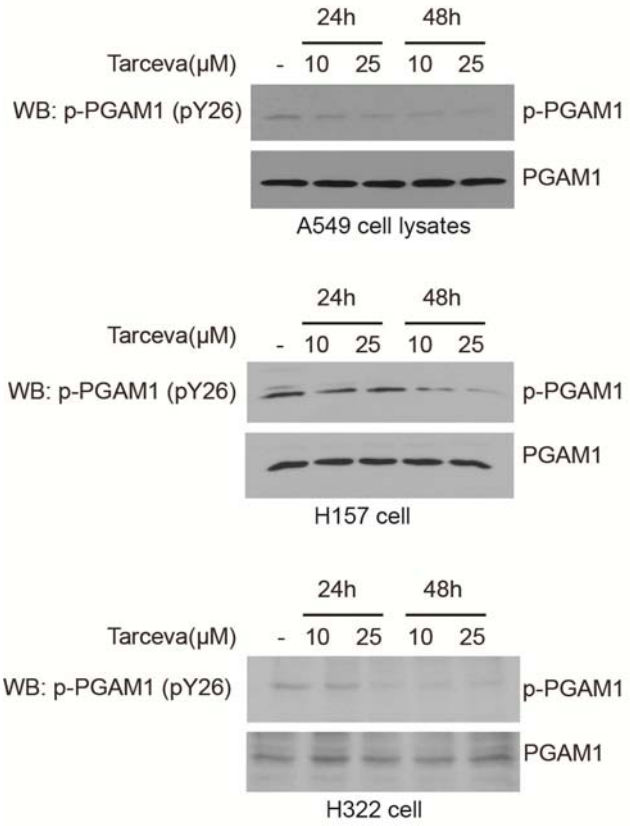

Fig.1. Treatment with EGFR inhibitor Tarceva (10 or 25 μM) for indicated time periods results in decreased Y26 phosphorylation of PGAM1 in lung cancer cells including A549 (*upper*), H157 (*middle*) and H322 (*lower*) cells.

- *We will also examine whether phosphorylation of PGAM1 at Y26 by EGFR results in increased 2,3-BPG binding (Month 3-4).*

Progress: As proposed, our structural studies (5) revealed that both H11 and Y92 are directly proximal to the active site where both cofactor (2,3-BPG) and substrate (3-PG) bind (Fig. 2A) (9), suggesting that Y92 may be crucial for 2,3-BPG binding and PGAM1 activity, consistent with our observation that substitution of Y92 abolishes PGAM1 enzyme activity (Fig. 1f-1g of (5)). This is also consistent with a previous report that S14, T23, G24, R90, Y92, K99, R116 and R117 are involved in binding of cofactor 2,3-BPG and substrate 3-PG, which share the same binding pocket on PGAM1 (1). Y26 is also close to the catalytic site (Fig. 2A); since Y26-phoshorylation by FGFR1 enhances PGAM1 in the presence of 2,3-BPG , this suggests a potential mechanism wherein Y26 phosphorylation by FGFR1 may stabilize the H11-phosphorylated PGAM1.

To test this hypothesis, we incubated active rFGFR1 with purified, recombinant PGAM1 WT and Y26F mutant in an *in vitro* kinase assay, followed by incubation with a competitive 2,3-BPG fluorescent analogue (8-hydroxy-1,3,6-pyrenetrisulfonate) (6, 7) (Fig. 2B). The decrease in fluorescence (ex: 362 nm, em: 520 nm) compared with buffer control was measured as 2,3-BPG binding ability. Phosphorylation of PGAM1 WT by EGFR resulted in a significant increase in the amount of bound 2,3-BPG analogue, whereas substitution of PGAM1 Y26 abolished enhanced binding of cofactor in the presence of recombinant EGFR (rEGFR) (Fig. 2C).

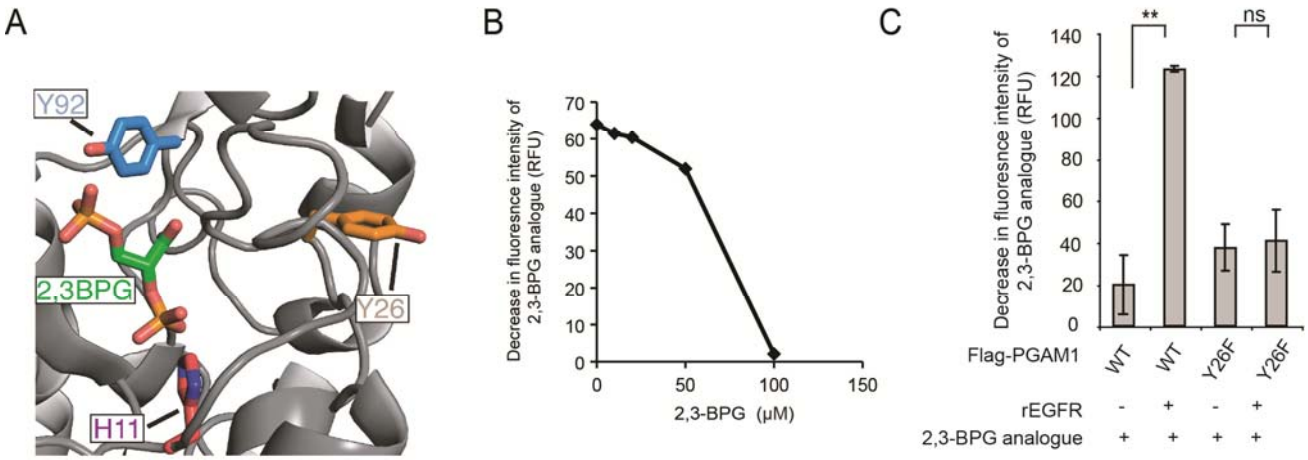

Fig.2. Y26 phosphorylation promotes cofactor 2,3-BPG binding to PGAM1. (A) Cartoon representation of 2,3-BPG location from structure 3FDZ superposed on PGAM1 (PDB ID: 1YFK). H11 and Y92 are directly proximal to and Y26 is also close to cofactor (2,3-BPG)/substrate (3-PG) binding site. (B) 2,3-BPG analogue (8-hydroxy-1,3,6-pyrenetrisulfonate) competes with 2,3-BPG for binding to rPGAM1 protein, where 3 μM 2,3-BPG analogue was mixed with different concentrations of 2,3-BPG in reaction mixture containing 100 mM Tris-HCl (pH 7.5). Fluorescence intensity of 2,3-BPG analogue (ex: 362 nm, em: 520 nm) was measured before and 5 min after the addition of 2.3 μM rPGAM1 protein to the reaction mixture. Decrease in fluorescence intensity of 2,3-BPG analogue indicates 2,3-BPG analogue binding to rPGAM1 protein. The values are presented as relative fluorescence units (RFU). (C) Purified Flag-PGAM1 WT or Y26F were incubated with recombinant EGFR followed by treatment with cofactor (represented by 2,3-BPG analogue, 8-hydroxy-1,3,6-pyrenetrisulfonate). The cofactor binding affinity was determined by decrease in fluorescence intensity of the analogue. The values are presented as relative fluorescence units (RFU).

- *We will continue the collaboration with Dr. Yibin Kang at Princeton University to address the question of whether Y26 phosphorylation promotes His11 phosphorylation of PGAM1 by quantitative mass spectrometric analysis (Month 5-8).*

Progress: As proposed, Dr. Yibin Kang's group at Princeton University performed a quantitative mass spectrometry-based study (Fig. 3A). The results revealed that the H11 phosphorylation level of Y26F mutant is significantly lower compared to PGAM1 WT in an in vitro kinase assay using PGAM1 proteins incubated with rFGFR1 in the presence of 2,3-BPG (Fig. 3B-3C). Similar results were obtained when using Flag-tagged mouse PGAM1 (mPGAM1) WT and Y26F from "rescue" human lung cancer H1299 cells, which overexpress oncogenic FGFR1, with stable knockdown of endogenous human PGAM1 (hPGAM1) and rescue expression of Flag-mPGAM1 WT or Y26F mutant, respectively (Fig. 3D-3E). These results suggest that Y26 phosphorylation may enhance PGAM1 activity by stabilizing the H11-phosphorylated PGAM1.

The detailed experimental procedure and methods were described in our recent paper published in *Nature Communications* (5) (please see attached reprint in appendices).

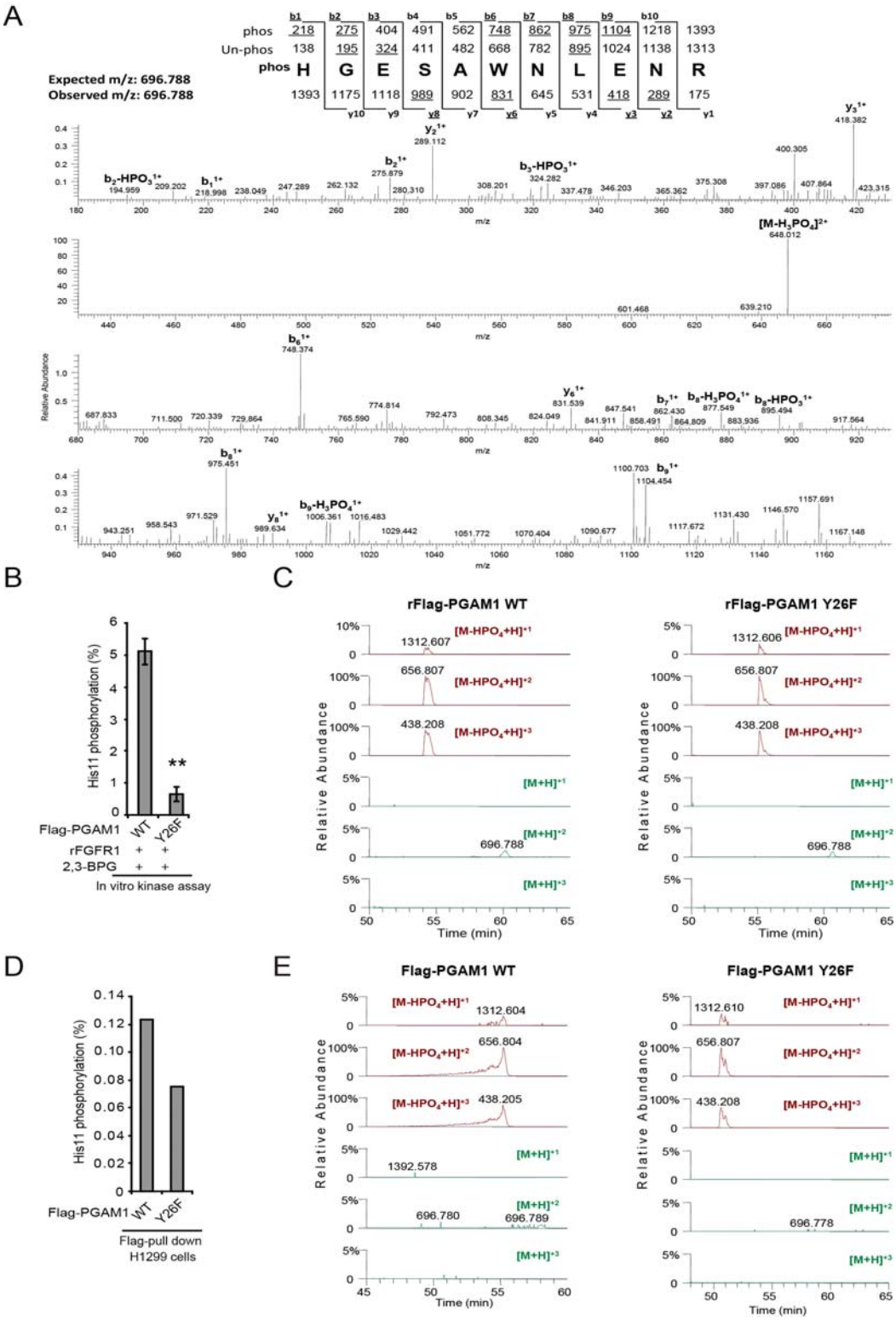

Fig.3. Y26 phosphorylation results in increased H11 phosphorylation of PGAM1 in vitro and in vivo. (A) Detection of H11 phosphorylation in PGAM1 using LC-MS/MS. Tandem mass spectrometry (MS/MS) spectrum of phosphorylated PGAM1 peptide pHGESAWNLENR (residue number 11-21) collected using CID fragmentation. Underlined nominal masses above and below the sequence denote the b and y ions respectively that were annotated from the spectrum. The expected and observed mass to charge ratio (m/z) for the [M+2H+]2+ precursor ion is provided. [M-H3PO4]+2 represents molecular ion with loss of the phosphate group. (B-C) Phosphorylation by rFGFR1 leads to increased H11 phosphorylation of Flag-PGAM1 WT but not Y26F in the presence of 10μM 2,3-BPG (B). C shows relative quantification of H11-phosphorylated PGAM1 using reverse phase liquid chromatography. MS data for HGESAWNLENR (upper three red spectra in each panel) and pHGESAWNLENR (lower three green spectra in each panel) were used to calculate the relative levels of phosphorylated and unphosphorylated peptide across all observable charge states in Flag-tagged PGAM1 WT and Y26F mutant incubated with active FGFR1 and 2,3-BPG for one hour (C, left and right, respectively). The relative abundance was normalized to the largest peak of each scan, which corresponds to 5.5E7 (C, left) and 2.26E7 (C, right). (D-E) Rescue cells expressing mouse PGAM1 (mPGAM1) Y26F demonstrate reduced H11 phosphorylated levels compared to cells with mPGAM1 WT (D). WT or Y26F: cells with stable knockdown of endogenous hPGAM1 and rescue expression of mPGAM1 WT or Y26F mutant, respectively. E shows relative quantification of H11-phosporylated PGAM1 using reverse phase liquid chromatography with Flag-tagged PGAM1 WT and Y26F mutant proteins isolated from rescue H1299 cells (E, left and right, respectively). The relative abundance was normalized to the largest peak of each scan, which corresponds to 1.12E7 (E, left) and 1.96E7 (E, right).

Additional work: As we reported in the recent Nature Communications paper (5), to further understand the structural properties of Y26-phosphorylation-enhanced activation of H11-phosphorylated PGAM1, we crystalized human PGAM1 with phosphorylated H11 (1.65 Å; please see Supplementary Table S1 of (5)) from purified PGAM1 protein incubated with 2,3-BPG, in which the occupancy of phosphate on H11 was refined to be 0.70; mass spectrometry analysis of the 2,3-BPG-treated PGAM1 supports that the majority of PGAM1 protein was phosphorylated (please see Supplementary Fig. S1a of (5)). We also crystalized the apo-form of non-phosphorylated wild type human PGAM1 (2.08 Å) as previously reported (9). Both structures of the H11-phosphorylated and non-phosphorylated forms were superposed with a RMSD value of 0.34 Å (please see Supplementary Fig. 1b of (5)).

Upon comparison between these two structures, we found a major conformational change at the loop 12-23 in the H11 phosphorylated form, which is close to H11 that is in the active site of PGAM1 (Fig. 4A). Further structural analysis revealed that, in the structure of non-phosphorylated PGAM1 form, Y26 docks on W16 in the flexible loop (Fig. 4B-4C), while the negative charged E19 is located in the positively charged active site, blocking access of cofactor (2,3-BPG) and substrate (3-PG) to the active site (Fig. 4c). Moreover, E19 forms hydrogen bonds with residues S14 and S23 on the loop, which stabilize the conformation of non-phosphorylated PGAM1 (Fig. 4c). In contrast, Y26 is exposed to the surface in the structure of the H11-phosphorylated form of PGAM1, whereas E19 flips away from the active site to allow the negatively charged phosphate group of phosphorylated H11 to be accommodated (Fig. 4D). In addition, the phosphorylated-H11 forms extensive hydrogen bonds with adjacent residues, including R10, R62, E89, H186 and G187, through its phosphate group (Fig. 4D). These hydrogen bonds also contribute to the stabilization of the phosphorylated-histidine group captured in the crystal, which, otherwise, is generally unstable in the aqueous solution with a half-life around 30 minutes (8).

These data together suggest a model in which Y26-phosphorylation may shift the protein conformation to release the negatively charged E19 that blocks the active site (Fig. 4E), thus promoting 2,3-BPG binding and consequently H11 phosphorylation, which may also help to keep the active site open for substrate (3-PG) binding (Fig. 4F). Please see below for detailed discussion.

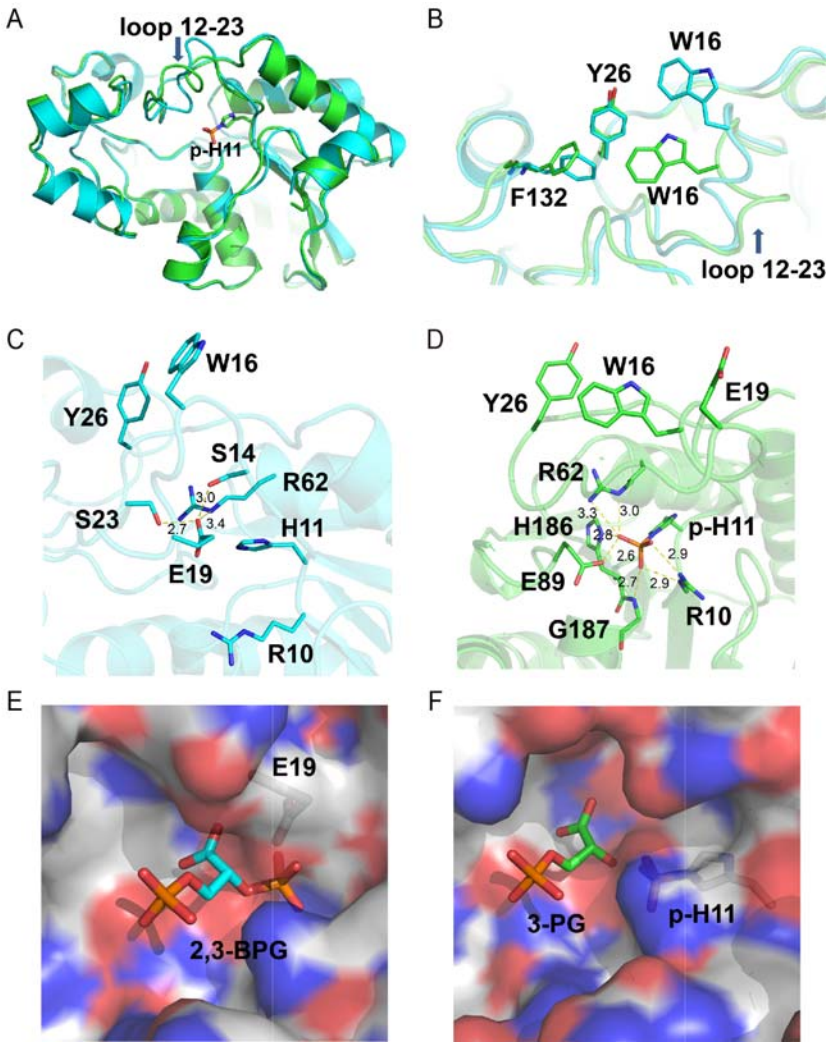

Fig.4. Y26 phosphorylation may cause conformational change to release E19 that blocks active site of PGAM1. (A) Superposition of PGAM1 wild type (cyan) and H11-phosphorylated form (green). Phosphorylated H11 is shown in stick and loop 12-23 with the large conformational change is marked. (B) Comparison of Y26 surrounding residues between wild type PGAM1 (cyan) and H11-phosphorylated form (green). (C) Interactions between E19 and adjacent residues in Y26 buried wild type PGAM1. (D) Interactions between phosphorylated H11 and adjacent residues in Y26 exposed phosphorylated PGAM1. (E) Superposed cofactor 2,3-BPG in the active site of non-phosphorylated PGAM1. There is a clash between E19 and phosphate group of 2,3-BPG. (f) Superposed substrate 3-PG in active site of H11-phosphorylated PGAM1 showing that it is ready to react with phosphorylated H11.

- *We will generate diverse lung cancer cell lines with stable knockdown of endogenous PGAM1 followed by rescue expression of mouse PGAM1 WT and Y➔F mutants. We will use H1299, A549, H157 and H322 lung cancer cells (Month 9-12).*

Progress: As proposed, we generated "rescue" cells using diverse human lung cancer cells including H1299, H157 and H322 cells as described (2-4) by shRNA-mediated stable knockdown of endogenous hPGAM1 and rescue expression of Flag-tagged mPGAM1 WT or Y26F (Fig. 5). These cell lines will be used to determine the role of Y26 phosphorylation of PGAM1 in lung cancer cell metabolism and lung tumor growth as proposed in the rest of Task1 and Task2.

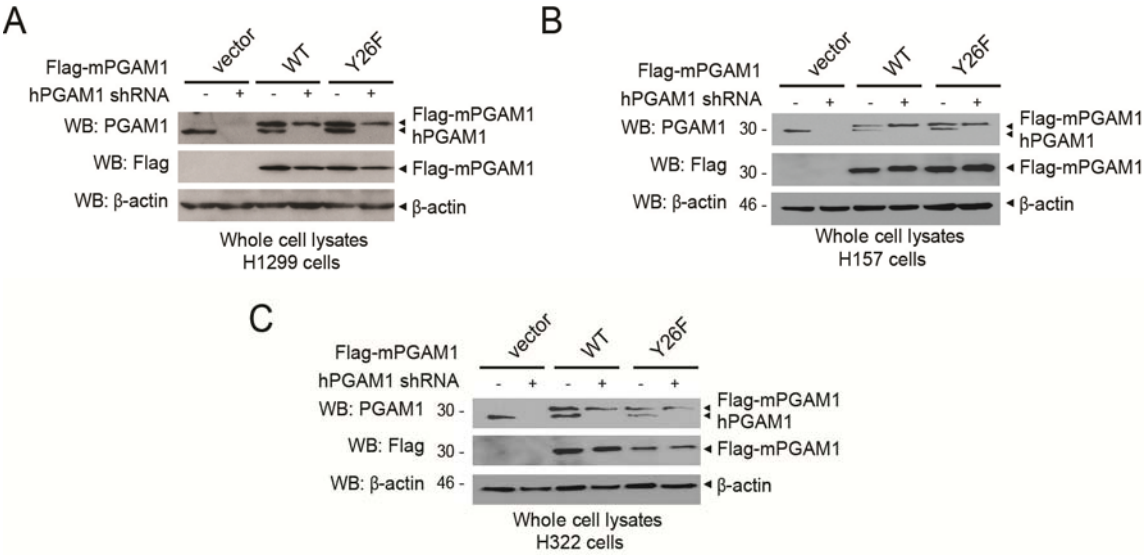

Fig.5. Generation of recuse cell lines using human lung cancer H1299 (A), H157 (B) and H322 (C) cells with stable knockdown of endogenous hPGAM1 and rescue expression of mPGAM1 WT or Y26F.

Key Research Accomplishments

So far we have demonstrated (and published) that:

- PGAM1 controls 3-PG and 2-PG levels to coordinate glycolysis and biosynthesis.
- 3-PG binds to and inhibits 6PGD in the oxidative PPP.
- 2-PG potentiates PHGDH to provide feedback control of 3-PG levels.
- PGAM1 is a promising anti-cancer target in treatment of lung cancer.
- Y26 phosphorylation activates PGAM1 by releasing inhibitory E19 that blocks the active site, stabilizing cofactor 2,3-bisphosphoglycerate binding and H11 phosphorylation.
- Y26-phosphorylation of PGAM1 is common in human cancer cells and contributes to regulation of 3-PG and 2-PG levels, promoting cancer cell proliferation and tumor growth.

Reportable Outcomes

1. We published two papers in top tier journals including Cancer Cell (featured article) and Nature Communications during the funded period (01-09-2012 to 31-08-2013) as listed below. The reprints in PDF files are attached as appendices.

    - Hitosugi, T., Zhou, L., Elf, S., Fan, J., Kang, H.-B., Seo, J.H., Shan, C., Dai, Q., Zhang, L., Xie, J., Gu, T.-L., Jin, P., Aleckovic, M., LeRoy, G., Kang, Y., Sudderth, J.A., DeBerardinis R.J., Luan, C., Chen, G.Z., Muller, S.M., Shin, D.M., Owonikoko, T.K., Lonial, S., Arellano, M., Khoury, H.J., Khuri, F.R., Lee, B.H., Ye, K., Boggon, T.J., Kang, S., He, C., and Chen, J. (2012) Phosphoglycerate mutase 1 coordinates glycolysis and biosynthesis to promote tumor growth. Cancer Cell November 13, 2012; 22(5): 585-600. Featured by Cancer Cell, Nature Chemical Biology, SciBX

        Preview: PGAMgnam Style: A Glycolytic Switch Controls Biosynthesis Barbara Chaneton and Eyal Gottlieb (2012) Cancer Cell November 13, 2012; 22(5): 565-6

    - Hitosugi, T., Zhou, L., Fan, J., Elf, S., Zhang, L., Xie, J., Wang, Y., Gu, T.-L., Aleckovic, M., LeRoy, G., Kang, Y., Kang, H.-B., Seo, J.H., Shan, C., Jin, P., Gong, W., Lonial, S., Arellano, M., Khoury, H.J., Chen, G.Z., Shin, D.M., Khuri, F.R., Boggon, T.J., Kang, S., He, C., and Chen, J. (2013) Y26 phosphorylation of PGAM1 provides a metabolic advantage to tumours by stabilizing the active conformation. Nature Communications 4, Article number:1790; doi:10.1038/ncomms2759

2. Shannon E. Elf, a graduate student who was supported by the current grant, graduated with PhD degree in July 2013. She is currently working as a postdoctoral fellow in Dana-Farber Cancer Institute/Harvard Medical School in Boston, Massachusetts

3. We were invited to speak at national and international conferences to present work from the current funded proposal.

    2013 Speaker, Keystone Symposium Tumor Metabolism (X4) joint with the meeting on PI 3-Kinase and Interplay with Other Signaling Pathways (X3), Keystone Resort, Keystone, Colorado

    2013 Speaker, Symposium "*Molecular and Cellular Biology*", American Association of Cancer Research 104th annual meeting, Washington, DC

    2013 Speaker, *The 2013 Frontier Forum in Medical Sciences and the 13th National Meeting on Tumor Pharmacology and Chemotherapy*, Chinese Academy of Engineering, Chinese Anti-Cancer Association and Chinese Pharmacological Society, Luo Yang, China

    2013 Speaker, *2013 FASEB meeting on Hematologic Malignancies*, Saxtons River, Vermont

Conclusion

We have successfully accomplished all the proposed work in the funded proposal during the report time period (first 12 months). Moreover, we published two important papers in high impact journals including *Cancer Cell* (featured article) and *Nature Communications*.

Our work has significant impact on lung cancer cell metabolism and therapeutic development to treat lung cancer patients. The current understanding of the Warburg effect consists of an increase in aerobic glycolysis in cancer cells. The connection between glycolysis and PPP/biosynthesis is based upon a model in which glycolytic intermediates can be diverted into PPP and biosynthesis pathways as precursors. Our findings demonstrate that PGAM1 regulates the concentrations of glycolytic metabolites 3-PG and 2-PG, which function as signaling molecules to directly affect the catalytic activity of enzymes involved in PPP and biosynthesis, representing an additional link between glycolysis, PPP and biosynthesis.

Moreover, we report that Y26 phosphorylation of PGAM1 is common in human cancers including lung cancer, providing a proliferative advantage. Structural analyses revealed a novel mechanism in which Y26 phosphorylation enhances PGAM1 activation by stabilizing active conformation of PGAM1. We were also the first to crystalize H11-phosphorylated PGAM1 and structural analysis suggests that phospho-H11 activates PGAM1 at least in part by promoting substrate 3-PG binding. Thus, Y26 phosphorylation of PGAM1 represents a novel, acute mechanism underlying PGAM1 upregulation in cancer cells in addition to chronic changes regulated by *TP53*.

"So What Section": Our studies suggest that protein expression and enzyme activity levels of PGAM1 are important for lung cancer cell proliferation and tumor growth. Our compound PGMI-004A exhibits promising efficacy in treatment of xenograft nude mice injected with human lung cancer H1299 cells in vivo with minimal toxicity, as well as in diverse human cancer cells and primary leukemia cells from human patients in vitro with no obvious off target effect and minimal toxicity to human cells. These translational studies provide "proof of principle" to suggest anti-PGAM1 as a promising therapy in clinical treatment of lung tumors that in general heavily rely on the Warburg effect.

References

1. **Bond, C. S., M. F. White, and W. N. Hunter.** 2002. Mechanistic implications for Escherichia coli cofactor-dependent phosphoglycerate mutase based on the high-resolution crystal structure of a vanadate complex. J Mol Biol **316:**1071-1081.
2. **Hitosugi, T., J. Fan, T. W. Chung, K. Lythgoe, X. Wang, J. Xie, Q. Ge, T. L. Gu, R. D. Polakiewicz, J. L. Roesel, G. Z. Chen, T. J. Boggon, S. Lonial, H. Fu, F. R. Khuri, S. Kang, and J. Chen.** 2011. Tyrosine phosphorylation of mitochondrial pyruvate dehydrogenase kinase 1 is important for cancer metabolism. Molecular cell **44:**864-877.
3. **Hitosugi, T., S. Kang, M. G. Vander Heiden, T. W. Chung, S. Elf, K. Lythgoe, S. Dong, S. Lonial, X. Wang, G. Z. Chen, J. Xie, T. L. Gu, R. D. Polakiewicz, J. L. Roesel, T. J. Boggon, F. R. Khuri, D. G. Gilliland, L. C. Cantley, J. Kaufman, and J. Chen.** 2009. Tyrosine phosphorylation inhibits PKM2 to promote the Warburg effect and tumor growth. Science signaling **2:**ra73.
4. **Hitosugi, T., L. Zhou, S. Elf, J. Fan, H. B. Kang, J. H. Seo, C. Shan, Q. Dai, L. Zhang, J. Xie, T. L. Gu, P. Jin, M. Aleckovic, G. Leroy, Y. Kang, J. A. Sudderth, R. J. Deberardinis, C. H. Luan, G. Z. Chen, S. Muller, D. M. Shin, T. K. Owonikoko, S. Lonial, M. L. Arellano, H. J. Khoury, F. R. Khuri, B. H. Lee, K. Ye, T. J. Boggon, S. Kang, C. He, and J. Chen.** 2012. Phosphoglycerate mutase 1 coordinates glycolysis and biosynthesis to promote tumor growth. Cancer Cell **22:**585-600.
5. **Hitosugi, T., L. Zhou, J. Fan, S. Elf, L. Zhang, J. Xie, Y. Wang, T. L. Gu, M. Aleckovic, G. LeRoy, Y. Kang, H. B. Kang, J. H. Seo, C. Shan, P. Jin, W. Gong, S. Lonial, M. L. Arellano, H. J. Khoury, G. Z. Chen, D. M. Shin, F. R. Khuri, T. J. Boggon, S. Kang, C. He, and J. Chen.** 2013. Tyr26 phosphorylation of PGAM1 provides a metabolic advantage to tumours by stabilizing the active conformation. Nat Commun **4:**1790.
6. **MacQuarrie, R., and Q. H. Gibson.** 1972. Ligand binding and release of an analogue of 2,3-diphosphoglycerate from human hemoglobin. J Biol Chem **247:**5686-5694.
7. **MacQuarrie, R., and Q. H. Gibson.** 1971. Use of a fluorescent analogue of 2,3-diphosphoglycerate as a probe of human hemoglobin conformation during carbon monoxide binding. J Biol Chem **246:**5832-5835.
8. **Nairn, J., T. Krell, J. R. Coggins, A. R. Pitt, L. A. Fothergill-Gilmore, R. Walter, and N. C. Price.** 1995. The use of mass spectrometry to examine the formation and hydrolysis of the phosphorylated form of phosphoglycerate mutase. FEBS letters **359:**192-194.
9. **Wang, Y., Z. Wei, L. Liu, Z. Cheng, Y. Lin, F. Ji, and W. Gong.** 2005. Crystal structure of human B-type phosphoglycerate mutase bound with citrate. Biochem Biophys Res Commun **331:**1207-1215.

Appendices

We include PDF Reprints of following publications:

1. Hitosugi, T., Zhou, L., Elf, S., Fan, J., Kang, H.-B., Seo, J.H., Shan, C., Dai, Q., Zhang, L., Xie, J., Gu, T.-L., Jin, P., Aleckovic, M., LeRoy, G., Kang, Y., Sudderth, J.A., DeBerardinis R.J., Luan, C., Chen, G.Z., Muller, S.M., Shin, D.M., Owonikoko, T.K., Lonial, S., Arellano, M., Khoury, H.J., Khuri, F.R., Lee, B.H., Ye, K., Boggon, T.J., Kang, S., He, C., and **Chen, J.** (2012) Phosphoglycerate mutase 1 coordinates glycolysis and biosynthesis to promote tumor growth. ***Cancer Cell*** November 13, 2012; 22(5): 585-600. Featured by *Cancer Cell*, *Nature Chemical Biology*, *SciBX*

> **Preview:** PGAMgnam Style: A Glycolytic Switch Controls Biosynthesis
> Barbara Chaneton and Eyal Gottlieb (2012) ***Cancer Cell*** November 13, 2012; 22(5): 565-6

2. Hitosugi, T., Zhou, L., Fan, J., Elf, S., Zhang, L., Xie, J., Wang, Y., Gu, T.-L., Aleckovic, M., LeRoy, G., Kang, Y., Kang, H.-B., Seo, J.H., Shan, C., Jin, P., Gong, W., Lonial, S., Arellano, M., Khoury, H.J., Chen, G.Z., Shin, D.M., Khuri, F.R., Boggon, T.J., Kang, S., He, C., and **Chen, J.** (2013) Y26 phosphorylation of PGAM1 provides a metabolic advantage to tumours by stabilizing the active conformation. ***Nature Communications*** 4, Article number:1790; doi:10.1038/ncomms2759

Cancer Cell
Article

Phosphoglycerate Mutase 1 Coordinates Glycolysis and Biosynthesis to Promote Tumor Growth

Taro Hitosugi,[1,12] Lu Zhou,[4,11,12] Shannon Elf,[1] Jun Fan,[1] Hee-Bum Kang,[1] Jae Ho Seo,[1] Changliang Shan,[1] Qing Dai,[4] Liang Zhang,[4] Jianxin Xie,[5] Ting-Lei Gu,[5] Peng Jin,[2] Masa Alečković,[6] Gary LeRoy,[6] Yibin Kang,[6] Jessica A. Sudderth,[7] Ralph J. DeBerardinis,[7] Chi-Hao Luan,[8] Georgia Z. Chen,[1] Susan Muller,[3] Dong M. Shin,[1] Taofeek K. Owonikoko,[1] Sagar Lonial,[1] Martha L. Arellano,[1] Hanna J. Khoury,[1] Fadlo R. Khuri,[1] Benjamin H. Lee,[9] Keqiang Ye,[3] Titus J. Boggon,[10] Sumin Kang,[1] Chuan He,[4,*] and Jing Chen[1,*]

[1]Department of Hematology and Medical Oncology, Winship Cancer Institute
[2]Department of Human Genetics
[3]Department of Pathology and Laboratory Medicine
Emory University School of Medicine, Atlanta, GA 30322, USA
[4]Department of Chemistry and Institute for Biophysical Dynamics, University of Chicago, Chicago, IL 60637, USA
[5]Cell Signaling Technology, Inc. (CST), Danvers, MA 01923, USA
[6]Department of Molecular Biology, Princeton University, Princeton, NJ 08544, USA
[7]UT Southwestern Medical Center, Dallas, TX 75390, USA
[8]Department of Molecular BioSciences, Northwestern University, Evanston, IL 60208, USA
[9]Novartis Institutes for BioMedical Research, Cambridge, MA 02139, USA
[10]Department of Pharmacology, Yale University School of Medicine, New Haven, CT 06520, USA
[11]Current address: School of Pharmacy, Fudan University, Shanghai 201203, China
[12]These authors contributed equally to this work
*Correspondence: chuanhe@uchicago.edu (C.H.), jchen@emory.edu (J.C.)
http://dx.doi.org/10.1016/j.ccr.2012.09.020

SUMMARY

It is unclear how cancer cells coordinate glycolysis and biosynthesis to support rapidly growing tumors. We found that the glycolytic enzyme phosphoglycerate mutase 1 (PGAM1), commonly upregulated in human cancers due to loss of *TP53*, contributes to biosynthesis regulation in part by controlling intracellular levels of its substrate, 3-phosphoglycerate (3-PG), and product, 2-phosphoglycerate (2-PG). 3-PG binds to and inhibits 6-phosphogluconate dehydrogenase in the oxidative pentose phosphate pathway (PPP), while 2-PG activates 3-phosphoglycerate dehydrogenase to provide feedback control of 3-PG levels. Inhibition of PGAM1 by shRNA or a small molecule inhibitor PGMI-004A results in increased 3-PG and decreased 2-PG levels in cancer cells, leading to significantly decreased glycolysis, PPP flux and biosynthesis, as well as attenuated cell proliferation and tumor growth.

INTRODUCTION

The Warburg effect in cancer cells consists of an increase in aerobic glycolysis and enhanced lactate production, which generates more ATPs more quickly than in normal cells that overwhelmingly rely on oxidative phosphorylation (Kroemer and Pouyssegur, 2008). In addition, tumor tissue traps more glucose than normal tissue does because cancer cells use elevated amounts of glucose as a carbon source for anabolic biosynthesis of macromolecules. These include nucleotides, amino acids, and fatty acids, to produce RNA/DNA, proteins, and lipids, respectively, which are necessary for cell proliferation and to accommodate the rapidly growing tumors (Kroemer and Pouyssegur, 2008). Interestingly, leukemia cells are also highly glycolytic (Elstrom et al., 2004; Gottschalk et al., 2004), despite the fact that such cells reside within the bloodstream at higher oxygen tensions than cells in most normal tissues.

Significance

The current understanding of the Warburg effect consists of an increase in aerobic glycolysis in cancer cells. The connection between glycolysis and PPP/biosynthesis is based on a model in which glycolytic intermediates can be diverted into PPP and biosynthesis pathways as precursors. Our findings demonstrate that PGAM1 regulates the concentrations of glycolytic metabolites 3-PG and 2-PG, which function as signaling molecules to directly affect the catalytic activity of enzymes involved in PPP and biosynthesis, representing an additional link between glycolysis, PPP, and biosynthesis. PGAM1 inhibitor PGMI-004A exhibits promising efficacy and minimal toxicity in treatment of xenograft nude mice and human primary leukemia cells, providing "proof of principle" for the development of PGAM1 inhibitors as anticancer agents.

During glycolysis, glycolytic intermediates including glucose-6-phosphate (G6P) can be diverted into the pentose phosphate pathway (PPP), which contributes to macromolecular biosynthesis by producing reducing potential in the form of reduced nicotinamide adenine dinucleotide phosphate (NADPH) and/or ribose-5-phosphate (R5P), the building blocks for nucleotide synthesis. NADPH is the most crucial metabolite produced by the PPP, because NADPH not only fuels macromolecular biosynthesis such as lipogenesis, but also functions as a crucial antioxidant, quenching the reactive oxygen species (ROS) produced during rapid proliferation of cancer cells. Glycolysis and glutaminolysis supply the carbon input required for the tricarboxylic acid cycle to function as a biosynthetic "hub" and permit the production of other macromolecules including amino acids and fatty acids (Cairns et al., 2011). Thus, cancer cells appear to coordinate glycolysis and anabolism to provide an overall metabolic advantage to cancer cell proliferation and disease development. However, the detailed mechanisms underlying this coordination remain largely unknown.

Phosphoglycerate mutase 1 (PGAM1) catalyzes the conversion of 3-phosphoglycerate (3-PG) to 2-phosphoglycerate (2-PG) during glycolysis. PGAM1 regulates a unique step in glycolysis, and most of the glycolytic intermediates that are used as precursors for anabolic biosynthesis are upstream of this step. In many cancers, including hepatocellular carcinoma and colorectal cancer, PGAM1 activity is increased compared to that in the normal tissues (Liu et al., 2008; Ren et al., 2010). PGAM1 gene expression is believed to be upregulated due to loss of *TP53* in cancer cells because *TP53* negatively regulates PGAM1 gene expression (Corcoran et al., 2006; Tennant et al., 2009, 2010). Here, we study the role of PGAM1 in the coordination of glycolysis and anabolic biosynthesis, as well as the mechanism by which PGAM1 promotes cancer cell proliferation and tumor growth.

RESULTS

PGAM1 Controls Intracellular 3-PG and 2-PG Levels and Is Important for Cancer Cell Glycolysis, Anabolic Biosynthesis, Proliferation, and Tumor Growth

To better understand how cancer cells coordinate glycolysis and anabolic biosynthesis, we examined the effects of targeted downregulation of the glycolytic enzyme PGAM1. Stable knockdown of PGAM1 in lung cancer H1299, breast cancer MDA-MB231, acute myeloid leukemia Molm14, and head and neck cancer 212LN cells resulted in decreased PGAM1 activity (Figure S1 available online). We next performed Global Metabolic Profiling (Metabolon) using cell lysate samples of parental H1299 cells and cells with stable knockdown of PGAM1. The results indicate that PGAM1 knockdown results in altered intracellular concentrations of 118 biochemicals (61 upregulated and 57 downregulated) with $p < 0.05$ using Welch's t-tests. Among these biochemicals, we observed that the PGAM1 substrate 3-PG levels are increased in PGAM1 knockdown compared to control cells (Tables S1 and S2). In consonance with this observation, we found that attenuation of PGAM1 by shRNA in diverse cancer cells leads not only to increased 3-PG (Figure 1A), but also decreased 2-PG (Figure 1B) levels compared to corresponding control cells harboring an empty vector (detailed data are shown in Table S3). The intracellular levels of 3-PG and 2-PG determined using different methods are comparable (Figures S1B and S1C). In addition, stable overexpression of PGAM1 in 3T3 cells results in increased 2-PG and decreased 3-PG levels, compared to control parental 3T3 cells (Figure S1D). These results suggest a crucial role for PGAM1 controlling the metabolite levels of its substrate 3-PG and product 2-PG in cancer cells.

We next examined the role of PGAM1 in cancer cell metabolism. We found that, compared to vector control cells, stable knockdown of PGAM1 results in a decreased glycolytic rate (Figure 1C) and lactate production (Figure 1D), as well as reduced glucose-dependent biosynthesis of RNA and lipids, accompanied by reduced NADPH/$NADP^+$ ratio (Figures 1E–1G, respectively). Because the PPP produces NADPH and R5P to contribute to macromolecular biosynthesis, we next examined whether PGAM1 contributes to PPP flux. Indeed, we found that oxidative PPP flux is reduced in PGAM1 knockdown compared to control vector cells (Figure 1H). Interestingly, attenuation of PGAM1 in cancer cells does not affect glucose uptake rate (Figure S1E), intracellular ATP levels (Figure 1I), or O_2 consumption rate (Figure 1J) in either the presence or absence of ATP synthase inhibitor oligomycin. These results suggest that downregulation of PGAM1 attenuates glycolysis, PPP and biosynthesis, but does not significantly affect glucose uptake or intracellular ATP levels.

In addition, we found that stable knockdown of PGAM1 results in decreased cell proliferation in diverse human cancer and leukemia cells (Figure 1K). Moreover, we performed a xenograft experiment in which nude mice were subcutaneously injected with control H1299 cells harboring an empty vector on the left flank and PGAM1 knockdown H1299 cells on the right flank (Figure 1L, left). The mice were monitored for tumor growth over 6 weeks. The masses of tumors derived from PGAM1 knockdown H1299 cells were significantly reduced compared to those of tumors formed by vector control cells (Figure 1L, right).

PGAM1 Knockdown Results in Elevated Levels of 3-PG, which Binds to and Inhibits 6PGD by Competing with Its Substrate, 6-PG

We next explored the molecular mechanism by which PGAM1 regulates the PPP. Our data suggest that the abnormally high levels of 3-PG in PGAM1 knockdown cells may be accounted for inhibition of oxidative PPP flux (Figure 1). To test this hypothesis, we examined the effect of 3-PG on glucose-6-phosphate dehydrogenase (G6PD), the first and most important enzyme of the oxidative PPP, which produces NADPH, and 6-phosphogluconate dehydrogenase (6PGD), an enzyme that also produces NADPH while converting 6-phosphogluconate into ribulose 5-phosphate in the presence of $NADP^+$. We performed in vitro 6PGD and G6PD assays in the presence of increasing concentrations of 3-PG. Physiologic concentrations of 3-PG in human cells are reported to be approximately 50–80 μM (Feig et al., 1971; Minakami et al., 1964; Mulquiney and Kuchel, 1999). As shown in Table S3, we determined that, in H1299, MDA-MB231, and Molm14 cells, the 3-PG levels are approximately 60–80 μM in control vector cells and 200–300 μM in PGAM1 knockdown cells, while the 3-PG concentrations are approximately 160 μM and 310 μM in 212LN control

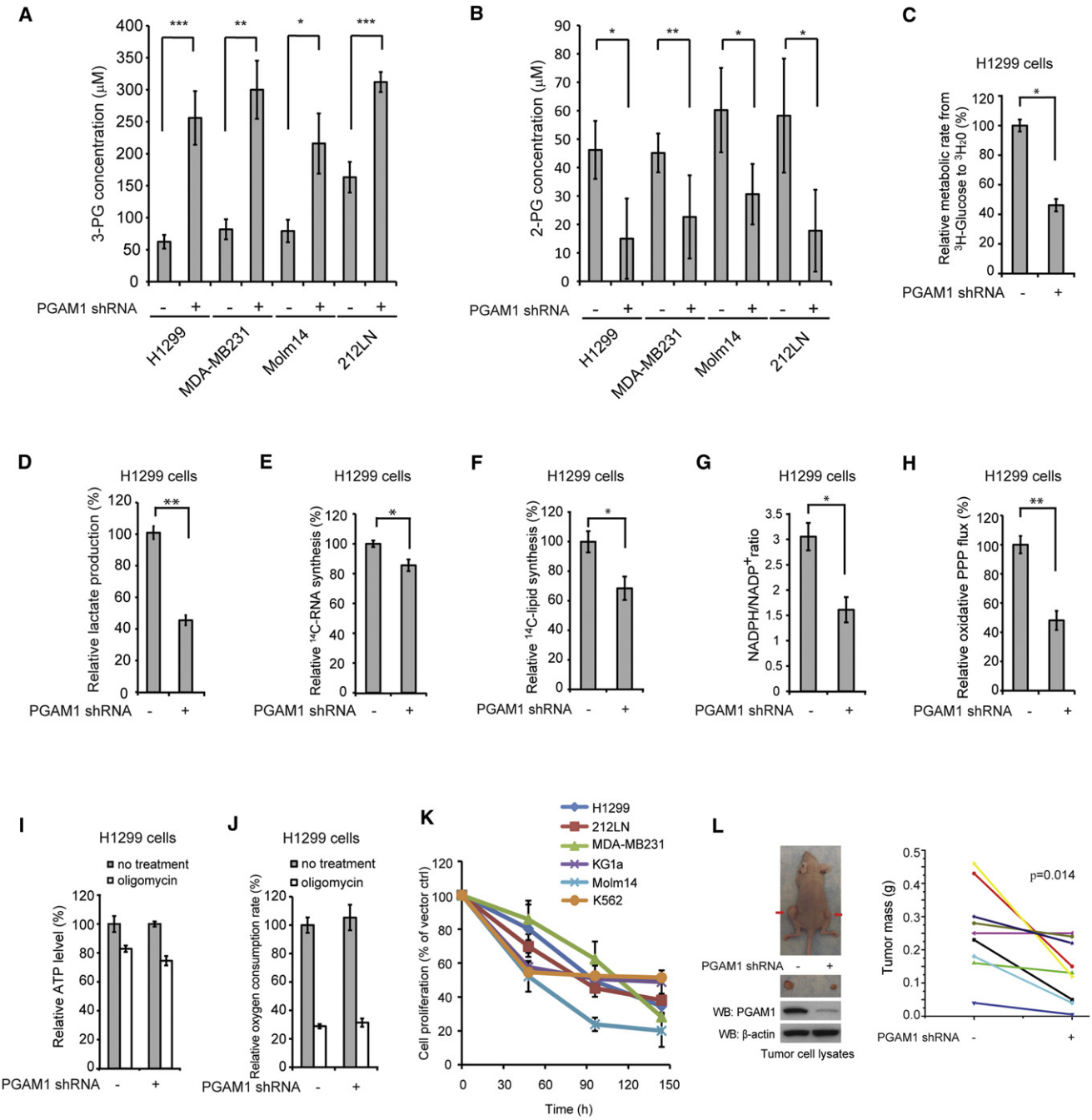

Figure 1. PGAM1 Controls Intracellular 3-PG and 2-PG Levels in Cancer Cells and Is Important for Glycolysis, Anabolic Biosynthesis, Cell Proliferation, and Tumor Growth

(A and B) Intracellular concentrations of 3-PG and 2-PG were determined in diverse PGAM1 knockdown cancer cells and compared to control cells. Detailed concentrations are listed in Table S3.

(C–J) H1299 cells with stable knockdown of PGAM1 and control cells harboring an empty vector were tested for glycolytic rate (C), lactate production (D), RNA biosynthesis (E), lipogenesis (F), NADPH/NADP$^+$ ratio (G), and oxidative PPP flux (H). The intracellular ATP levels (I) and oxygen consumption rate (J) in the presence or absence of 100 nM oligomycin (ATP synthase inhibitor) were also tested.

(K) Cell proliferation rates were determined by cell counting in diverse human cancer (H1299, 212LN, and MDA-MB231) and leukemia (KG1a, Molm14, and K562) cells with stable knockdown of PGAM1, which were normalized to the corresponding control cells harboring an empty vector.

(L) Stable knockdown of PGAM1 by shRNA attenuates tumor growth potential of H1299 cells in xenograft nude mice. Left: Dissected tumors (indicated by red arrows) in a representative nude mouse and expression of PGAM1 in tumor lysates are shown. Right: PGAM1 knockdown cells show significantly reduced tumor formation in xenograft nude mice compared to cells harboring empty vector control (p values were determined by a two-tailed paired Student's t test).

The error bars represent mean values ± SD from three replicates of each sample (*0.01 < p < 0.05; **0.001 < p < 0.01; ***p < 0.001). See also Figure S1 and Tables S1–S3.

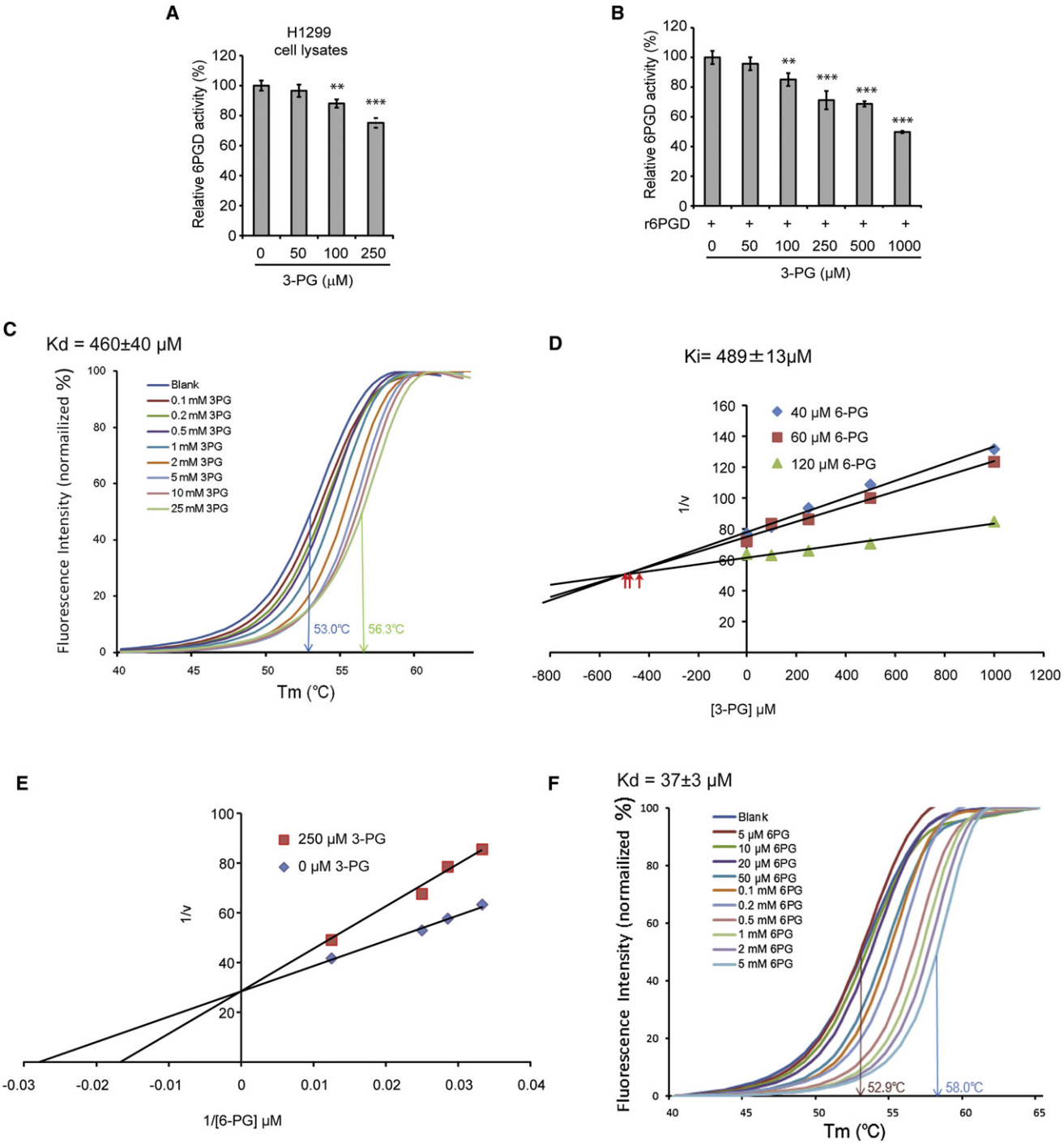

Figure 2. Attenuation of PGAM1 Results in Increased Intracellular Levels of 3-PG, which Binds to and Inhibits 6PGD by Competing with Its Substrate 6-PG

(A and B) Enzyme activity of 6PGD in H1299 cell lysates (A) or recombinant 6PGD (r6PGD) (B) was determined in the presence of increasing concentrations of 3-PG. Relative 6PGD activity was normalized to the control samples without 3-PG treatment. 3-PG levels in control H1299 cells with empty vector and PGAM1 knockdown are 62.5 ± 10.8 μM and 256 ± 41.9 μM, respectively. The error bars represent mean values ± SD from three replicates of each sample (**0.001 < p < 0.01; ***p < 0.001).

(C) Thermal shift melting curves of 6PGD and 3PG. Thermal shift assay was performed to examine the protein (6PGD) and "ligand" (3PG) interaction. Change of melting temperature (Tm) in a dose-dependent manner at concentrations from 100 μM to 25 mM demonstrates that 3-PG directly binds to the protein. Kd for 6PGD-3-PG interaction was determined to be 460 ± 40 μM.

(D) The Dixon plot shows that 3-PG inhibits 6PGD and the dissociation constant (Ki) was determined.

(E) The Lineweaver-Burk plot shows that 3-PG functions as a competitive inhibitor of 6PGD.

and PGAM1 knockdown cells, respectively. Thus, we next examined the effects of increasing concentrations of 3-PG on G6PD and 6PGD enzyme activities according to the aforementioned physiologic 3-PG levels in tumor cells.

We found that treatment with 3-PG concentrations analogous to those in PGAM1 knockdown H1299 cells (~250 μM) results in decreased enzyme activity of 6PGD (Figure 2A) in H1299 cell lysates or recombinant 6PGD (r6PGD) (Figure 2B), whereas the physiologic 3-PG concentrations determined in control H1299 cells (~60 μM) do not significantly affect 6PGD enzyme activity in both experiments. In control experiments, treatment with increasing concentrations of 3-PG did not significantly affect G6PD activity in H1299 cell lysates or rG6PD activity (Figure S2A). In addition, 2-PG did not affect 6PGD enzyme activity in H1299 cell lysates or r6PGD activity (Figure S2B). These results suggest that abnormally high levels of 3-PG, as in PGAM1 knockdown cells, may selectively and directly inhibit 6PGD but not G6PD.

To examine whether 3-PG binds to and inhibits 6PGD, we performed a thermal melt shift assay to examine the interaction of protein (6PGD) and "ligand" (3-PG). Incubation of increasing concentrations of 3-PG raises 6PGD melting temperature (Tm) in a dose-dependent manner, suggesting that 3-PG directly binds to the protein (Figure 2C). The Kd value for protein-"ligand" interaction was calculated to be 460 ± 40 μM. Moreover, we performed kinetics studies on the inhibition of 6PGD by 3-PG. As shown in Figure 2D, the Dixon plot indicates that 3-PG binds and inhibits 6PGD. The inhibition constant (Ki) was determined to be 489 ± 13 μM, in agreement with the Kd determined.

We next determined the intracellular concentration of 6-PG in H1299, MDA-MB231, and 212LN cells to be 34.9 ± 2.1 μM, 37.6 ± 0.7 μM, and 24.9 ± 0.4 μM, respectively. We performed additional enzyme kinetics assays to test whether 3-PG at a concentration analogous to that in PGAM1 knockdown H1299 cells (~250 μM) functions as a competitive or noncompetitive inhibitor of 6PGD in the presence of physiologic concentrations of 6-PG (~35 μM). As shown in Figure 2E, the Lineweaver-Burk plot demonstrates that 3-PG functions as a competitive inhibitor of 6PGD. Because the Kd value for protein (6PGD)-ligand (6-PG) interaction was calculated to be 37 ± 3 μM in a thermal melt shift assay (Figure 2F), these combined data suggest that at physiologic concentrations, 3-PG (~60–80 μM) cannot effectively compete with 6-PG (~35 μM) to inhibit 6PGD in cancer cells; however, upon attenuation of PGAM1, elevated cellular 3-PG levels (~250–300 μM) result in reduced 6PGD enzyme activity.

To further understand the structural properties of 3-PG-mediated inhibition of 6PGD, we crystallized the apo-form of 6PGD (1.39 Å), which was also soaked with 3-PG to obtain the 3-PG-bound form of 6PGD (1.53 Å) (Table S4). The Fo-Fc density analysis revealed that the electron density of 3-PG was located in the active site of the 3-PG-bound 6PGD structure (Figure 3A) but not in the apo-6PGD structure (Figure 3B). 3-PG interacts with several residues (Y191, T262, R287, R446) in the active site of 6PGD that are important for substrate binding and enzymatic activity of 6PGD (Li et al., 2006) (Figure 3A). Different conformations were observed for Arg 446 and His 452 in the 3-PG-bound 6PGD structure compared to the apo-form 6PGD structure (Figure 3C). An alignment of three different 6PGD structures with bound NADP, 6-PG, and 3-PG shows an overlap of 3-PG and 6-PG in the active site (Figure 3D). Together, these results demonstrate that 3-PG directly binds to 6PGD and inhibits 6PGD enzyme activity by competing with the cognate substrate 6-PG, representing a molecular mechanism to explain how PGAM1, as a glycolytic enzyme, contributes to the regulation of the oxidative PPP and consequently anabolic biosynthesis.

Rescue of Reduced 2-PG Levels in PGAM1 Knockdown Cells Results in Decreased 3-PG Levels by Activating 3-PG Dehydrogenase

To examine the effect of decreased 2-PG levels on cancer cell metabolism, we treated the aforementioned PGAM1 knockdown cancer cells with a cell permeable agent, methyl-2-PG, which converts to 2-PG in cells. We verified that in diverse PGAM1 knockdown cancer cells, treatment with methyl-2-PG results in increased 2-PG cellular levels comparable to those in the corresponding control vector cells (Figure 4A). We also observed that methyl-2-PG treatment rescues the reduced lactate production (Figure 4B) but has no significant effect on intracellular ATP levels (Figure S3A) in H1299 cells with stable knockdown of PGAM1 compared to control vector cells. This result suggests that rescuing cellular 2-PG levels reverses the inhibitory effect of PGAM1 knockdown on glycolysis and allows downstream glycolytic reactions to resume and ultimately produce lactate. However, such rescued glycolytic activity does not affect ATP levels, which is consistent with our previous observation (Figures 1I and 1J).

Surprisingly, we also found that methyl-2-PG treatment rescues the decreased oxidative PPP flux and biosynthesis of RNA and lipids, as well as partially restores the reduced cell proliferation in H1299 PGAM1 knockdown cancer cells compared to the corresponding control vector cells (Figures 4C–4F). Similar results were obtained using MDA-MB231 vector and PGAM1 knockdown cells (Figures S3B–S3E). These data suggest that the increased 2-PG levels in PGAM1 knockdown cells provide a feedback mechanism to rescue the abrogated PPP and anabolic biosynthesis upstream of PGAM1.

We tested this hypothesis by examining the effect of rescued 2-PG levels on 3-PG concentrations in PGAM1 knockdown cells. We found that treatment with methyl-2-PG results in decreased 3-PG concentrations in diverse PGAM1 knockdown cells to levels that are comparable to the 3-PG concentrations in the corresponding control vector cells (Figure 5A). These results further suggest that PGAM1 controls 2-PG levels in cancer cells, which contributes to PGAM1-dependent coordination of glycolysis and anabolic biosynthesis by adjusting 3-PG levels.

We next determined the molecular mechanism underlying 2-PG-dependent feedback regulation of intracellular 3-PG levels.

(F) Thermal shift melting curves of 6PGD and 6PG. Thermal shift assay was performed to examine the protein (6PGD) and ligand (6PG) interaction. Change of melting temperature (Tm) in a dose-dependent manner at concentrations from 5 μM to 5 mM demonstrates that 6-PG directly binds to the protein. Kd for 6PGD-6PG interaction was determined to be 37 ± 3 μM.
See also Figure S2.

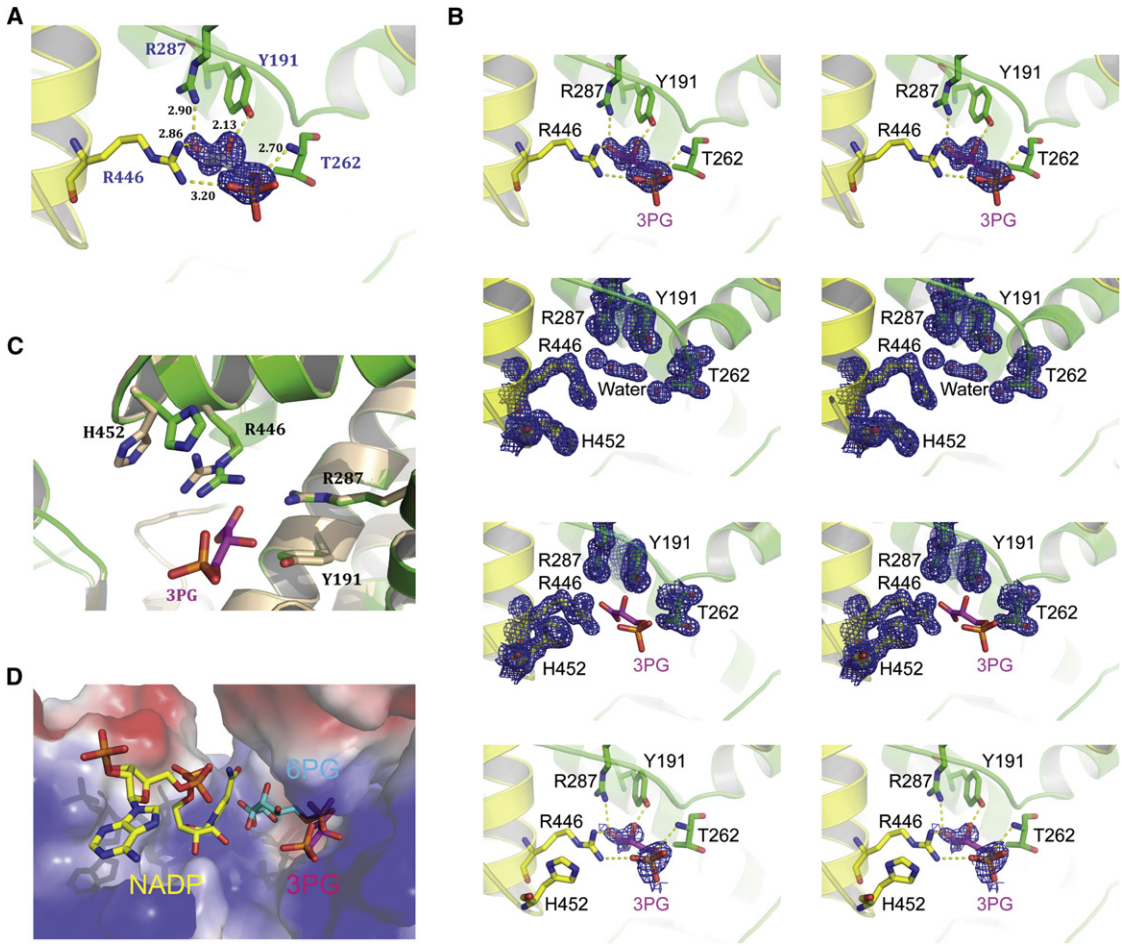

Figure 3. Co-Crystallization Analysis of 3-PG-Mediated Inhibition of 6PGD

(A) Stereo view of the Fo-Fc electron density map contoured at 3.0 σ around 3-PG. The Fo-Fc density map is shown as blue mesh. Residues of 6PGD interact with 3-PG are shown in stick.

(B) Upper top: Stereo view of the unbiased Fo-Fc electron density map contoured at 3.0 σ around 3PG. The Fo-Fc density map is shown as blue mesh. Residues interacting with 3-PG are shown in stick. Lower top: Stereo view of the 2Fo-Fc electron density map of 6PGD apo-form contoured at 1.2 σ at 3-PG binding pocket in the same orientation as in Figure 3A. The 2Fo-Fc density map is shown as blue mesh. Upper bottom: Stereo view of the 2Fo-Fc electron density map of 6PGD-3-PG complex contoured at 1.2 σ at 3-PG binding pocket in the same orientation as in Figure 3A. The 2Fo-Fc density map is shown as blue mesh. Lower bottom: Stereo view of simulated-annealing omit map contoured at 0.8 σ around 3-PG. The omit density map is shown as blue mesh.

(C) Structure comparison of the 6PGD apo-form (wheat) and the 6PGD-3-PG complex (green). Arg 446 and His 452 in the 6PGD-3-PG complex structure show different conformation.

(D) Surface electrostatic potential of the substrate binding pocket of 6PGD. The bound 3-PG (pink) competes with 6-PG (blue) but not NADP (yellow) in the active site. The model was built by aligning structures of 6PGD-NADP (PDB number: 2JKV), 6PGD-6-PG (PDB number: 3FWN), and 6PGD-3PG.

See also Table S4.

Besides conversion to 2-PG catalyzed by PGAM1 in glycolysis, 3-PG also serves as a precursor for serine synthesis and can be converted to 3-phosphohydroxypyruvate (pPYR) by 3-PG dehydrogenase (PHGDH). Because PGAM1 activity is attenuated in PGAM1 knockdown cells, it is possible that the rescued cellular 2-PG levels by methyl-2-PG treatment decreases 3-PG levels by activating PHGDH. We tested this hypothesis by examining the effect of 2-PG on PHGDH activity and we used PGAM1 knockdown cells to exclude the endogenous PGAM1 effect on 3-PG and 2-PG in the PHGDH enzyme activity reactions. Indeed, we found that treatment with 2-PG concentrations equivalent to those determined in control H1299 cells (~45 μM) or methyl-2-PG treated PGAM1 knockdown cells (~60 μM) results in higher PHGDH enzyme activity in H1299 PGAM1 knockdown cell lysates (Figure 5B, left). Similar results were obtained by treating 212LN PGAM1 knockdown cell lysates with increasing concentrations of 2-PG (Figure 5B, right). Moreover, treatment with increasing concentrations of 2-PG results in increased enzyme activity of recombinant PHGDH (rPHGDH) (Figure 5C). In contrast, 2-PG concentrations that correspond to those determined in PGAM1 knockdown cells (~15 μM) did not significantly affect PHGDH activity. Together, these studies reveal a feedback mechanism by which cellular 2-PG levels contribute to control of 3-PG levels in cells through regulation of PHGDH.

In addition, we found that stable knockdown of PGAM1 results in significantly decreased serine biosynthesis, while treatment

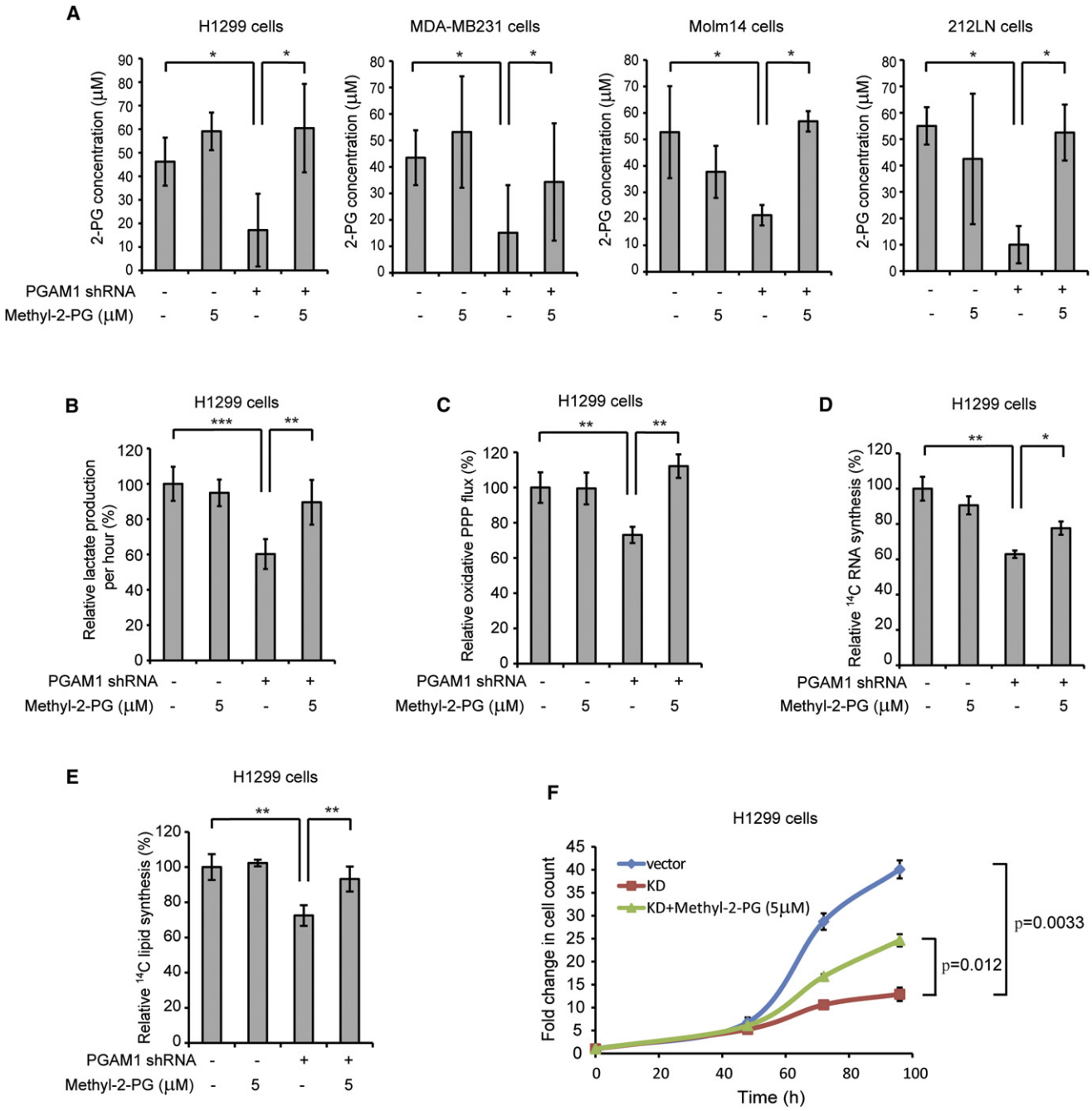

Figure 4. Rescue of Reduced 2-PG Levels in PGAM1 Knockdown Cells Reverses the Phenotypes due to Attenuation of PGAM1

(A) 2-PG levels in diverse cancer cells with stable knockdown of PGAM1 were determined in the presence and absence of cell-permeable methyl-2-PG.

(B–F) H1299 cells with stable knockdown of PGAM1 were tested for lactate production (B), oxidative PPP flux (C), biosynthesis of RNA (D) and lipids (E), and proliferation (F) in the presence and absence of methyl-2-PG.

The error bars represent mean values ± SD from three replicates of each sample (*0.01 < p < 0.05; **0.001 < p < 0.01; ***p < 0.001). See also Figure S3.

with methyl-2-PG rescues the phenotype (Figure 5D). Moreover, shRNA-mediated knockdown of PHGDH (Figure 5E) does not affect rescued 2-PG levels in PGAM1 knockdown cells upon treatment with methyl-2-PG, while PHGDH knockdown abolishes the methyl-2-PG-dependent decrease of the elevated 3-PG levels in H1299 PGAM1 knockdown cells (Figure 5F; left and right, respectively). These data support our hypothesis that PGAM1 controls 2-PG levels to regulate PHGDH, which consequently regulates 3-PG levels by diverting 3-PG in serine biosynthesis. Furthermore, knockdown of PHGDH in PGAM1 stable knockdown cells reverses the methyl-2-PG treatment dependent rescue of oxidative PPP flux as well as biosynthesis

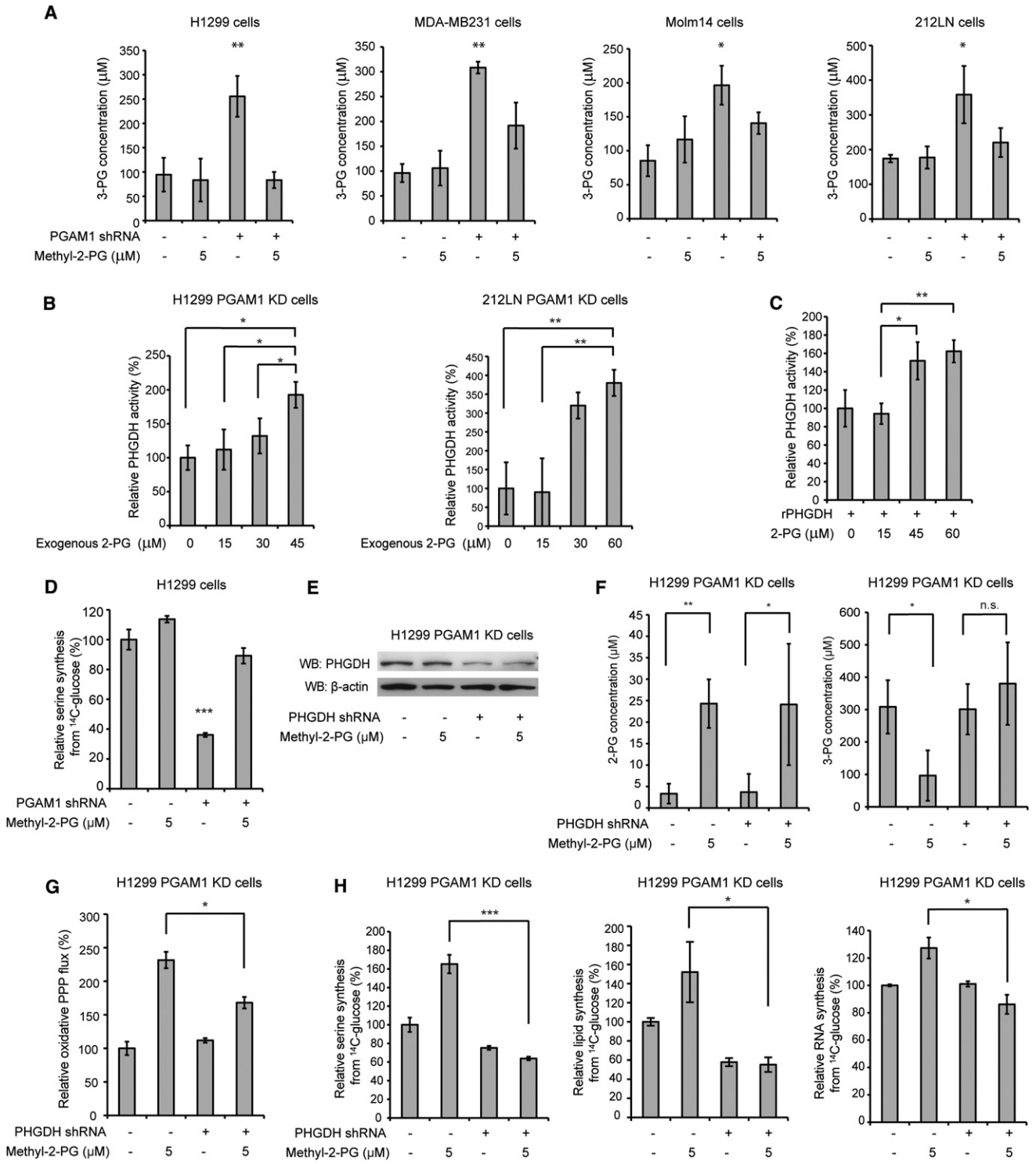

Figure 5. Rescue of Reduced 2-PG Levels due to PGAM1 Attenuation Results in Decreased 3-PG Levels by Activating PHGDH

(A) 3-PG levels in diverse cancer cells with stable knockdown of PGAM1 were determined in the presence and absence of methyl-2-PG.

(B and C) Enzyme activity of PHGDH in PGAM1 knockdown H1299 (B; left) or 212LN (B; right) cell lysates and recombinant PHGDH (rPHGDH) (C) were determined in the presence of increasing concentrations of 2-PG. Relative enzyme activity was normalized to the control samples without 2-PG treatment. 2-PG levels in control H1299 cells with empty vector and PGAM1 knockdown cells are 46.2 ± 10.2 μM and 15.0 ± 14.1 μM, respectively, while 2-PG levels in 212LN cells with empty vector and stable knockdown of PGAM1 are 58.3 ± 20.1 μM and 17.8 ± 14.4 μM, respectively.

(D) Serine biosynthesis rate of H1299 cells with stable knockdown of PGAM1 was determined by measuring ^{14}C incorporation into serine from ^{14}C-glucose in the presence and absence of methyl-2-PG. Relative serine biosynthesis was normalized to control cells harboring an empty vector without methyl-2-PG treatment.

of serine, lipids, and RNA (Figures 5G and 5H, respectively). These data together suggest that, besides being a glycolytic metabolite, 2-PG may also signal through PHGDH to provide regulation of PPP flux and anabolic biosynthesis, at least in part by regulating 3-PG levels.

PGAM1 Enzyme Activity Strikes a Balance between 3-PG and 2-PG Levels, which Coordinates Glycolysis and Biosynthesis to Promote Cancer Cell Proliferation

To study the role of PGAM1 enzyme activity in cancer metabolism and tumor development, we screened and developed a small molecule inhibitor of PGAM1. Currently the only reported PGAM1 inhibitor is MJE3, which specifically inhibits PGAM1 activity exclusively in intact cells, probably by targeting the active site of PGAM1 with certain modifications in vivo (Evans et al., 2005, 2007). We designed a screening strategy using coupled PGAM1 and enolase assays and identified three lead small molecule compounds, including alizarin, as PGAM1 inhibitors from a library of 2,000 US Food and Drug Adminstration-approved small molecule compounds (Figures 6A, S4A, and S4B). We focused on 1,2-dihydroxyanthraquinone, a.k.a. alizarin ($C_{14}H_8O_4$) (Figure 6B, top), which is an organic compound that is historically important as a prominent dye, originally derived from the roots of plants of the *Madder* genus. Treatment with alizarin results in decreased proliferation of human leukemia KG1a cells in a dose-dependent manner (Figures S4C and S4D).

We next identified Alizarin Red S (Figure 6B, middle) as a more potent PGAM1 inhibitor from a group of alizarin derivatives (Figures S4E and S4F). We designed a group of Alizarin Red S derivatives by adding hydrophobic groups through a sulfonamide bond (Figure S5A). Among these compounds, we focused on PGAM1 inhibitor 004A (PGMI-004A) (Figure 6B, bottom), which, although less potent than Red S in vitro, demonstrates enhanced potency to inhibit PGAM1 in leukemia KG1a cells compared to its parental compounds (Figures S5B and S5C). This may be due to the fact that PGMI-004A is more hydrophobic than alizarin and alizarin red S, which confers better cell permeability.

PGMI-004A inhibits PGAM1 with an IC_{50} of ~13.1 μM (Figure 6C) and the Kd value of the PGMI-004A-PGAM1 interaction was determined to be 7.2 ± 0.7 μM from fluorescence-based binding assay (Figure 6D). In a competitive binding assay where PGMI-004A was incubated with recombinant PGAM1 proteins in the presence of different concentrations of PGAM1 substrate 3-PG, we found that increasing concentrations of 3-PG caused an increase in the fluorescence intensity from PGMI-004A-unbound form of PGAM1 in the presence of different concentrations of PGMI-004A, but not in the absence of PGMI-004A (Figure 6E). This suggests that PGMI-004A may allosterically modulate the enzyme activity of PGAM1. The Ki value was determined to be 3.91 ± 2.50 μM using Dixon plot analysis (Figure 6F). In addition, we performed a thermal melt shift assay to examine the interaction of protein (PGAM1) and ligand (PGMI-004A). Incubation of increasing concentrations of PGMI-004A raises PGAM1 melting temperature (Tm) in a dose-dependent manner, suggesting that PGMI-004A directly binds to the protein (Figure 6G). The Kd value for protein-ligand interaction was calculated to be 9.4 ± 2.0 μM. Together, these results suggest that PGMI-004A directly binds to PGAM1 and inhibits its enzyme activity.

We found that inhibition of PGAM1 activity by PGMI-004A treatment results in decreased 2-PG and increased 3-PG levels in H1299 cells, which could be rescued by treatment with methyl-2-PG (Figure 7A). Moreover, treatment with PGMI-004A results in significantly reduced lactate production that was rescued by methyl-2-PG treatment (Figure 7B), but has no significant effect on intracellular ATP levels (Figure 7C). In consonance with these observations, the rescued lactate production due to methyl-2-PG treatment was abolished when enolase was knocked down or inhibited by specific inhibitor NaF in PGMI-004A treated cells (Figure S5D). These results also suggest that rescued 2-PG derived from methyl-2-PG is metabolized by cells to restore the decreased glycolysis due to PGAM1 inhibition in cancer cells. We also found that PGMI-004A treatment results in decreased oxidative PPP flux (Figure 7D) and NADPH/$NADP^+$ ratio (Figure 7E), as well as reduced biosynthesis of lipids and RNA (Figures 7F and 7G, respectively) and cell proliferation (Figure 7H) in H1299 cells. These phenotypes are similar to those observed in PGAM1 knockdown cells, which could be significantly rescued by treatment with methyl-2-PG, suggesting that PGMI-004A targets PGAM1 to inhibit cancer cell metabolism and proliferation.

In addition, we observed that PGMI-004A treatment results in decreased cell proliferation of diverse human cancer and leukemia cells (Figures 7I and 7J and S5E–S5H), but not control human dermal fibroblasts (HDF), human foreskin fibroblasts (HFF), human HaCaT keratinocyte cells and human melanocyte PIG1 cells (Figures 7K and S5I), suggesting minimal non-specific toxicity of PGMI-004A in normal, proliferating human cells.

Targeting PGAM1 by PGMI-004A Treatment Inhibits Cancer Cell Proliferation and Tumor Growth and Alters 3-PG and 2-PG Levels in Primary Leukemia Cells from Patients, Leading to Attenuated Leukemia Cell Proliferation

We next performed an in vivo drug treatment experiment. Initial toxicity studies by chronic injection of PGMI-004A to nude mice for 4 weeks revealed that 100 mg/kg/day administered intraperitoneally is a well-tolerated dose. In addition, continuous treatment with PGMI-004A (100 mg/kg/day) for 7 days did not result in significant alteration in body weight, complete blood cell counts, or hematopoietic properties of nude mice (Table S5). Histopathologic analyses revealed that no notable differences between the vehicle-treated and PGMI-004A-treated groups were evident (Figures S6A–S6D). We performed

(E) Western blot result shows shRNA-mediated knockdown of PHGDH in H1299 cells with stable knockdown of PGAM1 in the presence or absence of methyl-2-PG treatment.

(F) 2-PG (left) and 3-PG (right) levels in PGAM1 knockdown cells upon PHGDH knockdown were determined in the presence and absence of methyl-2-PG.

(G and H) PGAM1 stable knockdown cells treated with or without shRNA targeting PHGDH were tested for PPP flux (G) as well as biosynthesis of serine, lipids and RNA (H; left, middle, and right, respectively) in the presence and absence of methyl-2-PG.

The error bars represent mean values ± SD from three replicates of each sample (*0.01 < p < 0.05; **0.001 < p < 0.01; ***p < 0.001; n.s., not significant).

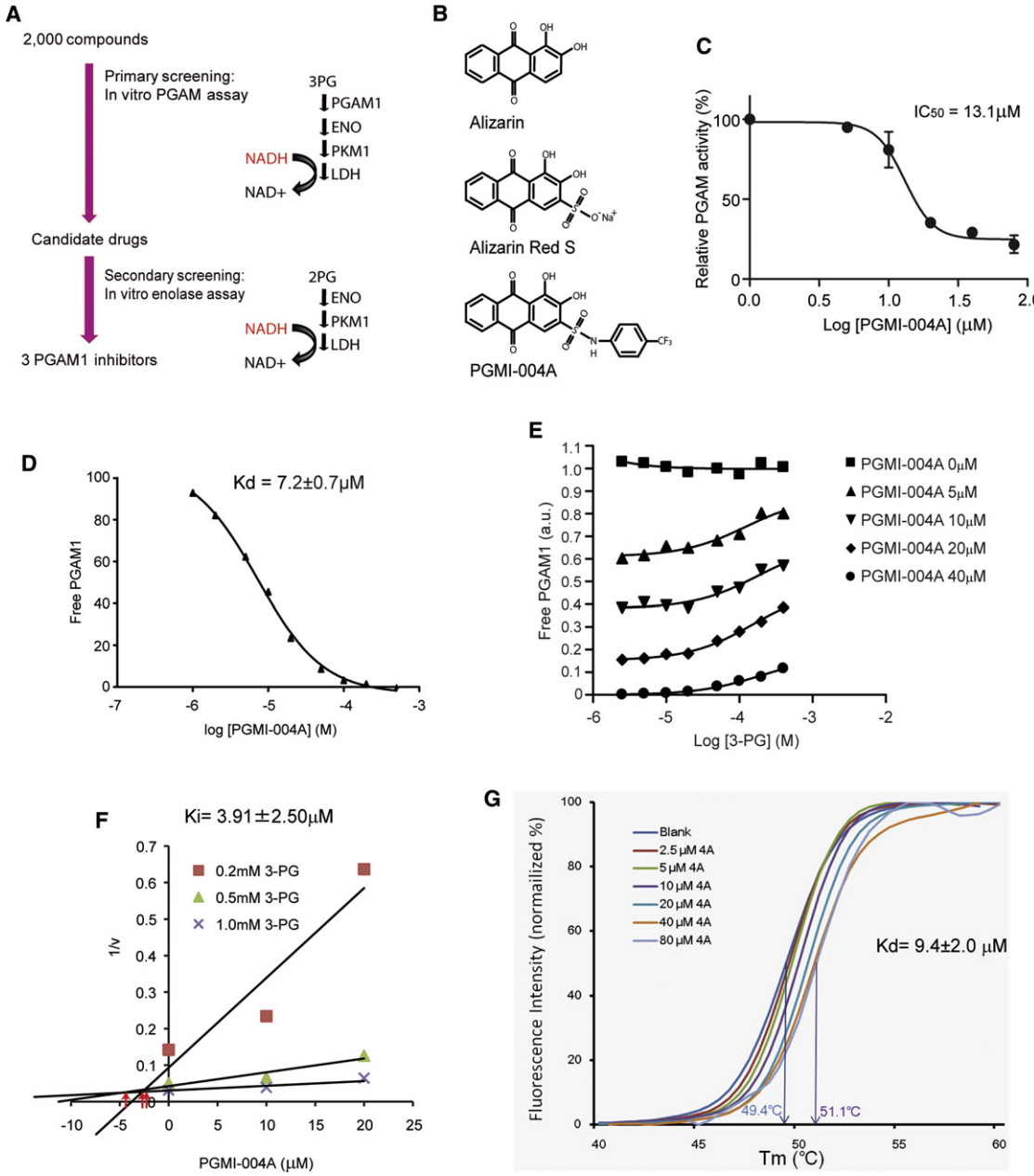

Figure 6. Identification and Characterization of a Small Molecule PGAM1 Inhibitor, PGMI-004A

(A) Schematic representation of the primary and secondary screening strategies to identify lead compounds as PGAM1 inhibitors.

(B) Structure of alizarin and its derivatives alizarin red S and PGAM1 inhibitor (PGMI)-004A.

(C) PGMI-004A inhibits PGAM1 with an IC_{50} of 13.1 μM, which was determined by incubating purified human PGAM1 proteins with increasing concentrations of PGMI-004A. The error bars represent mean values ± SD from three replicates of each sample.

(D) Kd value was determined as 7.2 ± 0.7 μM by incubating purified human PGAM1 proteins with increasing concentrations of PGMI-004A. The fluorescence intensity (Ex: 280 nm, Em: 350 nm) from tryptophan was measured (Schauerte and Gafni, 1989).

(E) Competitive binding assay of PGMI-004A with recombinant PGAM1 protein in the presence of increasing concentrations of PGAM1 substrate 3-PG. Increased free PGAM1 was determined by an increase in fluorescence intensity.

(F) Dixon plot analysis of PGAM1 enzyme assay in the presence of different concentrations of PGMI-004A and 3-PG. The reaction velocity (v) was determined by the rate of the decrease in fluorescence (ex: 340 nm, em: 460 nm) by NADH oxidation. Ki was determined to be 3.91 ± 2.50 μM.

(G) Thermal shift melting curves of PGAM1 and PGMI-004A. Thermal shift assay was performed to examine the protein (PGAM1) and "ligand" (inhibitor PGMI-004A) interaction. Change of melting temperature (Tm) in a dose-dependent manner at concentrations from 2.5 μM to 80 μM demonstrates that PGMI-004A directly binds to the protein. Kd for PGAM1-PGMI-004A interaction was determined to be 9.4 ± 2.0 μM.

See also Figure S4.

xenograft experiments by injecting H1299 cells into nude mice as described (Hitosugi et al., 2009). Six days postinjection, mice were divided into two groups (n = 8/group) and treated with either PGMI-004A (100 mg/kg/day) or vehicle for 21 days. We found that PGMI-004A treatment results in significantly decreased tumor growth and size in treated mice compared with mice receiving vehicle control (Figures 8A and 8B, respectively; Figures S6E and S6F). Moreover, treatment with PGMI-004A effectively inhibits PGAM1 enzyme activity in tumors in vivo in resected tumors from xenograft nude mice (Figure S6G). These combined data suggest that targeting PGAM1 by PGMI-004A inhibits PGAM1 in vivo, and that this inhibition causes specific toxicity to tumor cells.

We found that PGAM1 protein expression and enzyme activity levels are commonly upregulated in primary leukemia cells from diverse patients with acute myeloid leukemia (AML), chronic myelogenous leukemia (CML), or acute B lymphoblastic leukemia (B-ALL; n = 12), compared to control peripheral blood cells from healthy donors (n = 4) (Figure 8C). We next found that, consistent with our observations in cancer cell lines, inhibiting PGAM1 by PGMI-004A treatment results in increased 3-PG and decreased 2-PG levels in primary leukemia cells from a representative patient with AML (Figure 8D). PGMI-004A treatment also results in decreased cell viability and reduced PGAM1 activity and lactate production in the samples from seven (one CML and six AML) out of eight patients with leukemia. Figures 8E, S6H, and S6I show results using samples from patients with CML or AML as representatives, respectively. Moreover, methyl-2-PG treatment rescues the decreased cell viability (Figures 8F and 8G, left) and lactate production (Figure 8G, right) in primary leukemia cells from representative patients with AML. In addition, PGMI-004A treatment did not affect cell viability of mononucleocytes in peripheral blood samples from two healthy human donors (Figures 8H and S6J) and CD34+ cells isolated from bone marrow samples from four healthy donors (Figures 8I and S6K), suggesting promising anticancer potential of PGMI-004A with minimal toxicity to human blood cells. These combined results of translational studies suggest that PGAM1 is a promising therapeutic target in the treatment of human malignancies.

DISCUSSION

Our findings suggest that upregulation of PGAM1 by increased gene expression in cancer cells provides a metabolic advantage to cancer cell proliferation and tumor growth; PGAM1 coordinates glycolysis and anabolic biosynthesis, at least in part by controlling intracellular levels of its substrate 3-PG and product 2-PG (Figure 8J). Our results revealed a molecular mechanism by which 3-PG inhibits 6PGD by directly binding to the active site of 6PGD and competing with its substrate 6-PG. Attenuation of PGAM1 results in abnormal accumulation of 3-PG, which in turn inhibits 6PGD and consequently the oxidative PPP and anabolic biosynthesis. Moreover, our findings suggest that PGAM1 controls the intracellular levels of its substrate 3-PG not only directly through substrate consumption, but also indirectly by controlling levels of its product 2-PG. Physiologic concentrations of 2-PG promote the enzyme activity of PHGDH, which converts 3-PG to pPYR, reducing the cellular 3-PG levels. Upon attenuation of PGAM1, 2-PG is decreased to levels below the physiologic concentrations, leading to decreased PHGDH activity, which facilitates 3-PG accumulation. This represents a regulatory mechanism by which 2-PG activates PHGDH to provide feedback control of 3-PG levels. Thus, we suggest that PGAM1 activity is upregulated in cancer cells to promote glycolysis and keep the intracellular 3-PG levels low, which in turn permits high levels of the PPP and biosynthesis to fulfill the request of rapidly growing tumors. This is consistent with previous report that expression of TP53 suppresses oxidative PPP in cancer cells (Jiang et al., 2011). In addition, PGAM1 may also be responsible for maintaining the physiological levels of 2-PG to sustain PHGDH activity, which diverts 3-PG from glycolysis to serine synthesis and contributes to maintaining relatively low levels of 3-PG in cancer cells.

Inhibition of PGAM1 by shRNA or treatment with a small molecule inhibitor PGMI-004A results in altered glycolysis and anabolic biosynthesis, and reduced cancer cell proliferation and tumor growth. Interestingly, targeting PGAM1 does not significantly affect intracellular ATP levels. Decreased ATP production due to attenuated glycolysis in PGAM1 knockdown cells may be compensated by alternative mechanisms other than mitochondrial oxidative phosphorylation, or perhaps the ATP consumption in PGAM1 knockdown cells is decreased accordingly. Methyl-2-PG treatment rescues most of the aforementioned phenotypes. Rescued 2-PG levels in cells with attenuated PGAM1 reversed decreased lactate production by rescuing the glycolytic process downstream of PGAM1, as well as reduced oxidative PPP flux and biosynthesis of RNA and lipids, at least in part by decreasing elevated 3-PG levels. However, methyl-2-PG treatment only partially rescues the attenuated cell proliferation in PGAM1 knockdown cells or cells treated with PGMI-004A. This result suggests that PGAM1 may contribute to cell proliferation in both 2-PG-dependent and -independent manners.

The current understanding of the connection between glycolysis and PPP/biosynthesis is based on a model in which glycolytic intermediates can be diverted into PPP and biosynthesis pathways as precursors. Our results show that the concentrations of glycolytic metabolites such as 3-PG and 2-PG can directly affect the catalytic activity of enzymes involved in PPP and biosynthesis, which represents an additional link between glycolysis, PPP, and biosynthesis. Metabolites have been suggested to function as signaling molecules in the past. Examples include AMP, which is an allosteric activator for AMP-activated protein kinase (AMPK), a kinase that senses intracellular energy levels (ATP/AMP ratio) (Shackelford and Shaw, 2009), and glutamine, which activates leucine uptake, leading to mTOR activation (Nicklin et al., 2009). We found that the cellular levels of 3-PG and 2-PG, two key intermediates in glycolysis, have additional regulatory impact on metabolic enzymes to affect cell metabolism and consequently proliferation, which provides an example to suggest that glycolytic metabolites could also serve as signaling molecules to control cell metabolism and cellular responses. Moreover, our findings also describe a feedback mechanism by which the product levels (2-PG) of a metabolic enzyme (PGAM1) can regulate its substrate levels (3-PG) by affecting an alternative enzyme (PHGDH) that is involved in production of this substrate. Thus, this study showcases the

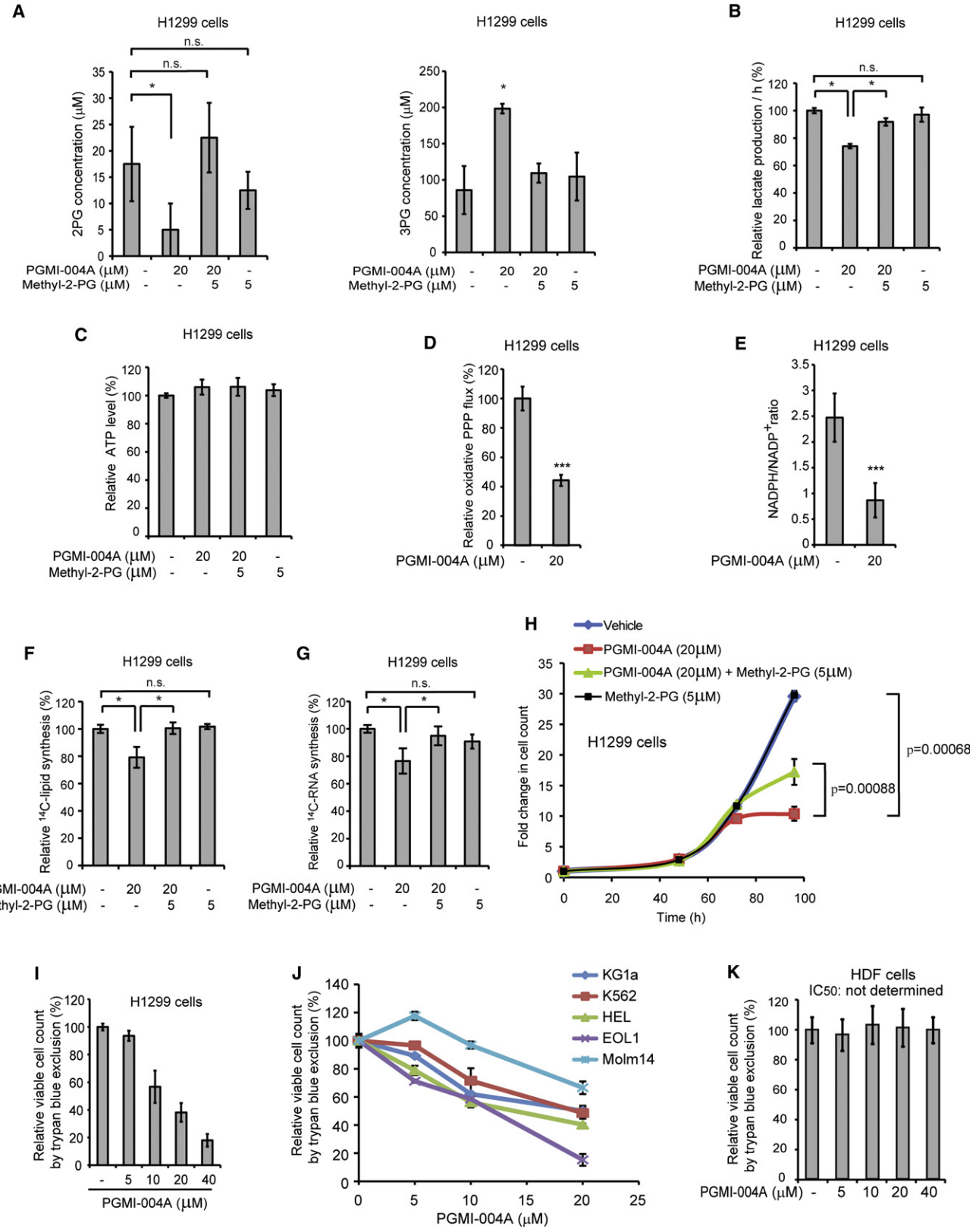
A
H1299 cells
2PG concentration (μM)
n.s.
n.s.
*
PGMI-004A (μM) - 20 20 -
Methyl-2-PG (μM) - - 5 5
H1299 cells
3PG concentration (μM)
*
PGMI-004A (μM) - 20 20 -
Methyl-2-PG (μM) - - 5 5
B
H1299 cells
Relative lactate production / h (%)
n.s.
* *
PGMI-004A (μM) - 20 20 -
Methyl-2-PG (μM) - - 5 5
C
H1299 cells
Relative ATP level (%)
PGMI-004A (μM) - 20 20 -
Methyl-2-PG (μM) - - 5 5
D
H1299 cells
Relative oxidative PPP flux (%)
***
PGMI-004A (μM) - 20
E
H1299 cells
NADPH/NADP+ratio
***
PGMI-004A (μM) - 20
F
H1299 cells
Relative 14C-lipid synthesis (%)
n.s.
* *
PGMI-004A (μM) - 20 20 -
Methyl-2-PG (μM) - - 5 5
G
H1299 cells
Relative 14C-RNA synthesis (%)
n.s.
* *
PGMI-004A (μM) - 20 20 -
Methyl-2-PG (μM) - - 5 5
H
Vehicle
PGMI-004A (20μM)
PGMI-004A (20μM) + Methyl-2-PG (5μM)
Methyl-2-PG (5μM)
H1299 cells
Fold change in cell count
p=0.00068
p=0.00088
Time (h)
I
H1299 cells
Relative viable cell count by trypan blue exclusion (%)
PGMI-004A (μM)
J
KG1a
K562
HEL
EOL1
Molm14
Relative viable cell count by trypan blue exclusion (%)
PGMI-004A (μM)
K
HDF cells
IC50: not determined
Relative viable cell count by trypan blue exclusion (%)
PGMI-004A (μM) - 5 10 20 40

complexity of cellular metabolism, demonstrating that control of the intracellular levels of a particular metabolite may involve diverse enzymes in different metabolic reactions, such that the balance of the intracellular levels of various metabolites may exert regulatory functions on enzymes in different pathways to control cellular metabolism. Such a mechanism can be explored for anticancer therapies.

Previous reports describe that targeting PGAM1 by a PGAM1-derived inhibitory peptide or PGAM inhibitor MJE3 attenuates cancer cell proliferation (Engel et al., 2004; Evans et al., 2005). In consonance with these observations, our studies suggest that protein expression and enzyme activity levels of PGAM1 are important for cancer cell proliferation and tumor growth. Our compound PGMI-004A exhibits promising efficacy in the treatment of xenograft nude mice in vivo with minimal toxicity, as well as in diverse human cancer cells and primary leukemia cells from human patients in vitro with no obvious off-target effect and minimal toxicity to human cells. These translational studies provide "proof of principle" to suggest anti-PGAM1 as a promising therapy in clinical treatment of tumors that heavily rely on the Warburg effect. However, the potential toxicity of PGAM inhibitors in vivo to normal postmitotic, metabolically active organs such as brain, liver, skeletal muscle, and heart, all of which are glycolytic, remains undetermined. This warrants further detailed toxicity and pharmacokinetics studies to improve the proposed anti-PGAM1 therapy in cancer treatment.

EXPERIMENTAL PROCEDURES

Cellular Metabolites Extraction and Measurement

Cellular metabolites were extracted and spectrophotometrically measured as described previously (Kauffman et al., 1969; Minakami et al., 1965) with some modifications. To determine cellular concentration of 2-PG and 3-PG, 100 μl of packed cell pellets were homogenized in 1.5 ml of hypotonic lysis buffer (20 mM HEPES (pH 7.0), 5 mM KCl, 1 mM $MgCl_2$, 5 mM DTT, and protease inhibitor cocktail). The homogenates were centrifuged in a cold room at 4°C for 10 min at maximum speed, and the supernatants were applied to Amicon Ultra tubes with 10KDa cut off filter (Millipore). The flow through containing the metabolites was used for the measurement. NADH, ADP, and $MgCl_2$ were added to the flow through to final concentrations of 0.14 mM, 1 mM, and 50 mM, respectively. Recombinant LDH and PKM1 proteins were added to final concentrations of 5 μg/ml and 10 μg/ml, respectively. Recombinant enolase protein was added to a final concentration of 50 μg/ml to measure cellular 2-PG. Once the reaction was initiated by enolase, a decrease in absorbance at 340 nm from NADH oxidation was measured by a DU800 spectrophotometer (Beckman). After termination of the enolase reaction, recombinant PGAM1 protein was added to a final concentration of 25 μg/ml and the decrease in absorbance at 340 nm was immediately monitored to measure cellular 3-PG. One hundred microliters of 2-PG and 3-PG (Sigma) diluted with 1.5 ml of hypotonic lysis buffer were used as the standards.

Protein Crystallization, Data Collection, and Structure Determination

For protein crystallization, 6PGD was crystallized by using the hanging drop vapor diffusion method. To soak in 3-PG, 0.2 μl of 5 mM 3-phosphoglycerate acid were added into the mixture and incubated for 2 hr. The crystals were then flash-frozen in liquid nitrogen with the same cryoprotectant solution. Because a high concentration of 3-PG causes the crystal to crack, a final 3-PG concentration of 833 μM was applied and an occupancy of 50% was obtained after refinement. For data collection, the crystal diffraction data of 6PGD apo-form and 6PGD-3-PG complex were collected at the macromolecular crystallography for life science beamline GM/CA-CAT (23-ID-F) and NE-CAT (24-ID-E) respectively at the Advanced Photon Source, Argonne National Laboratory. The data were processed with HKL2000 and the scaled data were used for molecular replacement. For phasing, model building and refinement, the structure of 6PGD apo-form was determined by molecular replacement using Molrep in the CCP4 suite, with the protein portion of the solved structure of 6PGD-6-PG as the search model (Protein Data Bank [pdb] number: 3FWN) (Chen et al., 2010). The structure was then refined by using Phenix (Haddadian et al., 2011). Manual rebuilding of the model was carried out using the molecular graphics program COOT based on electron density interpretation. Water molecules were incorporated into the model if they gave rise to peaks exceeding 3σ in Fo-Fc density maps. The structure of the 6PGD-3-PG complex was also determined by molecular replacement using Molrep with the solved structure of 6PGD apo-form as the search model, and then refined by using Phenix. Manual rebuilding of the model was carried out using the molecular graphics programs COOT. The final structures of apo-form and 6PGD-3-PG complex were visualized by using PyMol software.

Xenograft Studies

Approval of use of mice and designed experiments was given by the Institutional Animal Care and Use Committee of Emory University. Nude mice (Athymic Nude-Foxn1nu, female 6- to 8-week-old, Harlan) were subcutaneously injected with 10×10^6 H1299 cells harboring empty vector on the left flank, and cells with stable knockdown of endogenous hPGAM1 on the right flank, respectively. The tumors were harvested and weighed at the experimental endpoint, and the masses of tumors (g) derived from cells with and without stable knockdown of endogenous hPGAM1 in both flanks of each mouse were compared. Statistical analyses were performed by comparison in relation to the control group with a two-tailed paired Student's t test. For drug evaluation of PGMI-004A using xenograft mice, the drug was administered by daily intraperitoneal injection at a dose of 100 mg/kg from 6 days after subcutaneous injection of H1299 cells on right flank of each mouse. Tumor growth was recorded by measurement of two perpendicular diameters of the tumors over a 3 week course using the formula $4\pi/3 \times (\text{width}/2)^2 \times (\text{length}/2)$. The tumors were harvested and weighed at the experimental endpoint. The masses of tumors (g) treated with vehicle control (DMSO: PEG400:PBS at a ratio of 4:3:3) and PGMI-004A were compared and p values were determined by a two-tailed Student's t test.

Primary Tissue Samples from Patients with Leukemia and Healthy Donors

Approval of use of human specimens was given by the Institutional Review Board of Emory University School of Medicine. All clinical samples were

Figure 7. Inhibition of PGAM1 by PGMI-004A Reveals that PGAM1 Enzyme Activity Is Important for Regulation of 3-PG and 2-PG Levels and Coordination of Glycolysis and Biosynthesis to Promote Cancer Cell Proliferation

(A) 2-PG (left) and 3-PG (right) levels in H1299 cells treated with or without PGMI-004A were determined in the presence and absence of methyl-2-PG.

(B and C) Lactate production (B) and intracellular ATP levels (C) in H1299 cells treated with or without PGMI-004A were determined in the presence and absence of methyl-2-PG.

(D and E) H1299 cells treated with or without PGMI-004A were tested for oxidative PPP flux (D) and NADPH/$NADP^+$ ratio (E).

(F–H) H1299 cells treated with or without PGMI-004A were tested for biosynthesis of lipids (F) and RNA (G), as well as cell proliferation (H) in the presence and absence of methyl-2-PG.

(I–K) Cell viability of H1299 cells (I), diverse human leukemia cells (J) and control HDF cells (K) in the presence of increasing concentrations of PGMI-004A. Cell viability was determined by trypan blue exclusion.

The error bars represent mean values ± SD from three replicates of each sample (*$0.01 < p < 0.05$; ***$p < 0.001$; n.s., not significant).

See also Figure S5.

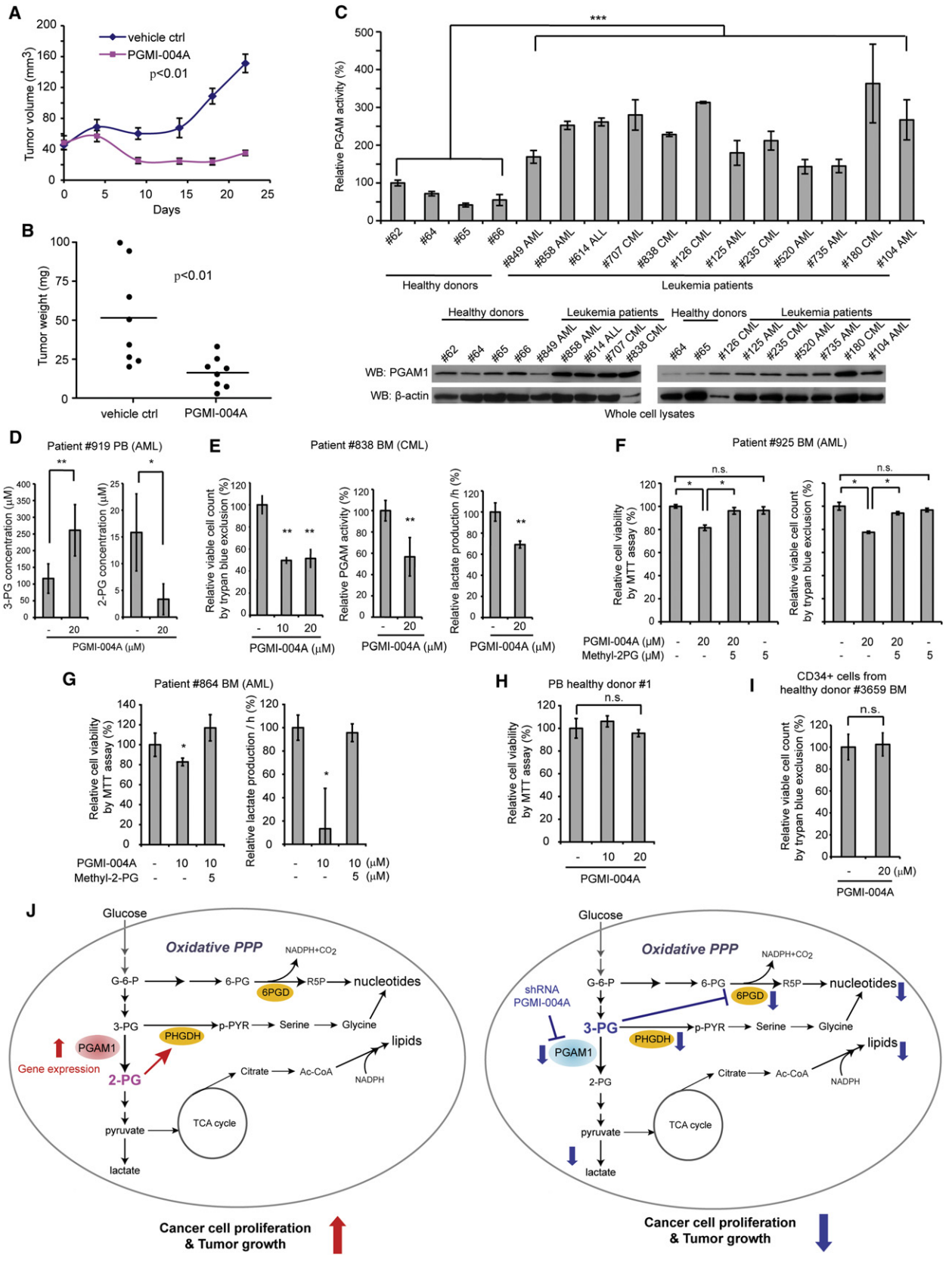
A
vehicle ctrl
PGMI-004A
p<0.01
Tumor volume (mm3)
Days
B
Tumor weight (mg)
p<0.01
vehicle ctrl
PGMI-004A
C
Relative PGAM activity (%)
***
Healthy donors
Leukemia patients
WB: PGAM1
WB: β-actin
Whole cell lysates
D
Patient #919 PB (AML)
3-PG concentration (μM)
2-PG concentration (μM)
PGMI-004A (μM)
E
Patient #838 BM (CML)
Relative viable cell count by trypan blue exclusion (%)
Relative PGAM activity (%)
Relative lactate production /h (%)
PGMI-004A (μM)
F
Patient #925 BM (AML)
Relative cell viability by MTT assay (%)
Relative viable cell count by trypan blue exclusion (%)
n.s.
PGMI-004A (μM)
Methyl-2PG (μM)
G
Patient #864 BM (AML)
Relative cell viability by MTT assay (%)
Relative lactate production / h (%)
PGMI-004A
Methyl-2-PG
H
PB healthy donor #1
Relative cell viability by MTT assay (%)
n.s.
PGMI-004A
I
CD34+ cells from healthy donor #3659 BM
Relative viable cell count by trypan blue exclusion (%)
n.s.
PGMI-004A
J
Glucose
Oxidative PPP
NADPH+CO2
G-6-P
6-PG
6PGD
R5P
nucleotides
3-PG
PHGDH
p-PYR
Serine
Glycine
PGAM1
Gene expression
2-PG
Citrate
Ac-CoA
lipids
NADPH
pyruvate
TCA cycle
lactate
shRNA PGMI-004A
Cancer cell proliferation & Tumor growth

obtained with informed consent with approval by the Emory University Institutional Review Board. Clinical information for the patients was obtained from the pathologic files at Emory University Hospital under the guidelines and with approval from the Institutional Review Board of Emory University School of Medicine and according to the Health Insurance Portability and Accountability Act. Only samples from patients that were not previously treated with chemotherapy or radiation therapy were used. Mononuclear cells were isolated from peripheral blood and bone marrow samples from patients with leukemia or peripheral blood samples from healthy donors using lymphocyte separation medium (Cellgro). Cells were cultured in RPMI 1640 medium supplemented with 10% fetal bovine serum and penicillin/streptomycin and incubated with increasing concentrations of PGMI-004A for up to 72 or 120 hr.

SUPPLEMENTAL INFORMATION

Supplemental Information includes six figures, five tables, and Supplemental Experimental Procedures and can be found with this article online at http://dx.doi.org/10.1016/j.ccr.2012.09.020.

ACKNOWLEDGMENTS

We thank Susan Sunay at the Hematology Division Tissue Bank, Winship Cancer Institute of Emory, for providing primary tissue samples from patients with leukemia, Drs. Sagar Lonial and Lawrence Boise for providing peripheral blood samples from healthy donors, and Dr. Yoke Wah Kow for human HaCaT and PIG1 cell lines. This work was supported in part by NIH Grants CA120272 (to J.C.), CA140515 (to J.C.), GM071440 (to C.H.), and the Pharmacological Sciences Training Grant T32 GM008602 (to S.E.). J.X. and T.-L.G. are employees of Cell Signaling Technology, Inc. T.H. is a Fellow Scholar of the American Society of Hematology. S.E. is an NIH pre-doctoral fellow and an ARCS Foundation Scholar. G.Z.C., D.M.S., F.R.K., S.K., and J.C. are Georgia Cancer Coalition Distinguished Cancer Scholars. S.K. is a Robbins Scholar. S.K. and J.C. are American Cancer Society Basic Research Scholars. J.C. is a Scholar of the Leukemia and Lymphoma Society.

Received: March 29, 2012
Revised: July 23, 2012
Accepted: September 12, 2012
Published: November 12, 2012

REFERENCES

Cairns, R.A., Harris, I.S., and Mak, T.W. (2011). Regulation of cancer cell metabolism. Nat. Rev. Cancer *11*, 85–95.

Chen, Y.Y., Ko, T.P., Chen, W.H., Lo, L.P., Lin, C.H., and Wang, A.H. (2010). Conformational changes associated with cofactor/substrate binding of 6-phosphogluconate dehydrogenase from Escherichia coli and Klebsiella pneumoniae: Implications for enzyme mechanism. J. Struct. Biol. *169*, 25–35.

Corcoran, C.A., Huang, Y., and Sheikh, M.S. (2006). The regulation of energy generating metabolic pathways by p53. Cancer Biol. Ther. *5*, 1610–1613.

Elstrom, R.L., Bauer, D.E., Buzzai, M., Karnauskas, R., Harris, M.H., Plas, D.R., Zhuang, H., Cinalli, R.M., Alavi, A., Rudin, C.M., and Thompson, C.B. (2004). Akt stimulates aerobic glycolysis in cancer cells. Cancer Res. *64*, 3892–3899.

Engel, M., Mazurek, S., Eigenbrodt, E., and Welter, C. (2004). Phosphoglycerate mutase-derived polypeptide inhibits glycolytic flux and induces cell growth arrest in tumor cell lines. J. Biol. Chem. *279*, 35803–35812.

Evans, M.J., Saghatelian, A., Sorensen, E.J., and Cravatt, B.F. (2005). Target discovery in small-molecule cell-based screens by in situ proteome reactivity profiling. Nat. Biotechnol. *23*, 1303–1307.

Evans, M.J., Morris, G.M., Wu, J., Olson, A.J., Sorensen, E.J., and Cravatt, B.F. (2007). Mechanistic and structural requirements for active site labeling of phosphoglycerate mutase by spiroepoxides. Mol. Biosyst. *3*, 495–506.

Feig, S.A., Shohet, S.B., and Nathan, D.G. (1971). Energy metabolism in human erythrocytes. I. Effects of sodium fluoride. J. Clin. Invest. *50*, 1731–1737.

Gottschalk, S., Anderson, N., Hainz, C., Eckhardt, S.G., and Serkova, N.J. (2004). Imatinib (STI571)-mediated changes in glucose metabolism in human leukemia BCR-ABL-positive cells. Clin. Cancer Res. *10*, 6661–6668.

Haddadian, E.J., Gong, H., Jha, A.K., Yang, X., Debartolo, J., Hinshaw, J.R., Rice, P.A., Sosnick, T.R., and Freed, K.F. (2011). Automated real-space refinement of protein structures using a realistic backbone move set. Biophys. J. *101*, 899–909.

Hitosugi, T., Kang, S., Vander Heiden, M.G., Chung, T.W., Elf, S., Lythgoe, K., Dong, S., Lonial, S., Wang, X., Chen, G.Z., et al. (2009). Tyrosine phosphorylation inhibits PKM2 to promote the Warburg effect and tumor growth. Sci. Signal. *2*, ra73.

Jiang, P., Du, W., Wang, X., Mancuso, A., Gao, X., Wu, M., and Yang, X. (2011). p53 regulates biosynthesis through direct inactivation of glucose-6-phosphate dehydrogenase. Nat. Cell Biol. *13*, 310–316.

Figure 8. PGMI-004A Treatment Results in Increased 3-PG and Decreased 2-PG Levels, and Reduced Cell Proliferation of Primary Leukemia Cells from Patients, and Attenuated Tumor Growth in Xenograft Nude Mice In Vivo

(A and B) Tumor growth (A) and tumor size (B) in xenograft nude mice injected with H1299 cells were compared between the group of mice treated with PGMI-004A and the control group treated with vehicle control. p values were determined by a two-tailed Student's t test.

(C) PGAM1 protein expression (lower) and enzyme activity (upper) levels were examined using primary leukemia cells from diverse human patients with AML, CML, or B-ALL and compared to control peripheral blood cells from healthy donors.

(D) Effect of PGMI-004A treatment on 3-PG (left) and 2-PG (right) levels in human primary leukemia cells isolated from peripheral blood samples from a representative patient with AML.

(E) Effect of PGMI-004A treatment on cell viability (left), PGAM1 activity (middle), and lactate production (right) in human primary leukemia cells from a representative patient with CML.

(F and G) Effect of methyl-2-PG treatment on decreased cell viability (F; G left) and lactate production (G right) in PGMI-004A-treated human primary leukemia cells from patients with AML.

(H and I) PGMI-004A shows no toxicity in treatment (120 hr) of peripheral blood cells (H) and CD34+ cells isolated from bone marrow samples (I) from representative healthy human donors.

(J) Proposed model: role of PGAM1 in cancer cell metabolism.

Left: PGAM1 activity is upregulated in cancer cells to promote glycolysis and keep the intracellular 3-PG levels low, which in turn permits high levels of the PPP and biosynthesis to fulfill the request of rapidly growing tumors. PGAM1 also maintains the physiologic levels of 2-PG to sustain PHGDH activity, which diverts 3-PG from glycolysis to serine synthesis and contributes to maintaining relatively low levels of 3-PG in cancer cells. These effects in concert provide a metabolic advantage to cancer cell proliferation and tumor growth.

Right: When PGAM1 is inhibited, 3-PG levels are elevated, which in turn inhibit 6PGD and consequently the oxidative PPP and anabolic biosynthesis. At the same time, 2-PG is decreased to levels below the physiologic concentrations, leading to decreased PHGDH activity, which facilitates 3-PG accumulation. Such metabolic changes result in attenuated cell proliferation and tumor development.

The error bars represent mean values ± SD from three replicates of each sample (*$0.01 < p < 0.05$; **$0.001 < p < 0.01$; ***$p < 0.001$; n.s., not significant). See also Figure S6 and Table S5.

Kauffman, F.C., Brown, J.G., Passonneau, J.V., and Lowry, O.H. (1969). Effects of changes in brain metabolism on levels of pentose phosphate pathway intermediates. J. Biol. Chem. *244*, 3647–3653.

Kroemer, G., and Pouyssegur, J. (2008). Tumor cell metabolism: cancer's Achilles' heel. Cancer Cell *13*, 472–482.

Li, L., Dworkowski, F.S., and Cook, P.F. (2006). Importance in catalysis of the 6-phosphate-binding site of 6-phosphogluconate in sheep liver 6-phosphogluconate dehydrogenase. J. Biol. Chem. *281*, 25568–25576.

Liu, L., Wang, S., Zhang, Q., and Ding, Y. (2008). Identification of potential genes/proteins regulated by Tiam1 in colorectal cancer by microarray analysis and proteome analysis. Cell Biol. Int. *32*, 1215–1222.

Minakami, S., Takayasu, S., Suzuki, C., and Yoshikawa, H. (1964). The hydrogen ion concentrations and erythrocyte glycolysis. Biochem. Biophys. Res. Commun. *17*, 748–751.

Minakami, S., Suzuki, C., Saito, T., and Yoshikawa, H. (1965). Studies on erythrocyte glycolysis. I. Determination of the glycolytic intermediates in human erythrocytes. J. Biochem. *58*, 543–550.

Mulquiney, P.J., and Kuchel, P.W. (1999). Model of 2,3-bisphosphoglycerate metabolism in the human erythrocyte based on detailed enzyme kinetic equations: equations and parameter refinement. Biochem. J. *342*, 581–596.

Nicklin, P., Bergman, P., Zhang, B., Triantafellow, E., Wang, H., Nyfeler, B., Yang, H., Hild, M., Kung, C., Wilson, C., et al. (2009). Bidirectional transport of amino acids regulates mTOR and autophagy. Cell *136*, 521–534.

Ren, F., Wu, H., Lei, Y., Zhang, H., Liu, R., Zhao, Y., Chen, X., Zeng, D., Tong, A., Chen, L., et al. (2010). Quantitative proteomics identification of phosphoglycerate mutase 1 as a novel therapeutic target in hepatocellular carcinoma. Mol. Cancer *9*, 81.

Schauerte, J.A., and Gafni, A. (1989). Long-lived tryptophan fluorescence in phosphoglycerate mutase. Biochemistry *28*, 3948–3954.

Shackelford, D.B., and Shaw, R.J. (2009). The LKB1-AMPK pathway: metabolism and growth control in tumour suppression. Nat. Rev. Cancer *9*, 563–575.

Tennant, D.A., Durán, R.V., Boulahbel, H., and Gottlieb, E. (2009). Metabolic transformation in cancer. Carcinogenesis *30*, 1269–1280.

Tennant, D.A., Durán, R.V., and Gottlieb, E. (2010). Targeting metabolic transformation for cancer therapy. Nat. Rev. Cancer *10*, 267–277.

PGAMgnam Style: A Glycolytic Switch Controls Biosynthesis

Barbara Chaneton[1] and Eyal Gottlieb[1,*]
[1]Cancer Research UK, The Beatson Institute for Cancer Research, Switchback Road, Glasgow G61 1BD, UK
*Correspondence: e.gottlieb@beatson.gla.ac.uk
http://dx.doi.org/10.1016/j.ccr.2012.10.014

Therapeutic strategies that target glycolysis and biosynthetic pathways in cancer cells are currently the main focus of research in the field of cancer metabolism. In this issue of *Cancer Cell*, Hitosugi and colleagues show that targeting PGAM1 could be a way of "killing two birds with one stone".

The metabolism of cancer cells differs from that of many normal cells and is mostly characterized by higher rates of glucose metabolism under normal oxygen levels. This trait enables cancer cells to satisfy their demand for both energy and biosynthetic building blocks required for proliferation. For that reason, it is not surprising that many glycolytic enzymes are commonly overexpressed in tumors (Tennant et al., 2009). Phosphoglycerate mutase (PGAM1) catalyzes the conversion of 3-phosphoglycerate (3PG) into 2-phosphoglycerate (2PG) as part of the glycolytic pathway using a phospho-histidine residue at the enzyme's catalytic domain (His11) as a phosphate donor/acceptor and 2,3-bisphosphoglycerate as an intermediate metabolite (Fothergill-Gilmore and Watson, 1989). In humans, PGAM1 is widely expressed at levels that vary among different tissues as well as during differentiation and transformation. PGAM1 is overexpressed in several types of cancer (Fothergill-Gilmore and Watson, 1989; Ren et al., 2010). Because PGAM1 expression is negatively regulated by the tumor suppressor TP53, the loss of the latter may cause increased expression of PGAM1 in cancer. This portrays PGAM1 as a potential therapeutic target, and indeed, pharmacological inhibition of PGAM1 reduced proliferation of breast cancer cells (Evans et al., 2005). Furthermore, in cancer cells that overexpress the tightly-regulated isoform of pyruvate kinase PKM2, PGAM1 phosphorylation on His11, and hence PGAM1's activity, are induced by phosphoenolpyruvate, the substrate of pyruvate kinase (Vander Heiden et al., 2010).

The notion that metabolites can act as signaling molecules in distant metabolic pathways is gaining significant attention and support (Figure 1A). Some of the best known examples are the activation of PKM2, which catalyzes the last step of glycolysis, by fructose 1,6-bisphosphate (an upstream glycolytic intermediate) and the inhibition of phosphofructokinase-1 (another key regulated glycolytic enzyme) by phosphoenolpyruvate, citrate, and ATP (Ashizawa et al., 1991; Evans et al., 1981). These regulatory loops ensure that glycolytic intermediates are optimally utilized and channeled into the appropriate metabolic pathway to balance energetic and anabolic demands. Recently, the amino acid serine was demonstrated to bind and directly activate PKM2 in order to control the bifurcation point from glycolysis to serine biosynthesis (Chaneton et al., 2012). In line with this concept, this issue of *Cancer Cell* features the work by Hitosugi et al. (2012), which demonstrates that, in addition to their involvement in glycolysis, both the substrate and product of PGAM1 (3PG and 2PG, respectively) modulate two other biosynthetic pathways derived from glycolysis: the oxidative branch of the pentose phosphate pathway (PPP) and the serine biosynthesis pathway (Figure 1A).

Hitosugi et al. (2012) studied the prospective therapeutic approach of PGAM1 inhibition in cancer cells and the associated metabolic consequences. Silencing the expression of PGAM1 with short-hairpin RNA caused an increase in the intracellular levels of 3PG and a decrease in 2PG levels, which is associated with a block in the glycolytic flow. Surprisingly, the downregulation of PGAM1 levels also inhibited the entry of glucose 6-phosphate into the oxidative PPP, a process which supports de novo nucleotide biosynthesis. Hitosugi et al. (2012) demonstrated that the increase in 3PG directly causes the inactivation of the PPP enzyme 6-phosphogluconate dehydrogenase (6PGD) by competing with its substrate 6-phosphogluconate. What's more, the decrease in 2PG levels upon PGAM1 downregulation was accompanied by a reduction in phosphoglycerate dehydrogenase (PHGDH) activity, which utilizes 3PG as a substrate and carries out the first regulated step in the serine biosynthesis pathway (Figure 1B). Interestingly, the cell permeable analog of 2PG (methyl-2-PG) rescued PGAM1-silenced cells by increasing the flux of 3PG into the serine biosynthesis pathway through PHGDH and, with that, alleviated the inhibition of the PPP by 3PG while also rescuing glycolysis. Furthermore, a screen for small molecule inhibitors of PGAM1 identified an allosteric inhibitor that affected cell metabolism and growth of xenografted tumors in vivo in a manner similar to PGAM1 silencing. These observations strengthen the concept that targeting PGAM1 pharmacologically may be beneficial for cancer therapy not only by reducing an important energy source of cancer cells, but also by preventing anabolic processes required for cell growth and proliferation.

The work by Hitosugi et al. (2012) not only provides new insights into the complex mechanism of metabolic regulation (by identifying 2PG and 3PG as signaling molecules that regulate biosynthetic pathways), but also emphasizes the potential effectiveness of exploiting such complexity, which allows for the targeting of both energetic and anabolic processes with a single drug. However, one of the main challenges in targeting cancer metabolism is the robustness

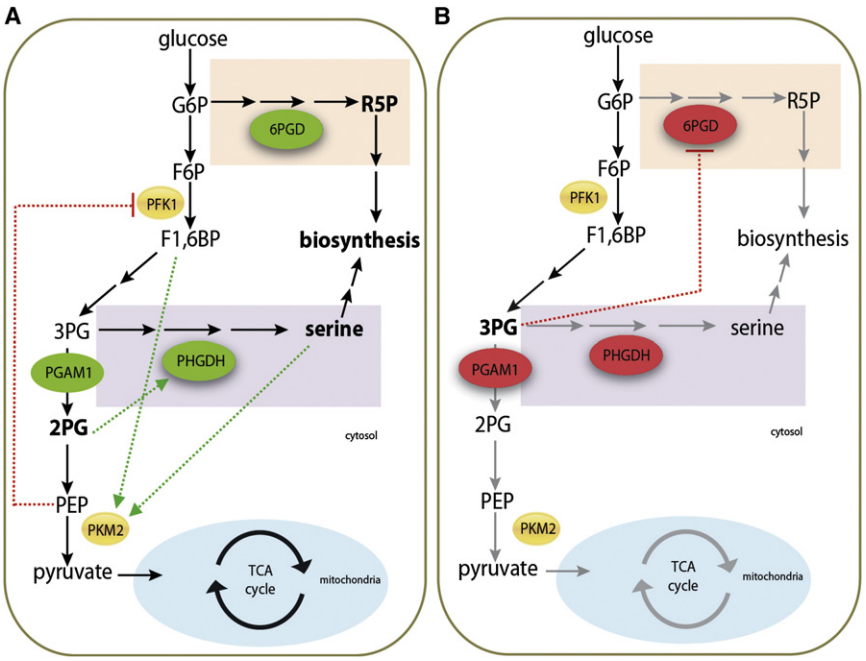

Figure 1. The Dual Catabolic and Anabolic Roles of PGAM1 that Make It a Useful Target for Cancer Treatment

(A) Glycolysis and biosynthetic processes that "branch" from glucose metabolism are required to support growth and proliferation of cells. These processes must be tightly controlled and adjusted to meet cellular needs. Intricate regulatory loop signals exist to enable such control. These include phosphofructokinase-1 (PFK1) inhibition by phosphoenolpyruvate (PEP) and the activation of pyruvate kinase (PK) M2 isoform (PKM2) (the predominant isoform expressed in proliferating cells) by fructose 1,6-bisphosphate (F1,6BP) and serine. PGAM1 is overexpressed in many cancer cells supporting energetic demands by enabling increased glycolytic flux. At the same time, its product 2-phosphoglycerate (2PG) stimulates phosphoglycerate dehydrogenase (PHGDH), which catalyzes the first and rate-limiting step in the serine biosynthesis pathway (purple rectangle).

(B) Upon inhibition of PGAM1, an increase in 3-phosphoglycerate (3PG) and a decrease in 2PG occur. This leads to a decrease in glycolytic flow and energy production by PK as well as the tricarboxylic acid (TCA) cycle in the mitochondria. In addition, the reduction in 2PG due to PGAM1 inhibition prevents the channeling of 3PG into the serine biosynthetic pathway, leading to further accumulation of 3PG. Accumulated 3PG, in turn, inhibits 6-phosphogluconate dehydrogenase (6PGD) in the pentose phosphate pathway (brown rectangle) and ribosome 5-phosphate (R5P) production. In effect, the inhibition of PGAM1, a glycolytic enzyme, not only limits glycolysis, but also two important anabolic processes required for cell proliferation.

Green or red dotted lines indicate direct positive or negative regulatory effects and green or red ovals represent active or inactive enzymes, respectively. Black or gray arrows represent active or inhibited reactions, respectively.

and plasticity of metabolic networks that allow cancer cells to adapt and overcome impediments. In addition, a consideration for long- and short-term toxicity to metabolically active normal tissues must be taken into account when a core glucose metabolic pathway is being targeted. Encouragingly, the in vivo work reported by Hitosugi et al. (2012) demonstrated a good therapeutic index for such a strategy.

REFERENCES

Ashizawa, K., Willingham, M.C., Liang, C.M., and Cheng, S.Y. (1991). J. Biol. Chem. *266*, 16842–16846.

Chaneton, B., Hillmann, P., Zheng, L., Martin, A.C., Maddocks, O.D., Chokkathukalam, A., Coyle, J.E., Jankevics, A., Holding, F.P., Vousden, K.H., et al. (2012). Nature. Published online October 14, 2012. http://dx.doi.org/10.1038/nature11540.

Evans, M.J., Saghatelian, A., Sorensen, E.J., and Cravatt, B.F. (2005). Nat. Biotechnol. *23*, 1303–1307.

Evans, P.R., Farrants, G.W., and Hudson, P.J. (1981). Philos. Trans. R. Soc. Lond. B Biol. Sci. *293*, 53–62.

Fothergill-Gilmore, L.A., and Watson, H.C. (1989). Adv. Enzymol. Relat. Areas Mol. Biol. *62*, 227–313.

Hitosugi, T., Zhou, L., Elf, S., Fan, J., Kang, H.-B., Seo, J.H., Shan, C., Dai, Q., Zhang, L., Xie, J., et al. (2012). Cancer Cell *22*, this issue, 585–600.

Ren, F., Wu, H., Lei, Y., Zhang, H., Liu, R., Zhao, Y., Chen, X., Zeng, D., Tong, A., Chen, L., et al. (2010). Mol. Cancer *9*, 81.

Tennant, D.A., Durán, R.V., Boulahbel, H., and Gottlieb, E. (2009). Carcinogenesis *30*, 1269–1280.

Vander Heiden, M.G., Locasale, J.W., Swanson, K.D., Sharfi, H., Heffron, G.J., Amador-Noguez, D., Christofk, H.R., Wagner, G., Rabinowitz, J.D., Asara, J.M., and Cantley, L.C. (2010). Science *329*, 1492–1499.

nature COMMUNICATIONS

ARTICLE

Received 24 Sep 2012 | Accepted 18 Mar 2013 | Published 30 Apr 2013

DOI: 10.1038/ncomms2759

Tyr26 phosphorylation of PGAM1 provides a metabolic advantage to tumours by stabilizing the active conformation

Taro Hitosugi[1,*], Lu Zhou[2,*], Jun Fan[1], Shannon Elf[1], Liang Zhang[2], Jianxin Xie[3], Yi Wang[3], Ting-Lei Gu[3], Masa Alečković[4], Gary LeRoy[4], Yibin Kang[4], Hee-Bum Kang [1], Jae-Ho Seo[1], Changliang Shan[1], Peng Jin[5], Weimin Gong[6], Sagar Lonial[1], Martha L. Arellano[1], Hanna J. Khoury[1], Georgia Z. Chen[1], Dong M. Shin[1], Fadlo R. Khuri[1], Titus J. Boggon[7], Sumin Kang[1], Chuan He[2] & Jing Chen[1]

How oncogenic signalling coordinates glycolysis and anabolic biosynthesis in cancer cells remains unclear. We recently reported that the glycolytic enzyme phosphoglycerate mutase 1 (PGAM1) regulates anabolic biosynthesis by controlling intracellular levels of its substrate 3-phosphoglycerate and product 2-phosphoglycerate. Here we report a novel mechanism in which Y26 phosphorylation enhances PGAM1 activation through release of inhibitory E19 that blocks the active site, stabilising cofactor 2,3-bisphosphoglycerate binding and H11 phosphorylation. We also report the crystal structure of H11-phosphorylated PGAM1 and find that phospho-H11 activates PGAM1 at least in part by promoting substrate 3-phosphoglycerate binding. Moreover, Y26 phosphorylation of PGAM1 is common in human cancer cells and contributes to regulation of 3-phosphoglycerate and 2-phosphoglycerate levels, promoting cancer cell proliferation and tumour growth. As PGAM1 is a negative transcriptional target of *TP53,* and is therefore commonly upregulated in human cancers, these findings suggest that Y26 phosphorylation represents an additional acute mechanism underlying phosphoglycerate mutase 1 upregulation.

[1] Department of Haematology and Medical Oncology, Winship Cancer Institute of Emory, Emory University School of Medicine, Atlanta, Georgia 30322, USA. [2] Department of Chemistry and Institute for Biophysical Dynamics, The University of Chicago, Chicago, Illinois 60637, USA. [3] Cell Signalling Technology, Inc. (CST), Danvers, Massachusetts 01923, USA. [4] Department of Molecular Biology, Washington Road, LTL 255, Princeton University, Princeton, New Jersey 08544, USA. [5] Department of Human Genetics, Emory University School of Medicine, Atlanta, Georgia 30322, USA. [6] Institute of Biophysics, Chinese Academy of Sciences, Beijing, China. [7] Department of Pharmacology, Yale University School of Medicine, New Haven, Connecticut 06520, USA. * These authors contributed equally to this work. Correspondence and requests for materials should be addressed to J.C. (email: jchen@emory.edu).

The Warburg effect describes the observation that tumour cells take up more glucose than normal tissue and favour glycolysis even in the presence of oxygen. This phenomenon is not limited to solid tumours, as leukaemia cells are also highly glycolytic[1,2]. One metabolic advantage of the Warburg effect is that a boost in aerobic glycolysis in tumour cells generates more ATP more quickly than normal cells that rely on oxidative phosphorylation[3]. Moreover, tumour cells use glycolytic intermediates for anabolic biosynthesis of macromolecules including nucleotides, amino acids and fatty acids, which are used to produce RNA/DNA, proteins and lipids, respectively. These 'building blocks' are necessary for cell proliferation, and their expeditive production is crucial to fulfill the demands of rapidly growing tumours[3]. However, how tumour cells coordinate glycolysis and anabolic biosynthesis remains largely unknown.

We recently reported that the glycolytic enzyme phosphoglycerate mutase 1 (PGAM1) regulates anabolic biosynthesis by controlling intracellular levels of its substrate 3-phosphoglycerate

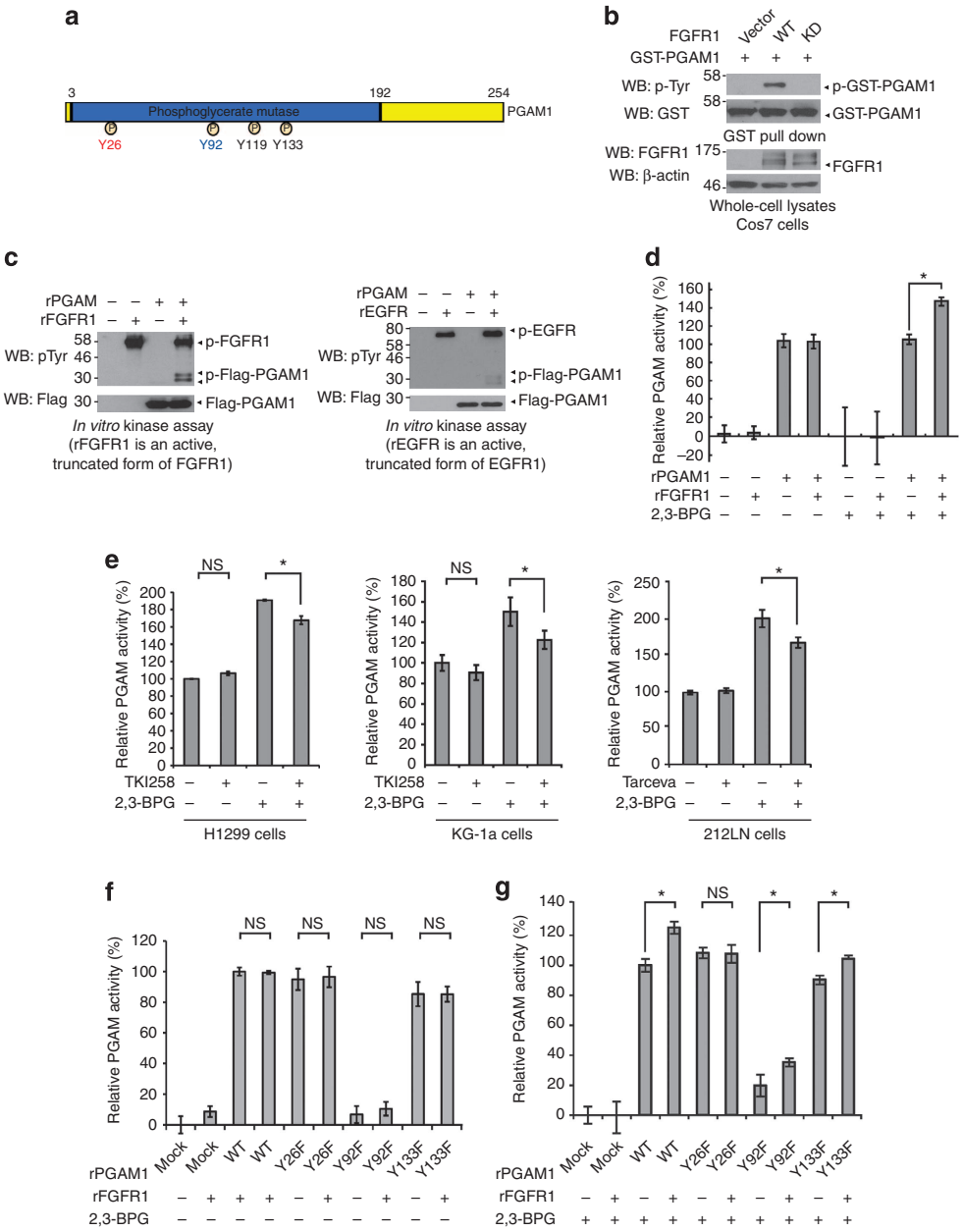

Figure 1 | Y26 phosphorylation enhances PGAM1 activity. (**a**) Schematic representation of PGAM1 with identified tyrosine phosphorylation sites in phospho-proteomics studies. (**b**) Immunoblotting of cell lysates for tyrosine phosphorylation of GST-PGAM1 when coexpressed with FGFR1 WT or a kinase-dead form (KD). (**c**) Active, rFGFR1 (left) and EGFR (rEGFR; right) were incubated with Flag-PGAM1 in *in vitro* kinase assays. Tyrosine phosphorylation of Flag-PGAM1 was assessed by western blot. (**d**) Enzyme activity of recombinant PGAM1 (rPGAM1) treated with or without rFGFR1 was measured in the presence or absence of 10 μM 2,3-BPG. (**e**) PGAM1 activity in the presence or absence of 2,3-BPG in cell lysates from human lung cancer H1299 (left) and leukaemia KG-1a cells (middle) treated with FGFR1 inhibitor TKI258, or head and neck cancer 212LN cells (right) treated with EGFR inhibitor Tarceva. (**f**–**g**) Activity of diverse PGAM1 Y→F mutants treated with FGFR1 in the presence (**g**) or absence (**f**) of 10 μM 2,3-BPG. The values were normalised to the activity level of WT PGAM1 without FGFR1 treatment. The error bars represent mean values ± s.d. from three independent experiments (*$0.01 < P < 0.05$; **$P < 0.01$).

(3-PG) and product 2-phosphoglycerate (2-PG)[4]. PGAM1 catalyses the conversion of 3-PG to 2-PG, a crucial step in glycolysis. PGAM1 is activated upon binding of the cofactor 2,3-bisphosphoglycerate (2,3-BPG), which phosphorylates PGAM1 at histidine 11 (H11) by transferring the C3 phosphate group to H11 (ref. 5). During the conversion of 3-PG to 2-PG by PGAM1, phospho-H11 of PGAM1 is positioned to facilitate transfer of phosphate from phospho-H11 to C-2 of the substrate 3-PG. This creates a 2,3-BPG intermediate in the catalytic pocket, which in turn 're-phosphorylates' H11 by transferring the C3 phosphate group back to H11 to return the enzyme to its initial H11-phosphorylated, fully activated state and allow for release of product 2-PG. Such a 'ping-pong' mechanism of PGAM1 activation involving catalytic H11 phosphorylation by 2,3-BPG has been known for decades, and is supported by kinetic studies[6,7] and isolation of the phospho-H11 containing peptide[8]. However, the structural mechanisms underlying 2,3-BPG binding and how H11 phosphorylation activates PGAM1 remain unknown.

PGAM1 activity has been reported to be upregulated in many cancers, including hepatocellular carcinoma and colorectal cancer[9,10], probably due to increased *PGAM1* gene expression resulting from loss of *TP53*, as PGAM1 is a negative transcriptional target of *TP53* (refs 11–13). In consonance with this, we found that PGAM1 protein expression and enzyme activity levels are upregulated in human primary leukaemia cells from diverse leukaemia patients with acute myeloid leukaemia, chronic myelogenous leukaemia and B-cell acute lymphoblastic leukaemia[4]. Moreover, we found that 3-PG binds to and inhibits 6-phosphogluconate dehydrogenase (6PGD) in the oxidative pentose phosphate pathway (PPP), while 2-PG activates 3-PG dehydrogenase (PHGDH) to provide feedback control of 3-PG levels. Inhibition of PGAM1 by shRNA or a small molecule inhibitor PGMI-004A results in increased 3-PG and decreased 2-PG levels in cancer cells, leading to significantly decreased glycolysis, PPP flux, biosynthesis, cell proliferation and tumour growth.

Here, we report that Y26 phosphorylation of PGAM1 is common in human cancers, providing a proliferative advantage. Structural analyses revealed a novel mechanism in which Y26 phosphorylation enhances PGAM1 activation by stabilising the active conformation of PGAM1. We were also the first to crystalise H11-phosphorylated PGAM1 and structural analysis suggests that phospho-H11 activates PGAM1 at least in part by promoting substrate 3-PG binding. Thus, Y26 phosphorylation of PGAM1 represents a novel, acute mechanism underlying PGAM1 upregulation in cancer cells in addition to chronic changes regulated by *TP53*.

Results

Y26 phosphorylation enhances 2,3-BPG-dependent PGAM1 activity. Our phospho-proteomics studies identified PGAM1 as phosphorylated at multiple tyrosine sites including Y26, Y92, Y119 and Y133 in murine haematopoietic Ba/F3 cells expressing constitutively active ZNF198–FGFR1 fusion tyrosine kinase[14] (Fig. 1a). In consonance with this observation, GST-tagged PGAM1 was tyrosine phosphorylated in COS7 cells transiently co-transfected with plasmids encoding FGFR1 wild-type (WT), but not in cells co-expressing GST-PGAM1 and a kinase-dead form of FGFR1 (Fig. 1b). We further confirmed this in an *in vitro* kinase assay where active, recombinant FGFR1 (rFGFR1) or EGFR (rEGFR) directly phosphorylated purified, Flag-tagged recombinant PGAM1 (rPGAM1) at tyrosine residues (Fig. 1c).

PGAM1 is believed to be activated upon binding of cofactor 2,3-BPG, which was suggested to 'phosphorylate' PGAM1 at histidine 11 (H11) by transferring the C3 phosphate to H11 (ref. 5). In a PGAM1 enzyme assay coupled with the FGFR1 *in vitro* kinase assay, we found that rFGFR1 significantly enhanced rPGAM1 enzyme activity only in the presence but not absence of 2,3-BPG (Fig. 1d). Notably, purified PGAM1 in the absence of 2,3-BPG shows comparable level of enzyme activity as PGAM1 in the presence of 2,3-BPG, indicating that the purified recombinant PGAM1 is H11-phosphorylated and activated to a certain extent, which may be due to modification from bacteria or 3-PG applied in the experiments contaminated with 2,3-BPG as previously described[15]. Nevertheless, these data suggest that FGFR1-dependent tyrosine phosphorylation 'further' enhances PGAM1 activation.

In addition, in a PGAM1 enzyme activity assay, incubation with cofactor 2,3-BPG significantly activates PGAM1 in cell lysates from FGFR1-expressing lung cancer H1299 and leukaemia KG-1a cells (Fig. 1e; left and middle, respectively) and EGFR-expressing head and neck cancer 212LN cells (Fig. 1e; right), while treatment with the FGFR1 small molecule inhibitor TKI258 or EGFR inhibitor Tarceva significantly decreases PGAM1

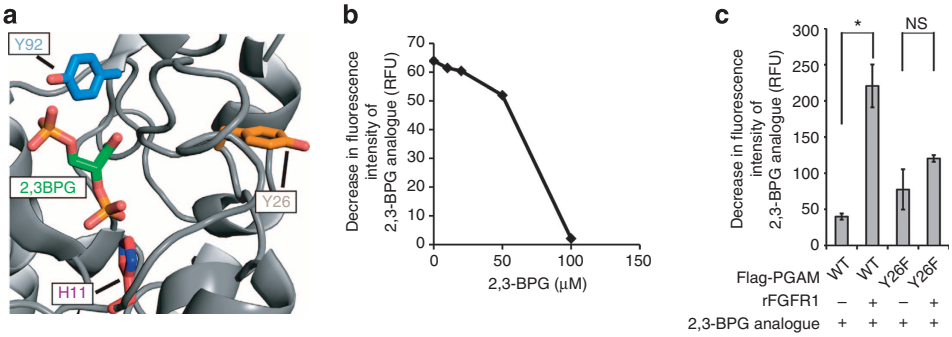

Figure 2 | Y26 phosphorylation promotes cofactor 2,3-BPG binding to PGAM1. (**a**) Cartoon representation of 2,3-BPG location from structure 3FDZ superposed on PGAM1 (PDB accession code: 1YFK). H11 and Y92 are directly proximal to and Y26 is also close to cofactor (2,3-BPG)/substrate (3-PG) binding site. (**b**) 2,3-BPG analogue (8-hydroxy-1,3,6-pyrenetrisulfonate) competes with 2,3-BPG for binding to rPGAM1 protein, where 3 μM 2,3-BPG analogue was mixed with different concentrations of 2,3-BPG in reaction mixture containing 100 mM Tris-HCl (pH 7.5). Fluorescence intensity of 2,3-BPG analogue (ex: 362 nm, em: 520 nm) was measured before and 5 min after the addition of 2.3 μM rPGAM1 protein to the reaction mixture. Decrease in fluorescence intensity of 2,3-BPG analogue indicates 2,3-BPG analogue binding to rPGAM1 protein. The values are presented as relative fluorescence units (RFU). (**c**) Purified Flag-PGAM1 WT or Y26F were incubated with cofactor (represented by 2,3-BPG analogue, 8-hydroxy-1,3,6-pyrenetrisulfonate). The cofactor binding affinity was determined by decrease in fluorescence intensity of the analogue. The values are presented as RFU. The error bars represent mean values ± s.d. from three independent experiments (*$0.01<P<0.05$; **$P<0.01$).

enzyme activity, only in the presence but not absence of 2,3-BPG in H1299 and KG-1a or 212LN cells, respectively.

We next performed mutational analysis and found that, in the absence of 2,3-BPG, tyrosine phosphorylation by FGFR1 did not alter enzyme activity of rPGAM1 WT, Y26F or Y133F. Interestingly, Y92F mutant lost PGAM1 enzyme activity in the presence and absence of rFGFR1, suggesting that Y92 is intrinsically required for PGAM1 enzyme activity (Fig. 1f). In contrast, in the presence of 2,3-BPG, rFGFR1 significantly activates rPGAM1 WT and Y133F mutant (Fig. 1g). However, substitution of Y26 abolished the FGFR1-dependent increase in the PGAM1 enzyme activity. Y92F mutant again showed a very low level of PGAM1 activity, however, incubation with rFGFR1 resulted in significantly increased PGAM1 enzyme activity of Y92F in the presence of 2,3-BPG (Fig. 1g). These data together suggest that Y26 phosphorylation is responsible for mediating FGFR1-dependent, 'enhanced' activation of PGAM1 in the presence of 2,3-BPG.

Y26 phosphorylation PGAM1 enhances H11 phosphorylation. Structural studies revealed that both H11 and Y92 are directly proximal to the active site where both cofactor (2,3-BPG) and substrate (3-PG) bind (Fig. 2a)[16], suggesting that Y92 may be crucial for 2,3-BPG binding and PGAM1 activity, consistent with our observation that substitution of Y92 abolishes PGAM1 enzyme activity (Fig. 1f,g). This is also consistent with a previous report that S14, T23, G24, R90, Y92, K99, R116 and R117 are involved in binding of cofactor 2,3-BPG and substrate 3-PG, which share the same binding pocket on PGAM1 (ref. 17). Y26 is also close to the catalytic site (Fig. 2a); as Y26-phoshorylation by FGFR1 enhances PGAM1 in the presence of 2,3-BPG, this suggests a potential mechanism wherein Y26 phosphorylation by FGFR1 may stabilise the H11-phosphorylated PGAM1.

To test this hypothesis, we incubated active rFGFR1 with purified, recombinant PGAM1 WT and Y26F mutant in an *in vitro* kinase assay, followed by incubation with a competitive 2,3-BPG fluorescent analogue (8-hydroxy-1,3,6-pyrenetrisulfonate)[18,19] (Fig. 2b). The decrease in fluorescence (ex: 362 nm, em: 520 nm) compared with buffer control was measured as 2,3-BPG binding ability. Phosphorylation of PGAM1 WT by FGFR1 resulted in a significant increase in the amount of bound 2,3-BPG analogue, whereas substitution of PGAM1 Y26 abolished enhanced binding of cofactor in the presence of rFGFR1 (Fig. 2c).

Moreover, a quantitative mass spectrometry-based study (Fig. 3a) revealed that the H11 phosphorylation levels of Y26F mutant is significantly lower compared with PGAM1 WT in an *in vitro* kinase assay using PGAM1 proteins incubated with rFGFR1 in the presence of 2,3-BPG (Fig. 3b,c). Similar results were obtained when using Flag-tagged mouse PGAM1 (mPGAM1) WT and Y26F from 'rescue' H1299 cells with stable knockdown of endogenous human PGAM1 (hPGAM1) and rescue expression of Flag-mPGAM1 WT or Y26F mutant, respectively (Fig. 3d,e). These results suggest that Y26 phosphorylation may enhance PGAM1 activity by stabilising the H11-phosphorylated PGAM1.

Y26 phosphorylation stabilises H11-phosphorylated PGAM1. To further understand the structural properties of Y26-phosphorylation-enhanced activation of H11-phosphorylated PGAM1, we crystalised human PGAM1 with phosphorylated H11 (1.65 Å; Supplementary Table S1) from purified PGAM1 protein incubated with 2,3-BPG, in which the occupancy of phosphate on H11 was refined to be 0.70; mass spectrometry analysis of the 2,3-BPG-treated PGAM1 supports that the majority of PGAM1 protein was phosphorylated (Supplementary Fig. S1a). We also crystalised the apo-form of non-phosphorylated WT human PGAM1 (2.08 Å) as previously reported[16]. Both structures of the H11-phosphorylated and non-phosphorylated forms were superposed with a RMSD value of 0.34 Å (Supplementary Fig. S1b).

Upon comparison between these two structures, we found a major conformational change at the loop 12–23 in the H11-phosphorylated form, which is close to H11 that is in the active site of PGAM1 (Fig. 4a). Further structural analysis revealed that, in the structure of non-phosphorylated PGAM1 form, Y26 docks on W16 in the flexible loop (Fig. 4b,c), while the negative charged E19 is located in the positively charged active site, blocking access of cofactor (2,3-BPG) and substrate (3-PG) to the active site (Fig. 4c). Moreover, E19 forms hydrogen bonds with residues S14 and S23 on the loop, which stabilise the conformation of non-phosphorylated PGAM1 (Fig. 4c). In contrast, Y26 is exposed to the surface in the structure of the H11-phosphorylated form of PGAM1, whereas E19 flips away from the active site to allow the negatively charged phosphate group of phosphorylated H11 to be accommodated (Fig. 4d). In addition, the phosphorylated-H11 forms extensive hydrogen bonds with adjacent residues, including R10, R62, E89, H186 and G187, through its phosphate group (Fig. 4d). These hydrogen bonds also contribute to the stabilisation of the phosphorylated-histidine group captured in the crystal, which, otherwise, is generally unstable in the aqueous solution with a half-life around 30 min (ref. 20).

These data together suggest a model in which Y26 phosphorylation may shift the protein conformation to release the negatively charged E19 that blocks the active site (Fig. 4e), thus promoting 2,3-BPG binding and consequently H11 phosphorylation, which may also help to keep the active site open for substrate (3-PG) binding (Fig. 4f). Please see below for detailed discussion.

Figure 3 | Y26 phosphorylation results in increased H11 phosphorylation of PGAM1 *in vitro* and *in vivo*. (**a**) Detection of H11 phosphorylation in PGAM1 using LC-MS/MS. Tandem mass spectrometry (MS/MS) spectrum of phosphorylated PGAM1 peptide pHGESAWNLENR (residue number 11–21) collected using collision-induced dissociation (CID) fragmentation. Underlined nominal masses above and below the sequence denote the b and y ions, respectively that were annotated from the spectrum. The expected and observed mass to charge ratio (m/z) for the $[M+2H^+]^{2+}$ precursor ion is provided. [M-H3PO4] + 2 represents molecular ion with loss of the phosphate group. (**b**,**c**) Phosphorylation by rFGFR1 leads to increased H11 phosphorylation of Flag-PGAM1 WT but not Y26F in the presence of 10 μM 2,3-BPG (**b**). Panel (**c**) shows relative quantification of H11-phosphorylated PGAM1 using reverse phase liquid chromatography. MS data for HGESAWNLENR (upper three red spectra in each panel) and pHGESAWNLENR (lower three green spectra in each panel) were used to calculate the relative levels of phosphorylated and unphosphorylated peptide across all observable charge states in Flag-tagged PGAM1 WT and Y26F mutant incubated with active FGFR1 and 2,3-BPG for one hour (**c**, left and right, respectively). The relative abundance was normalised to the largest peak of each scan, which corresponds to 5.5E7 (**c**, left) and 2.26E7 (**c**, right). (**d**,**e**) Rescue cells expressing mouse PGAM1 (mPGAM1) Y26F demonstrate reduced H11-phosphorylated levels compared with cells with mPGAM1 WT (**d**). WT or Y26F: cells with stable knockdown of endogenous hPGAM1 and rescue expression of mPGAM1 WT or Y26F mutant, respectively. Panel (**e**) shows relative quantification of H11-phosporylated PGAM1 using reverse phase liquid chromatography with Flag-tagged PGAM1 WT and Y26F mutant proteins isolated from rescue H1299 cells (**e**, left and right, respectively). The relative abundance was normalised to the largest peak of each scan, which corresponds to 1.12E7 (**e**, left) and 1.96E7 (**e**, right). The error bars represent mean values ± s.d. from two independent experiments (*$0.01 < P < 0.05$; **$P < 0.01$).

Y26 Phosphorylation of PGAM1 is common in human cancer cells. We also generated an antibody that specifically recognises PGAM1 phospho-Y26 (Supplementary Fig. S2a). We found that PGAM1 is commonly expressed and phosphorylated at Y26 in diverse leukaemia and multiple myeloma cells associated with various constitutively activated tyrosine kinase mutants, as well as various human solid tumour cells including lung, prostate, breast and head and neck cancer cells (Fig. 5a). In addition, we found

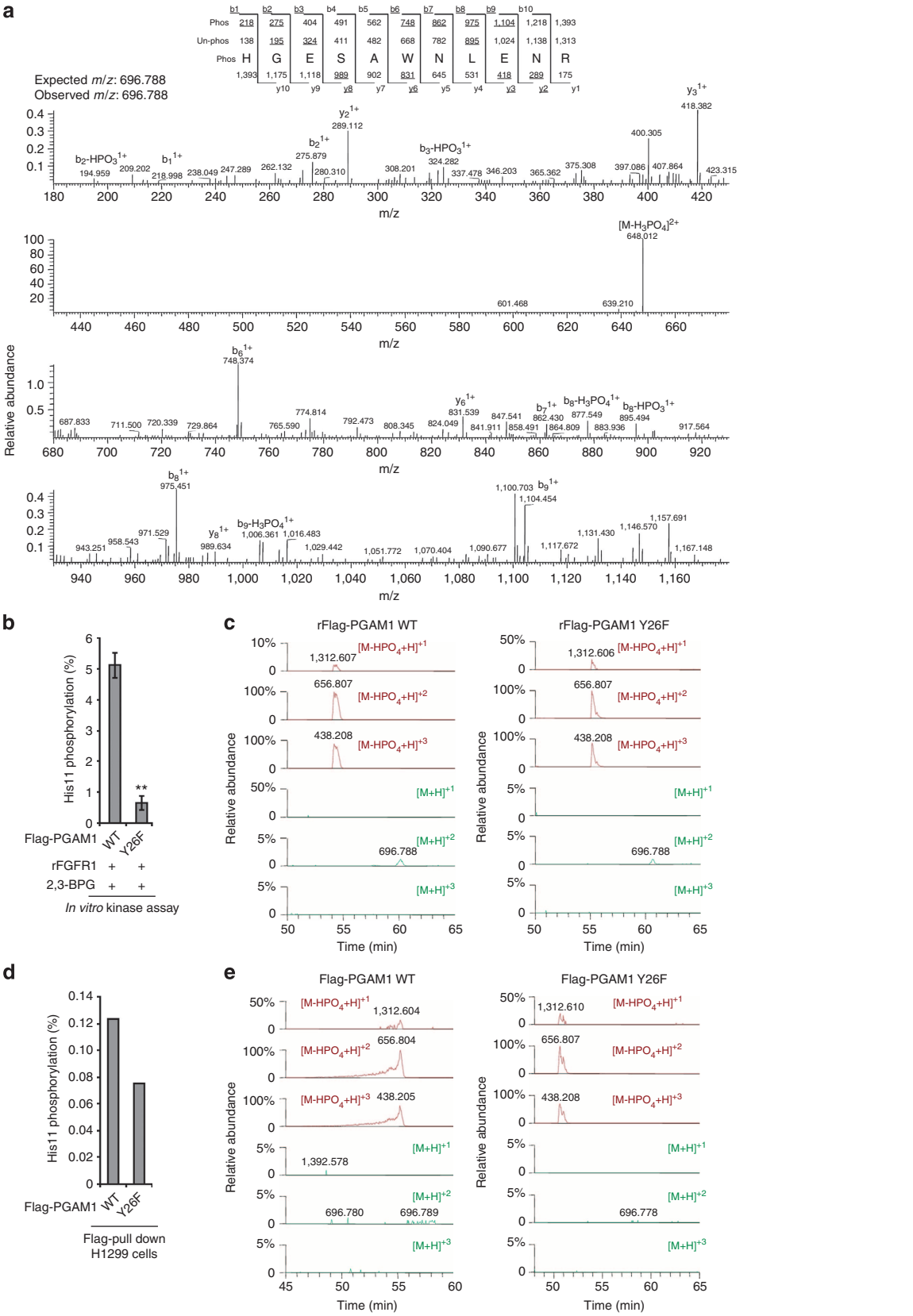

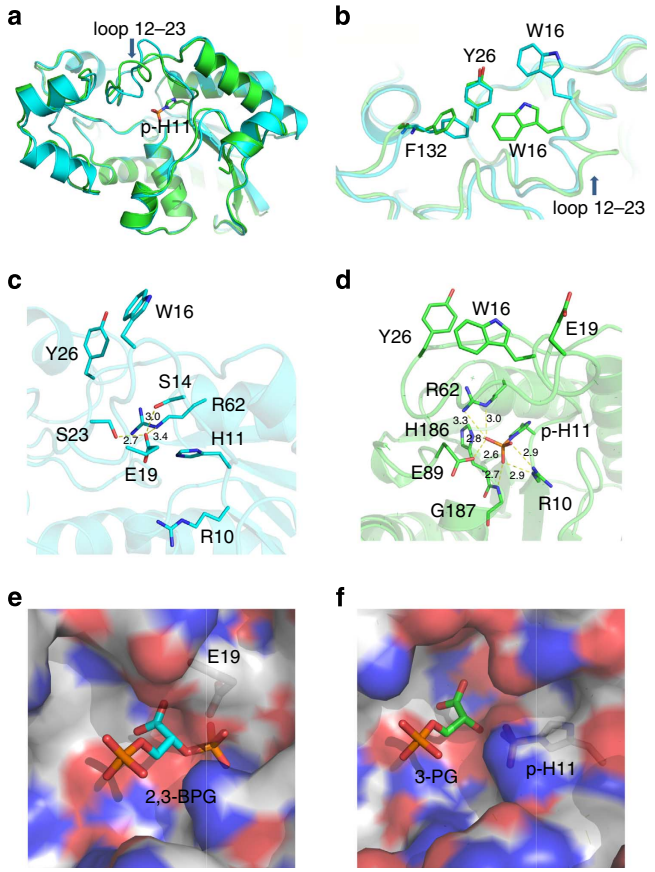

Figure 4 | Y26 phosphorylation may release E19 from blocking the active site of PGAM1. (**a**) Superposition of PGAM1 WT (cyan) and H11-phosphorylated form (green). Phosphorylated H11 is shown in stick and loop 12–23 with the large conformational change is marked. (**b**) Comparison of Y26 surrounding residues between WT PGAM1 (cyan) and H11-phosphorylated form (green). (**c**) Interactions between E19 and adjacent residues in Y26 buried WT PGAM1. (**d**) Interactions between phosphorylated H11 and adjacent residues in Y26 exposed phosphorylated PGAM1. (**e**) Superposed cofactor 2,3-BPG in the active site of non-phosphorylated PGAM1. There is a clash between E19 and phosphate group of 2,3-BPG. (**f**) Superposed substrate 3-PG in active site of H11-phosphorylated PGAM1 showing that it is ready to react with phosphorylated H11.

that PGAM1 protein expression and Y26 phosphorylation levels are upregulated in primary leukaemia cells from diverse acute myeloid leukaemia, chronic myelogenous leukaemia and B-cell acute lymphoblastic leukaemia patients ($n=5$), compared with control peripheral blood cells from healthy donors ($n=4$) (Supplementary Fig. S2b), and PGAM1 protein levels are significantly upregulated in head and neck tumour samples compared with normal tissue controls detected by immunohistochemical staining (Supplementary Fig. S2c). In *in vitro* kinase assays, purified PGAM1 proteins were directly phosphorylated at Y26 by diverse recombinant, active oncogenic tyrosine kinases including FGFR1, EGFR, FLT3 and JAK2 (Fig. 5b). Moreover, inhibiting FGFR1 by treatment with TKI258 resulted in decreased PGAM1 Y26 phosphorylation in FGFR1-expressing lung cancer H1299 cells and leukaemia KG-1a cells (Fig. 5c; left and right, respectively). In addition, inhibition of FLT3-ITD by TKI258 (Fig. 5d) and JAK2 by AG490 (Fig. 5e) resulted in decreased Y26 phosphorylation of PGAM1 in the pertinent human cancer cell lines.

Y26 phosphorylation of PGAM1 promotes tumour growth. In order to determine the role of Y26 phosphorylation of PGAM1 in cancer cell metabolism and tumour growth, we next generated 'rescue' H1299 cells as described[14] by RNAi-mediated stable knockdown of endogenous hPGAM1 and rescue expression of Flag-tagged mPGAM1 WT or Y26F (Fig. 6a). We found that, compared with mPGAM1 WT rescue cells, expression of the catalytically less active Y26F mutant attenuates PGAM1 activity in the presence of 2,3-BPG (Fig. 6b), which results in decreased glycolytic rate (Fig. 6c), oxidative PPP flux and NADPH/NADP$^+$ ratio (Fig. 6d,e, respectively), as well as reduced anabolic biosynthesis including RNA and lipid biosynthesis using ^{14}C-glucose as carbon source, accompanied by reduced NADPH/NADP$^+$ ratio (Fig. 6f,g, respectively). However, attenuation of PGAM1 by stable knockdown or expression of Y26F mutant does not affect lipid and RNA biosynthesis from ^{14}C-glutamine (Supplementary Fig. S2d,e, respectively). Interestingly, attenuation of PGAM1 in cancer cells does not affect the intracellular ATP levels (Fig. 6h) or O_2 consumption rate (Supplementary Fig. S2f), nor sensitivity of cells to treatment with oligomycin, a mitochondrial ATP synthase inhibitor, with regard to ATP levels and O_2 consumption rate (Fig. 6h and Supplementary Fig. S2f, respectively). These results together suggest that Y26 phosphorylation levels of PGAM1 are important for coordination between glycolysis and PPP/biosynthesis using glucose but not glutamine as a carbon source, while attenuation of PGAM1 does not significantly affect intracellular ATP levels.

In addition, we found that 'rescue' cells expressing mPGAM1 Y26F mutant demonstrate decreased cell proliferation compared with control cells expressing mPGAM1 WT (Fig. 6i). Moreover, we functionally validated these findings by performing xenograft experiments. Nude mice were injected with Flag-mPGAM1 WT rescue H1299 cells on the left flank and Y26F rescue cells on the right flank (Fig. 6j). Ten million cells of each cell line were injected and the mice were monitored for tumour growth over a 6-week time period. The masses of tumours derived from PGAM1 Y26F rescue cells were significantly reduced compared with those of tumours formed by Flag-mPGAM1 WT cells (Fig. 6j).

Y26 phosphorylation of PGAM1 regulates 3-PG and 2-PG levels. We recently reported that PGAM1 coordinates glycolysis and anabolic biosynthesis by controlling intracellular levels of its substrate 3-PG and product 2-PG, which consequently inhibits 6PGD in the oxidative PPP and activates 3-PHGDH in serine biosynthesis to provide feedback regulation of 3-PG levels, respectively[4]. In consonance with these findings, we found that, compared with the mPGAM1 WT rescue cells, rescue expression of the catalytically less active Y26F mutant results in increased 3-PG (Fig. 7a) and decreased 2-PG (Fig. 7b) levels, as well as reduced anabolic biosynthesis of RNA and lipids (Fig. 7c,d, respectively) and decreased cell proliferation (Fig. 7e), while treatment with a cell permeable form of 2-PG (methyl-2-PG) significantly rescues these phenotypes. These data together suggest that PGAM1 Y26 phosphorylation levels, in addition to PGAM1 protein expression levels[4], are also important to control intracellular 3-PG and 2-PG levels, which confers both metabolic and proliferative advantages to cancer cells.

Discussion

Upregulated expression of PGAM1, likely due to loss of *TP53*, has been demonstrated in diverse human tumours and leukaemias[4,9,10]. In the current report, our findings suggest that, besides the commonly increased gene expression of PGAM1 that is likely due to loss of *p53* in cancer cells, Y26 phosphorylation

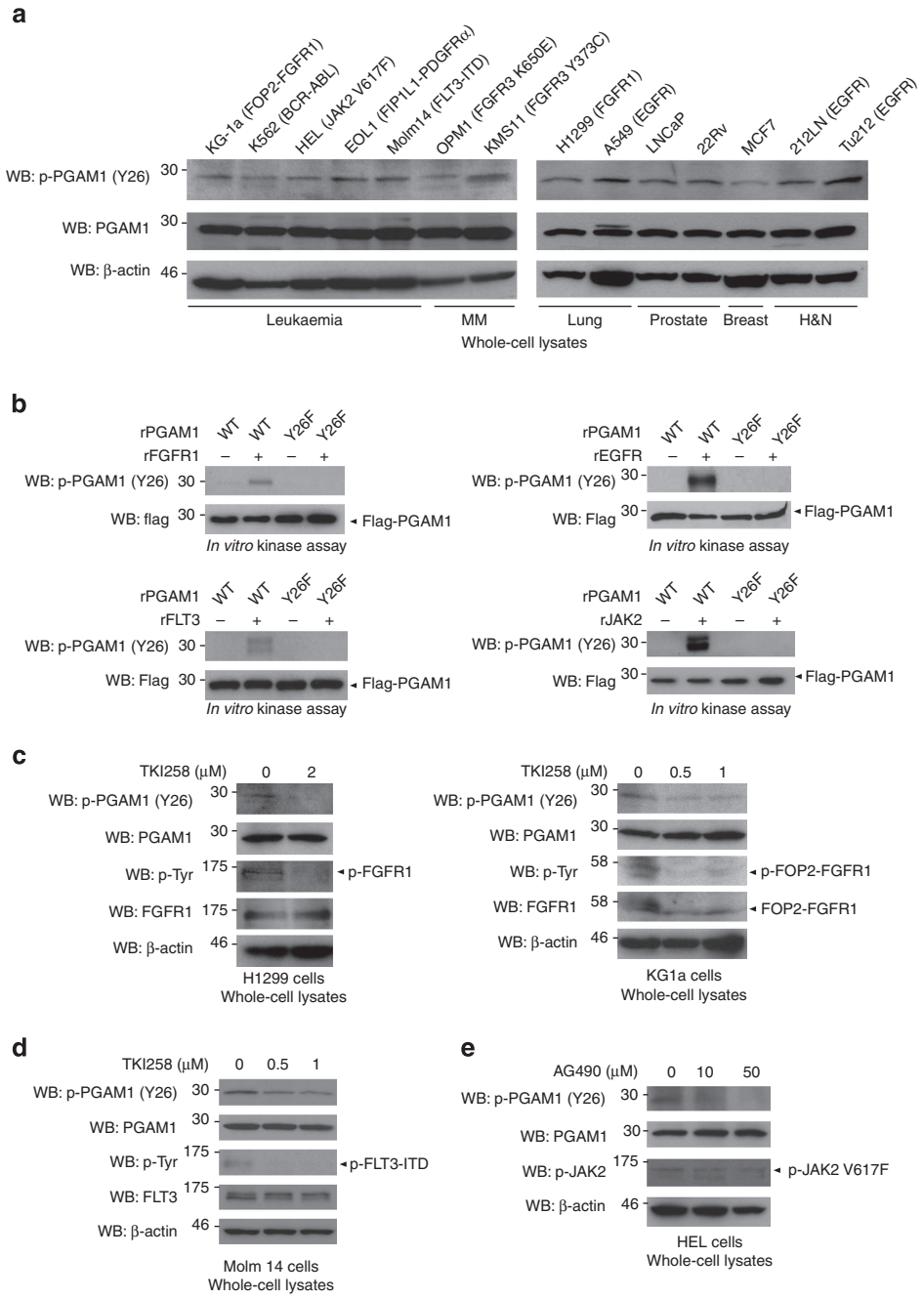

Figure 5 | Y26 phosphorylation is common in diverse cancer cells. (**a**) Protein expression and Y26 phosphorylation levels of PGAM1 in diverse human leukaemia, multiple myeloma (MM), lung, prostate, breast, and head and neck (H and N) cancer cells were assessed by western blot. Oncogenic tyrosine kinases associated with individual cancer cells are indicated. (**b**) Y26 phosphorylation levels of rPGAM1 incubated with active, recombinant rFGFR1, rEGFR, FLT3 (rFLT3) or JAK2 (rJAK2) in diverse *in vitro* kinase assay were detected by western blot. (**c**–**e**) Immunoblotting results showing Y26 phosphorylation levels of PGAM1 in lung cancer H1299 (**c**; left) and leukaemia KG-1a (**c**: right) cells upon treatment with FGFR1 inhibitor TKI258, in leukaemia Molm14 cells (associated with FLT3-ITD mutant) treated with TKI258 (**d**), and leukaemia HEL cells (associated with JAK2 V617F mutant) treated with JAK2 inhibitor AG490 (**e**).

represents an alternative molecular mechanism underlying PGAM1 upregulation in human cancers. Y26 phosphorylation of PGAM1 is common in diverse human cancers and has been detected in a number of phospho-proteomics studies performed by our collaborators at Cell Signalling Technology Inc. using a spectrum of human cancer cells and primary tissue samples from human cancer patients (http://www.phosphosite.org/siteAction.do?id=11589). As tyrosine kinase signalling is commonly upregulated in human cancers, our findings suggest that phosphorylation of Y26 enhances PGAM1 activity, which may represent a common, short-term molecular mechanism underlying upregulated PGAM1 activity in both leukaemias and solid tumours, in addition to the chronic upregulation of *PGAM1* gene expression that is believed to be due to loss of *TP53* in cancer cells.

Moreover, our findings that Y26 phosphorylation could stabilise the active conformation of PGAM1 suggest a novel mechanism by which PGAM1 activity is regulated. Our structural

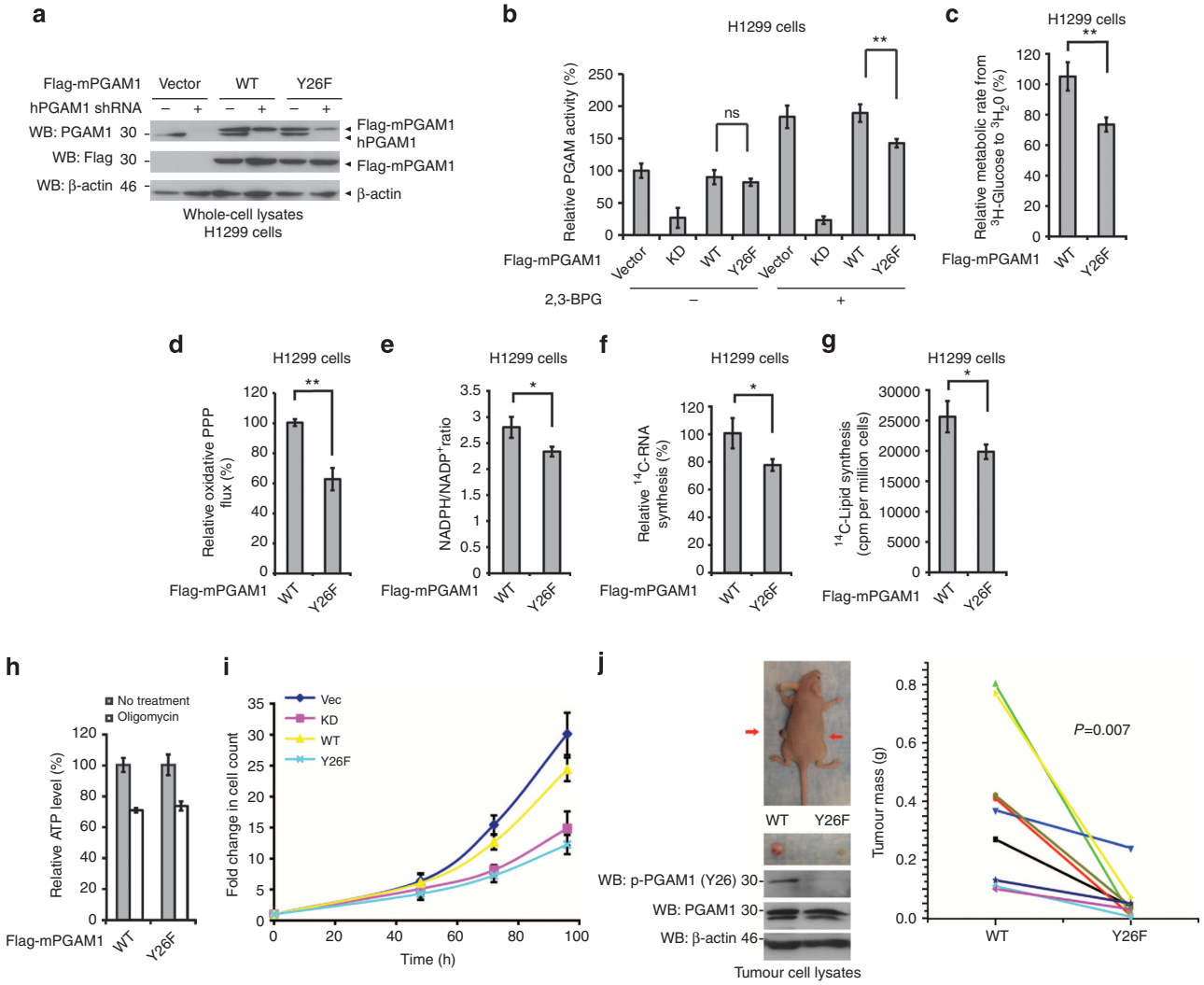

Figure 6 | Y26 phosphorylation of PGAM1 is important for glycolysis and anabolic biosynthesis as well as cell proliferation and tumour growth. (**a**) Generation of H1299 cells with stable knockdown of endogenous hPGAM1 and rescue expression of mPGAM1 WT or Y26F. (**b**) PGAM1 activity in rescue cells expressing mPGAM1 Y26F mutant was compared with that in control cells harbouring an empty vector or rescue cells expressing mPGAM1 WT, respectively, in the presence and absence of 2,3-BPG. (**c**–**h**) Glycolytic rate (**c**), oxidative PPP flux (**d**), NADPH/NADP$^+$ ratio (**e**), RNA biosynthesis (**f**), lipogenesis (**g**) and intracellular ATP levels in the presence or absence of 100 nM oligomycin (**h**) were measured in rescue cells expressing mPGAM1 Y26F mutant, compared with those in control rescue cells of mPGAM1 WT. (**i**,**j**) Rescue expression of catalytically less active Y26F mutant attenuates H1299 cell proliferation (**i**), as well as tumour growth potential of H1299 cells in xenograft nude mice (**j**). (**j**; left) Dissected tumours (indicated by red arrows) in a representative nude mouse; expression and Y26 phosphorylation levels of PGAM1 or mPGAM1 proteins in tumour lysates are shown. (**j**; right) Cells expressing mPGAM1 Y26F show significantly reduced tumour formation in xenograft nude mice compared with cells expressing mPGAM1 WT (*P*-values were determined by the paired Student's *t*-tests). The error bars represent mean values ± s.d. from three independent experiments (*$0.01<P<0.05$; **$P<0.01$).

analyses suggest that Y26 phosphorylation could shift the PGAM1 conformation that releases the negatively charged E19 from blocking the active site. By docking 2,3-BPG to the active site of PGAM1 based on a previously published crystal structure of bisphosphoglycerate mutase in complex with 2,3-BPG (Fig. 4e)[21], we observed that E19 blocks the active site of the protein and consequently prevents binding of the cofactor 2,3-BPG, which is required to transfer a phosphate group to H11, leading to H11 phosphorylation. As we obtained H11-phosphorylated PGAM1 crystal by incubating purified, recombinant PGAM1 protein with excess 2,3-BPG, it is likely that PGAM1 can be 'phosphorylated' by 2,3-BPG at H11 in the absence of Y26 phosphorylation. This also explains the results presented in Fig. 1d–g, which show that phosphorylation of PGAM1 by FGFR1 serves only to enhance PGAM1 activation in the presence of 2,3-BPG. However, our structural data suggest that activation of PGAM1 would benefit from a conformational change that precludes Y26 from forming hydrophobic interactions with W16. This is accomplished when Y26 is phosphorylated and thus negatively charged, which leads to exposure of Y26 to the surface. This further stabilises the active, H11-phosphorylated conformation, in which E19, a residue that blocks the active site of the non-phosphorylated protein (Fig. 4e), moves away to accommodate 2,3-BPG binding and consequently allow H11 phosphorylation. Moreover, the active site with exposed Y26 in the H11-phosphorylated PGAM1 is more accessible for the substrate 3-PG (Fig. 4f), and such a conformation is further stabilised by the multiple hydrogen bonds formed between phosphorylated H11 and its surrounding residues (Fig. 4d). The relatively low H11 phosphorylation quantified by MS using recombinant protein or cell lysates can be attributed to the fact that histidine phosphorylation is usually

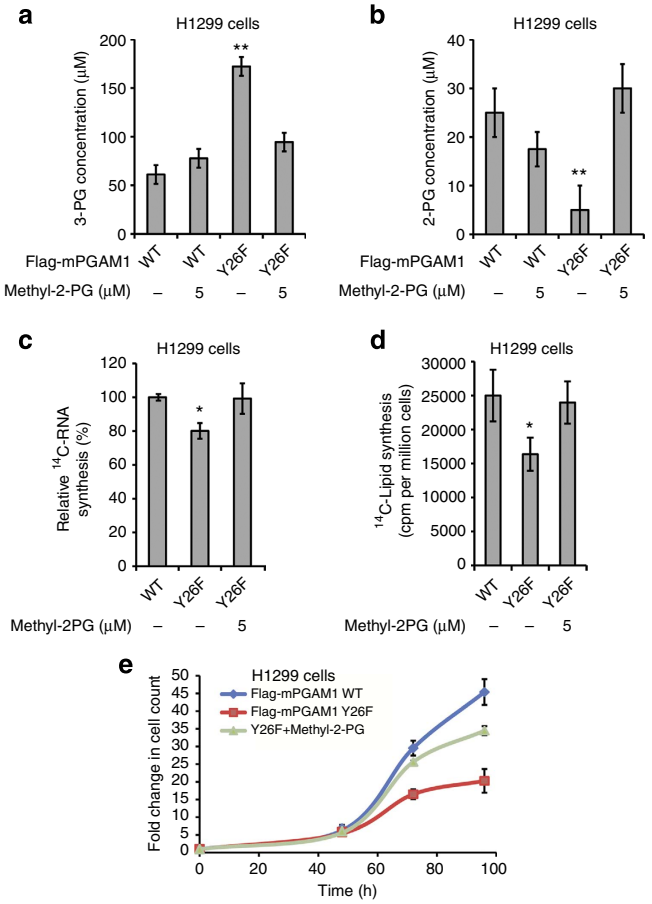

Figure 7 | Y26 phosphorylation of PGAM1 controls 3-PG and 2-PG levels to regulate biosynthesis and proliferation. (**a**–**e**) Intracellular 3-PG (**a**) and 2-PG levels (**b**), RNA biosynthesis (**c**), lipogenesis (**d**) and cell proliferation rate (**e**) in H1299 cells expressing mPGAM1 Y26F mutant were measured, compared with control cells with rescue expression of mPGAM1 WT, in the presence and absence of cell permeable methyl-2-PG. The error bars represent mean values ± s.d. from three independent experiments (*$0.01<P<0.05$; **$P<0.01$).

very unstable. In the protein (MALDI-MS and crystal) the phospho-H11 is stabilised with surrounding residues of phospho-H11 that contribute to its stability. Upon digestion to peptide, the stabilization effect of the protein is lost and the phosphorylated histidine is unstable with a half-life of 35 min. The fact that we observed H11 phosphorylation in the protein crystal structure strongly indicates the protein-mediated stabilization of this typically quite labile modification. Therefore, our findings suggest that Y26 phosphorylation can shift the protein conformation that contributes to PGAM1 activation and further stabilise the active form of PGAM1.

Furthermore, our findings for the first time elucidate the structural mechanism by which H11 phosphorylation contributes to PGAM1 activation. Phospho-H11 activates PGAM1 at least in part, by promoting substrate 3-PG binding. Recently, Vander Heiden *et al.*[22] showed that the pyruvate kinase substrate, phosphoenolpyruvate (PEP) can transfer a phosphate to PGAM1 to 'phosphorylate' the catalytic H11 on PGAM1, producing pyruvate in the absence of PKM2 activity. We tested this concept and found that FGFR1-dependent enhancement of PGAM1 activity is not altered in the presence of physiological levels of PEP (30 μM) (Supplementary Fig. S3). This suggests that Y26 phosphorylation- and PEP-dependent H11 phosphorylation are independent mechanisms that contribute to PGAM1 activation.

We recently reported that PGAM1 regulates anabolic biosynthesis by controlling intracellular levels of its substrate 3-PG and product 2-PG (ref. 4). The concentrations of these glycolytic metabolites can directly affect the catalytic activity of enzymes involved in PPP (3-PG binds to and inhibits 6PGD in the oxidative PPP) and biosynthesis (2-PG activates PHGDH in serine biosynthesis pathway), which represents a novel, additional link between glycolysis, PPP and biosynthesis. Inhibition of PGAM1 by shRNA or a small molecule inhibitor PGMI-004A results in increased 3-PG and decreased 2-PG levels in cancer cells, leading to significantly decreased glycolysis, PPP flux and biosynthesis, and reduced cancer cell proliferation and tumour growth[4]. In consonance with these findings, substitution of Y26 attenuates PGAM1 activity, leading to accumulation of 3-PG and reduction of 2-PG in cancer cells, accompanied by decreased glycolysis, PPP/anabolic biosynthesis and cell proliferation, as well as tumour growth in xenograft mice.

It is somewhat surprising that treatment with 5 μM methyl-2-PG rescues the decreased 2-PG level to ~30 μM in cells expressing PGAM1 Y26F mutant. We hypothesize that upon treatment, cell permeable methyl-2-PG enters the cell via passive diffusion, moving down its concentration gradient from outside the cell (5 μM) to inside the cell (0 μM). Once inside the cell, methyl-2-PG is hydrolysed to 2-PG, which is not cell permeable and chemically different from methyl-2-PG. Thus, the conversion of methyl-2-PG to 2-PG eliminates intracellular methyl-2-PG, which sustains the concentration gradient of methyl-2-PG across the cell membrane (extracellular 5 μM versus intracellular 0 μM). This in turn facilitates continuous diffusion of methyl-2-PG into cells, and if the diffusion and hydrolysis of methyl-2-PG occur more quickly than 2-PG consumption in glycolysis, restoration of physiological 2-PG levels (~30 μM) inside the cells could be eventually achieved.

Together, these data suggest that Y26 phosphorylation may provide a regulatory window for cancer cells to promptly respond to changes of nutrients and microenvironment, at least in part by altering intracellular levels of 3-PG and 2-PG to coordinate glycolysis and biosynthesis, providing a metabolic advantage to cancer cell proliferation and tumour growth.

Methods

Mass spectrometry analysis. Determination of histidine phosphorylation was performed using reversed phase high pressure liquid chromatography-mass spectrometry. The immunoprecipitated beads were washed with TBS and Flag-tagged PGAM1 proteins were eluted by 3 × FLAG peptide in TBS (Sigma) and directly subjected to MS analysis. PGAM1 WT and Y26F mutant samples were resolved using SDS–PAGE, and PGAM1 containing bands were excised. Bands were digested with trypsin (Promega) overnight at 25 °C, and tryptic peptides were extracted with repeated desiccation and swelling in acetonitrile and 100 mM ammonium bicarbonate, respectively. The extracted peptides were concentrated by vacuum centrifugation and desalted using in-house made C18STAGE Tips before mass spectrometric analysis. Samples were loaded by an Eksigent AS2 autosampler onto a 75-μm fused silica capillary column packed with 11 cm of C18 reverse phase resin (5 μm particles, 200 Å pore size; Magic C18; Michrom BioResources). Peptides were resolved on a 110-min 1–100% buffer B gradient (buffer A = 0.1 mol l^{-1} acetic acid, Buffer B = 70% acetonitrile in 0.1 mol l^{-1} acetic acid) at a flow rate of 200 ml min^{-1} (1200 series; Agilent). The HPLC was coupled to a mass spectrometer (LTQ-Orbitrap; ThermoFisher Scientific) with a resolution of 30,000 for full MS followed by seven data-dependent MS/MS analyses. Collision-induced dissociation was used for peptide fragmentation. Targeted runs were also performed to increase the likelihood of quantifying the labile histidine phosphorylation. Peptide abundance of the phosphorylated and unphosphorylated peptides was calculated by manual chromatographic peak integration of full MS scans using Qual Browser software (version 2.0.7; ThermoFisher Scientific Inc.). The relative abundance of the phosphorylated peptide was calculated as the ratio of the sum of the areas underneath the peaks of phosphorylated peptide to the sum of the areas underneath peaks corresponding to phosphorylated and unphosphorylated peptides (total peptide). The peptide sequence and histidine phosphorylation were confirmed by manual inspection of the MS/MS spectra.

Sample preparation of H11-phosphorylated PGAM1 protein. Purified PGAM1 protein (100 μM, in 20 mM Tris-HCl buffer, pH 7.4) mixed with 2,3-BPG (final concentration: 500 μM) and incubated for half an hour at room temperature. Excess 2,3-BPG was removed by desalting. Purified protein and 2,3-BPG-treated protein were directly analysed by MALDI-TOF mass spectrum using sinapic acid as matrix solution.

Crystallization of PGAM1 proteins and data collection. Crystals of PGAM1 were originally identified using the PEG ION crystallization screen kit (Hampton Research). Optimised crystals were produced using hanging drop vapour diffusion at 16 °C by mixing 1 μl of protein solution at 30–40 mg ml^{-1} with 1 μl reservoir solution containing 0.1 M MES pH 6.0, 8% PEG 3350. Crystals appeared after 1 h and continued to grow for several days. Non-phosphorylated PGAM1 was obtained by eluting with 500 mM imidazole from the Ni-NTA column and storing the PGAM1 under 277 K for 1 week. The protein was then washed by with buffer A (10 mM Tris, pH8.0, 500 mM NaCl) containing 20% glycerol three times and then purified by gel filtration. Phosphorylated PGAM1 crystals were obtained by treating WT PGAM1 with 5 mM 2,3-BPG for half an hour and excess 2,3-BPG were removed by buffer exchange before crystallization. Crystals were dehydrated by 50% PEG 6,000 for 24 h, and quickly frozen in liquid nitrogen. All diffraction data were collected at 100 K at the macromolecular crystallography for life science beamline LS-CAT (21-ID-F) and NE-CAT (24-ID-C), respectively, at the Advanced Photon Source, Argonne National Laboratory. Native data sets extending to 1.65 Å resolution were collected at 0.9795 Å wavelength (12.66 keV). The data were processed with HKL2000 and the scaled data were used for molecular replacement. Crystallographic statistics are summarized in Supplementary Table S1.

Data refinement. For phasing, model building and refinement, the structures of both PGAM1-apo form and phosphorylated PGAM1 were determined by molecular replacement using Phaser in the CCP4 suite, with the template protein as the search model (PDB accession code: 1YFK). The structures were then refined by using Phenix. Manual rebuilding of the model was carried out using the molecular graphics program COOT based on electron density interpretation. Water molecules were incorporated into the model if they gave rise to peaks exceeding 3σ in Fo-Fc density maps. The final refined models have good stereochemistry with 98.5% of the residues in the most favored regions of the Ramachandran plot with none in the disallowed regions (values calculated using PROCHECK from CCP4 suite).

Xenograft studies. Approval of use of mice and designed experiments was given by the Institutional Animal Care and Use Committee of Emory University. Nude mice (nu/nu, male 6–8-week old, Charles River Laboratories) were subcutaneously injected with 10×10^6 H1299 cells stably expressing mPGAM1 WT and Y26F with stable knockdown of endogenous hPGAM1 on the left and right flanks, respectively. Tumour growth was recorded by measurement of two perpendicular diameters of the tumours over a 6-week course using the formula $4\pi/3 \times (\text{width}/2)^2 \times (\text{length}/2)$. The tumours were harvested and weighed at the experimental endpoint, and the masses of tumours (g) derived from cells expressing mPGAM WT or Y26F mutant in both flanks of each mouse were compared. Statistical analyses have been done by comparison in relation to the control group with a two-tailed paired Student's *t*-test.

References

1. Elstrom, R. L. *et al.* Akt stimulates aerobic glycolysis in cancer cells. *Cancer Res.* **64,** 3892–3899 (2004).
2. Gottschalk, S., Anderson, N., Hainz, C., Eckhardt, S. G. & Serkova, N. J. Imatinib (STI571)-mediated changes in glucose metabolism in human leukemia BCR-ABL-positive cells. *Clin Cancer Res.* **10,** 6661–6668 (2004).
3. Kroemer, G. & Pouyssegur, J. Tumor cell metabolism: cancer's Achilles' heel. *Cancer Cell* **13,** 472–482 (2008).
4. Hitosugi, T. *et al.* Phosphoglycerate mutase 1 coordinates glycolysis and biosynthesis to promote tumor growth. *Cancer Cell* **22,** 585–600 (2012).
5. Grisolia, S. & Cleland, W. W. Influence of salt, substrate, and cofactor concentrations on the kinetic and mechanistic behavior of phosphoglycerate mutase. *Biochemistry* **7,** 1115–1121 (1968).
6. Rose, Z. B. & Dube, S. Rates of phosphorylation and dephosphorylation of phosphoglycerate mutase and bisphosphoglycerate synthase. *J. Biol. Chem.* **251,** 4817–4822 (1976).
7. Britton, H. G. & Clarke, J. B. Mechanism of the 2,3-diphosphoglycerate-dependent phosphoglycerate mutase from rabbit muscle. *Biochem. J.* **130,** 397–410 (1972).
8. Rose, Z. B., Hamasaki, N. & Dube, S. The sequence of a peptide containing the active site phosphohistidine residue of phosphoglycerate mutase from chicken breast muscle. *J. Biol. Chem.* **250,** 7939–7942 (1975).
9. Liu, L., Wang, S., Zhang, Q. & Ding, Y. Identification of potential genes/proteins regulated by Tiam1 in colorectal cancer by microarray analysis and proteome analysis. *Cell Biol. Int.* **32,** 1215–1222 (2008).
10. Ren, F. *et al.* Quantitative proteomics identification of phosphoglycerate mutase 1 as a novel therapeutic target in hepatocellular carcinoma. *Mol. Cancer* **9,** 81 (2010).
11. Corcoran, C. A., Huang, Y. & Sheikh, M. S. The regulation of energy generating metabolic pathways by p53. *Cancer Biol. Ther.* **5,** 1610–1613 (2006).
12. Tennant, D. A., Duran, R. V. & Gottlieb, E. Targeting metabolic transformation for cancer therapy. *Nat. Rev. Cancer* **10,** 267–277 (2010).
13. Tennant, D. A., Duran, R. V., Boulahbel, H. & Gottlieb, E. Metabolic transformation in cancer. *Carcinogenesis* **30,** 1269–1280 (2009).
14. Hitosugi, T. *et al.* Tyrosine phosphorylation inhibits PKM2 to promote the Warburg effect and tumor growth. *Sci. Signal* **2,** ra73 (2009).
15. Towne, J. C., Rodwell, V. W. & Grisolia, S. The microestimation, distribution, and biosynthesis of 2, 3-diphosphoglyceric acid. *J. Biol. Chem.* **226,** 777–788 (1957).
16. Wang, Y. *et al.* Crystal structure of human B-type phosphoglycerate mutase bound with citrate. *Biochem. Biophys. Res. Commun.* **331,** 1207–1215 (2005).
17. Bond, C. S., White, M. F. & Hunter, W. N. Mechanistic implications for Escherichia coli cofactor-dependent phosphoglycerate mutase based on the high-resolution crystal structure of a vanadate complex. *J. Mol. Biol.* **316,** 1071–1081 (2002).
18. MacQuarrie, R. & Gibson, Q. H. Ligand binding and release of an analogue of 2,3-diphosphoglycerate from human hemoglobin. *J. Biol. Chem.* **247,** 5686–5694 (1972).
19. MacQuarrie, R. & Gibson, Q. H. Use of a fluorescent analogue of 2,3-diphosphoglycerate as a probe of human hemoglobin conformation during carbon monoxide binding. *J. Biol. Chem.* **246,** 5832–5835 (1971).
20. Nairn, J. *et al.* The use of mass spectrometry to examine the formation and hydrolysis of the phosphorylated form of phosphoglycerate mutase. *FEBS Lett.* **359,** 192–194 (1995).
21. Wang, Y. *et al.* Seeing the process of histidine phosphorylation in human bisphosphoglycerate mutase. *J. Biol. Chem.* **281,** 39642–39648 (2006).
22. Vander Heiden, M. G. *et al.* Evidence for an alternative glycolytic pathway in rapidly proliferating cells. *Science* **329,** 1492–1499 (2010).

Acknowledgements

This work was supported in part by NIH grants CA120272 (J.C.), CA140515 (J.C.), GM071440 (C.H.), DoD grant W81XWH-12-1-0217 (J.C.), the Pharmacological Sciences Training Grant T32 GM008602 (S.E.) and the National Natural Science Funds of China No. 20902013 (L.Zhou). T.H. is a Fellow Scholar of the American Society of Haematology. J.X., Y.W. and T.-L.G. are employees of Cell Signaling Technology, Inc. G.Z.C., S.M.S., F.R.K., S.K. and J.C. are Georgia Cancer Coalition Distinguished Cancer Scholars. S.K. is a Robbins Scholar. S.K. and J.C. are American Cancer Society Basic Research Scholars. J.C. is a Scholar of the Leukaemia and Lymphoma Society. We thank Dr. Benjamin A. Garcia for providing mass spectrometry equipment and technical assistance.

Author contributions

T.H., L.Zhou, S.L., F.R.K., S.K., C.H. and J.C. designed this study. T.H. and J.F. performed experiments with help of S.E., H.-B.K., J.-H.S. and C.S., L.Zhou, L.Zhang and H.C. performed the crystallography experiments and data analysis with help of P.J. and W.G., J.X., Y.W. and T.-L.G. performed the phospho-proteomics studies and generated the specific phospho-PGAM1 (pY26) antibody. M.A., G.L. and Y.K. performed mass spectrometry analysis. S.E., M.L.A., H.J.K., G.Z.C. and D.M.S. performed experiments to detect Y26 phosphorylation in human patient tissue samples. T.J.B. performed structural analysis. T.H., L.Zhou, S.K., C.H. and J.C. wrote the manuscript. All authors read and approved the final manuscript.

Additional information

Accesssion codes: Coordinates and structure factors for PGAM1-apo and H11-phosphorylated PGAM1 have been deposited in the Protein Data Bank under accession codes 4GPI and 4GPZ, respectively.

Supplementary Information accompanies this paper at http://www.nature.com/naturecommunications

Competing financial interests: The authors declare no competing financial interests.

Reprints and permission information is available online at http://npg.nature.com/reprintsandpermissions/

How to cite this article: Hitosugi, T. *et al.* Tyr26 phosphorylation of PGAM1 provides a metabolic advantage to tumours by stabilizing the active conformation. *Nat. Commun.* 4:1790 doi: 10.1038/ncomms2759 (2013).